Max-Planck-Institut für Metallforschung
Stuttgart

Thermo-Mechanical Behavior of NiAl Thin Films

Patrick Wellner

Dissertation
an der
Universität Stuttgart

Bericht Nr. 144
Dezember 2003

Thermo-Mechanical Behavior of NiAl Thin Films

Von der Fakultät Chemie der Universität Stuttgart
zur Erlangung der Würde eines Doktors der
Naturwissenschaften (Dr. rer. nat.) genehmigte Abhandlung

Vorgelegt von

Patrick Wellner

aus Stuttgart

Hauptberichter:	Prof. Dr. E. Arzt
Mitberichter:	Prof. Dr. H. Clemens
Tag der mündlichen Prüfung:	5. Dezember 2003

Max-Planck-Institut für Metallforschung
und
Institut für Metallkunde der Universität Stuttgart

2003

Patrick Wellner

Thermo-Mechanical Behavior of NiAl Thin Films

109 pages, 53 figures, 6 tables

Abstract

Thin films based on the intermetallic alloy NiAl are used as protective coatings for high temperature applications because of their excellent oxidation resistance. However, insufficient mechanical strength of the coatings may lead to failure as a result of thermal stresses.

This work describes the influence of film thickness (0.2 to 3.1 μm) and Al content (45 to 52 at-% Al) on the yield strength, the fracture toughness and the creep strength of polycrystalline NiAl films. The NiAl films were sputter-deposited on Si substrates and were thermally cycled up to 700 °C. The stress evolution during thermal cycling was measured using a laser-optical substrate-curvature technique.

The fracture toughness of the NiAl films was found to depend on the chemical composition: upon thermal straining, Al-rich films exhibited crack formation while stoichiometric and Ni-rich films remained devoid of cracks. The fracture toughness of the Al-rich films was determined to be 2.2 to 2.9 MPa $m^{1/2}$, independent of film thickness. However, the fracture stress increased with decreasing film thickness. These results are discussed on the basis of thin film cracking models.

Plastic deformation in stoichiometric and Ni-rich films is strongly influenced by the thickness of the films. Upon cooling to room temperature, a strong increase in yield strength with decreasing film thickness was found. The yield strength increased from 420 MPa for 3.0 μm thick films to about 2000 MPa for 0.2 μm thick films. In contrast, heating above 400 °C yielded the opposite trend: thinner films showed stronger plastic deformation, which is related to a diffusional creep process. The influence of Al content and film thickness on the stress evolution of stoichiometric and Ni-rich films is discussed with respect to thin film deformation mechanisms.

Patrick Wellner

Thermo-mechanisches Verhalten dünner NiAl-Schichten

109 Seiten, 53 Abbildungen, 6 Tabellen

Kurzzusammenfassung

Dünne Schichten auf der Basis von intermetallischem NiAl finden ihren Einsatz als Schutzschichten für Hochtemperaturanwendungen aufgrund ihrer ausgezeichneten Oxidationsbeständigkeit. Mangelnde mechanische Stabilität der Schichten kann allerdings durch das Auftreten von thermischen Spannungen zum Schichtversagen führen.

In dieser Arbeit wird der Einfluss der Schichtdicke (0.2 bis 3.1 µm) und des Al-Gehalts (45 bis 52 at-% Al) auf die Bruchzähigkeit und den Widerstand gegenüber plastischem Fließen von polykristallinen NiAl-Schichten beschrieben. Die untersuchten Schichten wurden mittels Magnetron-Sputtern auf Si-Substrate aufgebracht und die Spannungsentwicklung während einer zyklischen, thermischen Beanspruchung bis 700 °C gemessen. Die Substrat-Krümmungs-Methode wurde zur Messung der Schichtspannung angewandt.

Diese Arbeit zeigt, dass die Bruchzähigkeit von NiAl-Schichten durch die chemische Zusammensetzung bestimmt wird. So wurde nach einer thermischen Behandlung Risse in Al-reichen Schichten gefunden, während stöchiometrische und Ni-reiche Schichten rissfrei blieben. Die Bestimmung der Bruchzähigkeit der Al-reichen Schichten ergab, unabhängig von der Schichtdicke, Werte von 2.2 bis 2.9 MPa $m^{1/2}$. Im Gegensatz dazu wurde eine Zunahme der Bruchspannung mit abnehmender Schichtdicke gemessen. Diese Ergebnisse werden anhand von Rissmodellen für Dünnschichtsysteme diskutiert.

Die plastische Verformbarkeit von stöchiometrischen und Ni-reichen Schichten hängt entscheidend von der Schichtdicke ab. So steigt die Streckgrenze bei niedrigen Temperaturen durch die Verringerung der Schichtdicke ungewöhnlich stark an. Für 0.2 µm dicke NiAl-Schichten wurden Streckgrenzen bis zu 2000 MPa gemessen, während die Streckgrenze von 3.0 µm dicken Schichten lediglich 420 MPa beträgt. Beim Aufheizen der Schichten auf Temperaturen oberhalb 400 °C zeigt sich der umgekehrte Trend: Dünnere Schichten zeigen stärkere plastische Verformung, was mit Diffusionskriechen in Zusammenhang gebracht wird. Der Einfluss der chemischen Zusammensetzung und der Schichtdicke auf die Spannungsentwicklung in stöchiometrischen und Ni-reichen Schichten wird mit Modellen der Dünnschichtmechanik erklärt.

Danksagung

Die vorliegende Arbeit wurde in der Zeit von Juni 2000 bis November 2003 am Max-Planck-Institut für Metallforschung und am Institut für Metallkunde der Universität Stuttgart durchgeführt. Herrn Prof. Dr. E. Arzt danke ich für die Möglichkeit, diese Arbeit in seiner Arbeitsgruppe durchzuführen.

Herrn Prof. Dr. H. Clemens danke ich für die freundliche Übernahme des Mitberichts.

Herrn Prof. Dr. Oliver Kraft und Herrn Dr. Gerhard Dehm gilt mein besonderer Dank; sie haben diese Arbeit betreut und immer ein offenes Ohr für mich gehabt. Die zahlreichen Diskussionen mit ihnen haben wesentlich zum Gelingen dieser Arbeit beigetragen. Ich hätte mir keine besseren Betreuer vorstellen können.

Herrn Dr. J. Andersons und Herrn Prof. Dr. H. Gao danke ich für die fruchtbaren Diskussionen.

Allen Serviceeinrichtungen und Technikern des Max-Planck-Institutes danke ich für ihre Unterstützung bei den experimentellen Arbeiten, von denen ich Frau Natascha Tomic und die Herren Gerhard Adam, Karl-Heinz Berckhemer und Siegfried Hansel besonders hervorheben möchte.

Außerdem möchte ich mich bei allen Mitarbeitern der Gruppe Arzt für die angenehme und kooperative Arbeitsatmosphäre bedanken.

Nicht zuletzt bedanke ich mich bei meiner Frau Randa und bei meinen Eltern für ihre Unterstützung.

Table of Contents

List of symbols

A	unit crack area [1 m^2]
a_l	crack length parallel to the surface [m]
a_s	substrate crack length [m]
b	Burgers vector length [m]
C	curvature [m^{-1}]
D_0	pre-exponential diffusion coefficient [m^2/s]
D_{gb}	grain boundary diffusion coefficient [m^2/s]
d	grain size [m]
E_f	Young's modulus of the film material [Pa]
E_f^*	plane-strain modulus of the film material [Pa]
E_s^*	plane-strain modulus of the substrate material [Pa]
G	energy release rate [J/m^2]
G_c	critical energy release rate [J/m^2]
g	numerical constant
h_f	film thickness [m]
h_s	substrate thickness [m]
K_c	critical stress intensity factor [MPa $m^{1/2}$]
k_B	Boltzmann's constant [$1.381 \cdot 10^{-23}$ J/K]
m_{el}	elastic slope [Pa/K]
m_{exp}	experimentally measured slope [Pa/K]
M_s	biaxial elastic modulus of the substrate [Pa]
P_{Al}	aluminum sputter power [W]
P_{Ni}	nickel sputter power [W]
p_{in}	inelastic proportion
Q_{gb}	activation energy for grain boundary diffusion [J/mol]
R	numerical constant
s	Schmid factor
	also: numerical constant

T	temperature [K]
T_{max}	maximum temperature [K]
t	time [s]
t_0	characteristic time [s]
ΔT_{in}	temperature interval referring to inelastic behavior [K]
ΔT_{el}	temperature interval referring to elastic behavior [K]
ΔT_{pl}	temperature interval referring to plastic behavior [K]
V_{film}	volume of the plastic zone in a film on a substrate [m^3]
V_{sheet}	volume of the plastic zone in a freestanding sheet [m^3]
W_{el}	elastic energy [J]
Z	numerical constant
α_i	thermal expansion coefficient of the material i [K^{-1}]
α	Dundurs parameter
β	Dundurs parameter
δ	grain boundary width [m]
ε_{pl}	plastic strain
ε_{th}	thermal strain
Γ	fracture energy [J/m^2]
Γ_f	fracture energy of the film [J/m^2]
Γ_s	fracture energy of the substrate[J/m^2]
γ_{coh}	cohesive energy [J/m^2]
γ_{sc}	surface energy [J/m^2]
η_f	numerical constant defining crack geometry in the film
η_s	numerical constant defining crack geometry in the substrate
φ	angle between glide plane normal and film normal [°]
λ	numerical constant
λ_1	numerical constant
λ_2	numerical constant
μ_{eff}	effective shear modulus [Pa]
μ_f	shear modulus of the film [Pa]
μ_i	shear modulus of the material i [Pa]
μ_s	shear modulus of the substrate [Pa]

ν_f	Poisson's ratio of the film material
σ_{el}	elastic stress [Pa]
σ_f	film stress [Pa]
σ_{fr}	fracture stress [Pa]
σ_{gb}	grain boundary stress [Pa]
σ_y	yield strength [Pa]
σ_0	film stress at the temperature T_0 [Pa]
τ_p	Peierls stress [Pa]
Ω	atomic volume [m^3]
ω_f	normalized energy release rate of the film
ω_s	normalized energy release rate of the substrate

1 Introduction

The reliability of structural components can be significantly improved by coatings. Protective coatings are widely used for different materials and applications ranging from wear resistant cutting tools to protection against environmental attack, e.g. the varnish on the outer skin of a ship. Especially in cutting edge fields, such as the aerospace industry, an increasing demand exists for enhanced surface properties. These requirements are fulfilled by coatings. For example, turbine blades in an aero engine must withstand temperatures of up to 1000 °C in the presence of corrosive gases. The turbine blades are therefore coated with a protective aluminide layer [1]. A typical aluminide coating is based on the intermetallic alloy NiAl, which forms a protective oxide at elevated temperatures. Besides the chemical properties, the mechanical response to stresses plays a crucial role in the reliability of the coating. Temperature changes induce thermal stresses in the coating, since the coating usually has a different thermal expansion coefficient compared to the underlying bulk material. Thermal stresses may cause damage or failure of the coating. For example, insufficient creep strength of the coating may lead to irreversible shape changes by plastic deformation at high temperatures or induce cracks upon cooling if the thermal stresses exceed the fracture stress of the coating.

Research of thin film systems has revealed that material properties may change significantly due to geometrical constraints. Film thickness is an important parameter that determines the mechanical properties of the films [2]. The thickness of thin films on substrates, e.g. coatings on structural components, are usually in the range of several micrometers for wear applications, down to a few nanometers in microelectronic devices.

Although NiAl-based coatings find technological application, little is known about the influence of size effects on the mechanical properties of NiAl. This study aims to correlate geometrical and microstructural size effects with the thermo-mechanical behavior of NiAl thin films with thicknesses of 0.2 to 3.1 μm. Furthermore, the influence of Al content is investigated in the range of 45 to 52 at-% Al. All films were deposited onto Si substrates as a model system and subjected to thermal cycling that induced thermal strains of up to 0.9 % in the NiAl films.

Chapter 2 summarizes the literature on the intermetallic phase NiAl, presents the current understanding of the mechanical behavior of thin metallic films, and outlines the motivation for this study. The results of the thermo-mechanical studies of NiAl thin films are reported and discussed in chapter 3 and 4. Chapter 3 focuses on the cracking behavior, while size effects on plasticity of NiAl films are described in chapter 4. Finally, chapter 5 briefly summarizes the main results of this work.

2 Literature review and motivation

The mechanical behavior of bulk NiAl and metallic thin films, which motivated this study, is introduced in this chapter. Further details required to interpret the experimental results will be given in the discussion sections of chapters 3 and 4.

2.1 Intermetallic phase NiAl

The search for new materials that can both withstand mechanical stresses at elevated temperatures and resist oxidation resulted in a broad scientific interest in intermetallics. The ordered intermetallic phase of NiAl has a melting temperature of 1638 °C [3] and shows excellent oxidation resistance due to the formation of a protecting alumina layer on the surface [4]. Furthermore, NiAl has a low density and possesses metal-like thermal and electrical conductivity. As a result of these desirable properties, NiAl has great potential for technical applications.

NiAl is thermodynamically stable between 45 to 60 at-% Ni below 400 °C (figure 2-1). Al-rich alloys are produced by the addition of Ni vacancies, and Ni-rich alloys are formed when Ni atoms replace Al atoms [5]. The chemical composition significantly influences the mechanical properties of NiAl. For example, the yield strength of NiAl at room temperature (RT) increases with deviation from stoichiometry toward both Ni-rich and Al-rich alloys, as summarized by Baker [6]. Furthermore, the volume diffusion coefficient for Ni diffusion in NiAl was found to strongly increase with deviation from stoichiometry [7]. As a consequence, the creep resistance of polycrystalline NiAl is reduced by changing the stoichiometric composition to both the Ni-rich or the Al-rich side [8] indicating a strong role of diffusional processes in high-temperature creep.

The major disadvantage of NiAl is its low fracture toughness below the brittle to ductile transition (BDT) temperature of approximately 400 °C [9-12]. The fracture toughness of polycrystalline NiAl was determined to be 4 to 12 MPa $m^{1/2}$, depending upon chemical composition, purity and grain size [9, 13, 14].

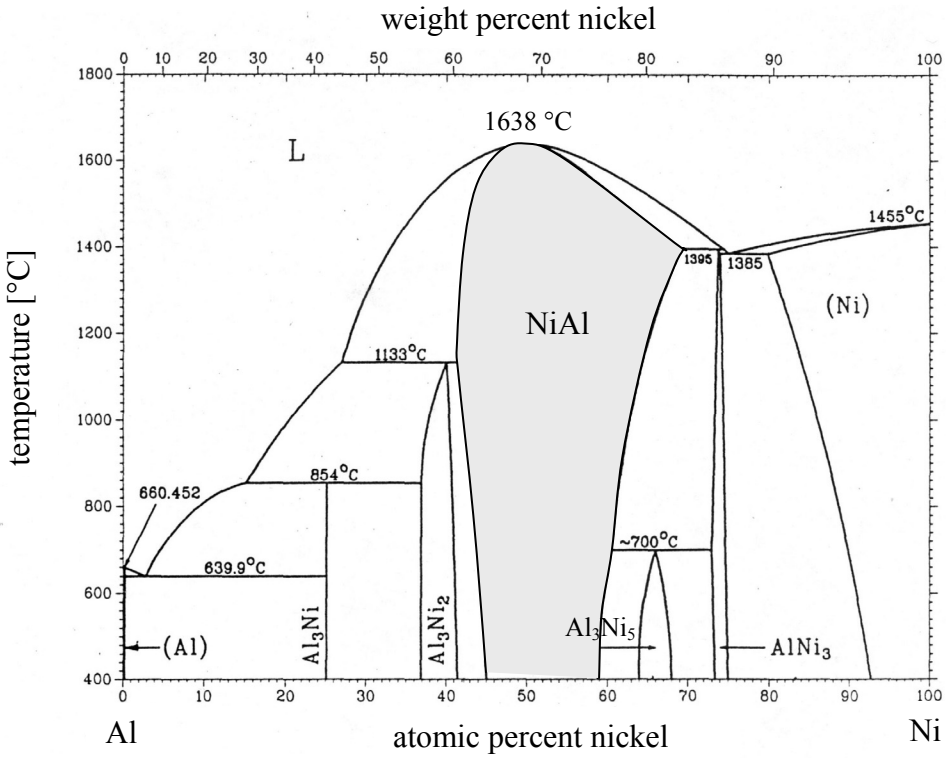

Figure 2-1 **Phase diagram of the system Al – Ni as proposed by Singleton et al. [3]. The intermetallic phase NiAl shows a wide homogeneity region.**

Plastic deformation below the BDT temperature is mainly attributed to dislocation motion on the {110}<001> slip system [15], which results in only three independent slip systems. The increased ductility above the BDT temperature is attributed to different mechanisms; the activation of additional slip systems and the climb of <001> dislocations are the most frequent explanations for the enhanced ductility found in the literature.

Very few investigations have been carried out on NiAl thin films so far. Hsu et al. [16], Zhong et al. [17] and Almeida et al. [18] studied the influence of substrate material and deposition conditions on NiAl film microstructure. The film texture was especially sensitive to deposition parameters such as pressure and sputtering power. However, the mechanical behavior of NiAl thin films is mainly unknown.

2.2 Cracking behavior of thin films bonded to a substrate

The major drawback for the technical application of intermetallics, in particular NiAl, is their brittle character below the BDT temperature. Stresses are not sufficiently relaxed by plastic deformation and thus cracks form. This is a common mechanism for failure of thin films.

The cracking behavior of thin films on substrates differs from bulk behavior due to the small film thicknesses and the presence of the substrate. In contrast to bulk behavior, where a propagating crack of critical length leads to fracture and total failure, a cracked film may still remain bonded to the substrate. This leads to multiple crack formation since a single crack reduces the film stress in the film only locally as a result of the constraining effect of the substrate. Furthermore, thin films on substrates are usually in a biaxial stress state, especially for thermal stresses induced by differences in thermal expansion coefficient between film and substrate. The constraining effect of the substrate on the released strain energy in a film under biaxial stress is schematically compared in figure 2-2 to a freestanding sheet under uniaxial loading.

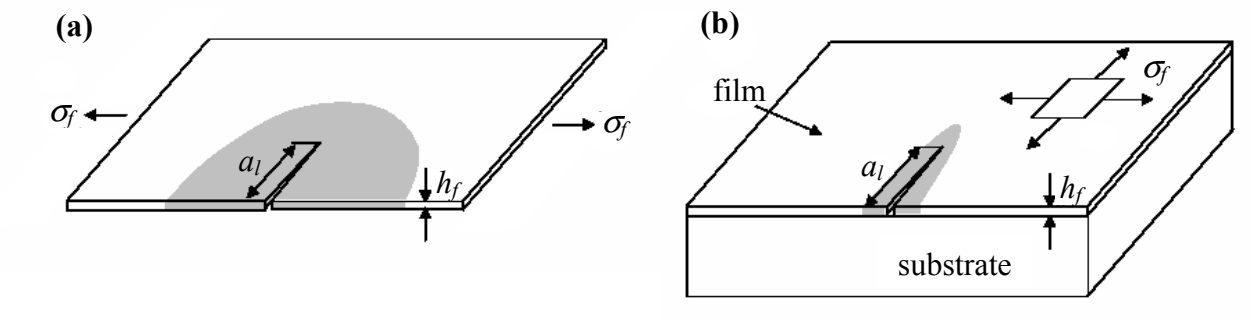

Figure 2-2 The volume (marked in grey) of strain energy released by the formation of a crack is larger in (a) a freestanding film under uniaxial tension than in (b) a film bonded to a substrate subjected to a biaxial film stress.

In a freestanding sheet, the volume V_{sheet} affected by the release of energy due to crack formation scales with the crack length a_l and the film thickness h_f according to $V_{sheet} \propto a_l^2 h_f$ (figure 2-2 a). In contrast, for a film on a substrate, the volume V_{film} in which the strain energy is released yields a stronger influence of the film thickness due to the

substrate constraint and scales as $V_{film} \propto a_l h_f^2$ (figure 2-2 b). For a film bonded to a substrate, the energy W_{el} released by the introduction of a crack is given by:

$$W_{el} \propto -\frac{\sigma_{fr}^{\ 2}}{E_f^*} a_l h_f^2, \tag{2-1}$$

where σ_{fr} is the film fracture stress, defined as the maximum stress prior to crack formation, and E_f^* represents the plane-strain elastic modulus of the film. The energy release rate G, defined as the reduction of the elastic energy associated with a crack advancing by unit area A (where $A \propto a_l h_f$), can be derived from equation (2-1) as follows:

$$G = -\frac{\partial W_{el}}{\partial A}. \tag{2-2}$$

Following this approach, the energy release rate for steady-state cracking is given by:

$$G = Z \frac{\sigma_{fr}^2 h_f}{E_f^*}, \tag{2-3}$$

This dependency implies that the film thickness plays the role of a critical crack length. Since the film thickness is homogeneous in most thin film systems, the driving force for crack propagation parallel to the surface is reached at every site along the film once the stress reaches the fracture stress. Due to the constrained energy release by the formation of a single crack, as described above, the experimentally observed formation of additional cracks is expected [19]. The crack propagation parallel to the surface is called channel cracking since the crack forms a channel of constant width as it propagates in the film.

The parameter Z in equation (2-3) comprises the elastic mismatch between film and substrate and the crack geometry. Several crack geometries for thin film cracking were mainly studied computationally: Isolated surface cracks [20], crack channeling including the formation of a network of cracks [21-24], debonding at the film/substrate interface [19, 25, 26] and crack penetration into the substrate [20, 27]. Typical values for the parameter Z as a function of cracking geometry and elastic mismatch are given in table 2-1.

Table 2-1 **Parameter Z of equation (2-3) for different crack geometries and elastic mismatches between film and substrate. E_f^* and E_s^* are the plane-strain elastic moduli of film and substrate, and h_f and a_s are the film thickness and the substrate crack length, respectively. The Z values are adopted from the works of Hutchinson and Suo [20], Beuth [21] and Ye et al. [27].**

parameter Z	isolated surface cracks (depth: 0.9 h_f)	crack channeling	substrate damage ($a_s = h_f$)	debonding at the interface	crack channeling and substrate damage ($a_s = h_f$)
no elastic mismatch	3.6	2.0	1.2	0.5	3.6
stiff film $E_f^* : E_s^* = 3 : 1$	6.7	3.1	2.3	0.4	7.7
compliant film $E_f^* : E_s^* = 1 : 3$	2.2	1.5	0.5	0.5	1.7

Even though thin film cracking was extensively studied on a theoretical basis, little experimental work has been carried out so far. Cracking in thin films is mainly treated in literature as a full elastic problem. Furthermore, it is assumed that the energy release rate is uniform along the crack front. As a consequence, the energy release rate and, thus, the fracture toughness is believed to be independent of film thickness. Hu and Evans [19] found experimental evidence for this assumption for Cr films on Al substrates as did Moody et al. [28] for Ta_2N films on AlN substrates. However, due to scatter in data and insufficient amount of tested samples with varying film thicknesses, clear experimental proof is still lacking. Especially for metallic films, plastic yielding in front of the crack tip cannot be excluded. For freestanding metallic sheets tested under uniaxial tension, it is well known that the sheet thickness affects the size of the plastic zone in front of the crack tip. Due to the plane-stress state near the surface, the plastic zone is larger compared to the center of the sheet, where a plane-strain state is present as sketched in figure 2-3 a. As a result, a change in sheet thickness affects the plastic zone size and, thus, the measured fracture toughness of the freestanding sheet. In contrast, the energy released by a crack propagating in a film bonded to a substrate is constrained, resulting in an ascendancy of the plane-strain state and a smaller plastic zone, as compared to a freestanding sheet. The models [19-27] discussed in the literature assume plane strain at each site of the crack front, even near the surface. In the case of plastic yielding in front of the crack tip, the plastic zone size and, thus, the energy release rate are expected to remain independent of the film thickness, as schematically shown in figure 2-3 b. It is unknown, whether this assumption is reasonable and correctly describes the cracking behavior of thin metallic films on substrates.

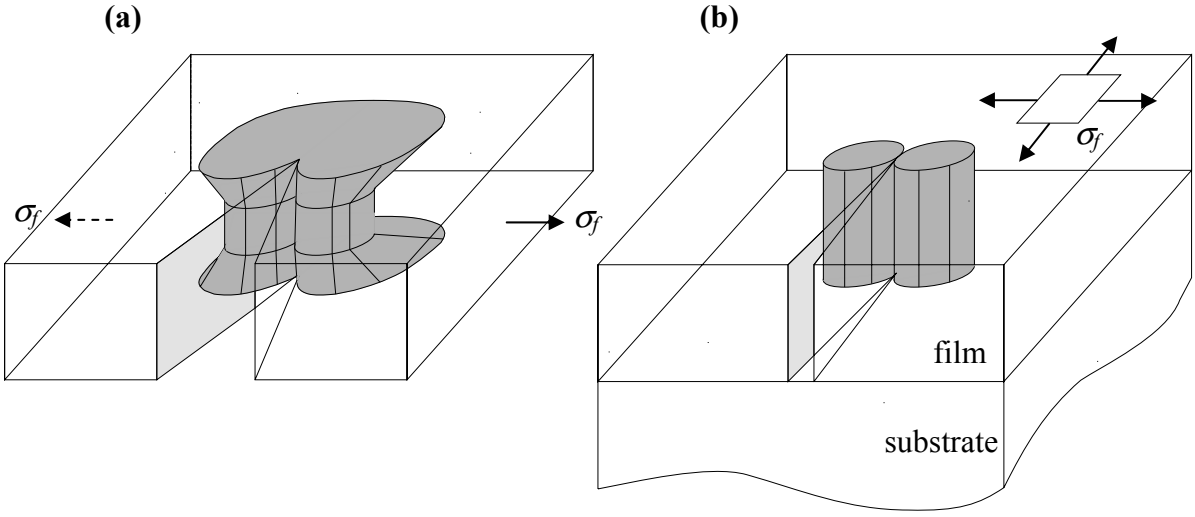

Figure 2-3 Sketch of the size of the plastic zone in front of the crack tip as expected for (a) a freestanding sheet in comparison to (b) a film on a substrate where plane strain is assumed at each site of the crack tip.

Although the fracture toughness of bulk NiAl has been studied, little is known about the cracking behavior of NiAl as a thin film bonded to a substrate. Specifically, the influence of film thickness on the cracking behavior, which is currently unknown, is a central theme of the first part of this study. A major question is whether the fracture toughness of NiAl films is independent of film thickness, as postulated by the models for thin film cracking. Furthermore, the influence of the chemical composition on the fracture toughness of thin NiAl films shall be examined and compared to literature values obtained on bulk NiAl.

2.3 Microstructural and geometrical size effects on plasticity

The geometric and microstructural confinements in thin films have an important impact on the deformation mechanisms and determine the mechanical properties of the films [2, 29]. For instance, the yield strength of thin metallic films increases significantly with decreasing film thickness and is typically much higher than in the corresponding bulk material. The dependence of flow stress on film thickness is shown for Cu [30], Al [31] and Ag [32] thin films in figure 2-4. For comparison, the flow stresses measured between RT and 40 °C were normalized to the shear moduli of the films. The increase in flow stress with decreasing film thickness is comparable for the various fcc metals. This behavior is commonly explained by the constrained dislocation motion in thin films. The film thickness and the grain size, which is usually in the range of the film thickness, limit dislocation-based plasticity. Several models were developed which account for the thickness / grain size effect on yield strength [2, 33-35]. Most authors report an inverse dependency of the yield strength σ_y on film thickness h_f and grain size d:

$$\sigma_y \propto \frac{1}{h_f} \text{ or } \frac{1}{d}. \tag{2-4}$$

Although the general trend is described by the existing models, the magnitude of stress enhancement with decreasing film thickness is generally underestimated. In a more recent approach, the activation of dislocations in the grain interior is considered, which yields a better agreement with some experimental data [36]. However, further developments are needed in order to correctly describe the dependency of yield strength on film thickness and grain size.

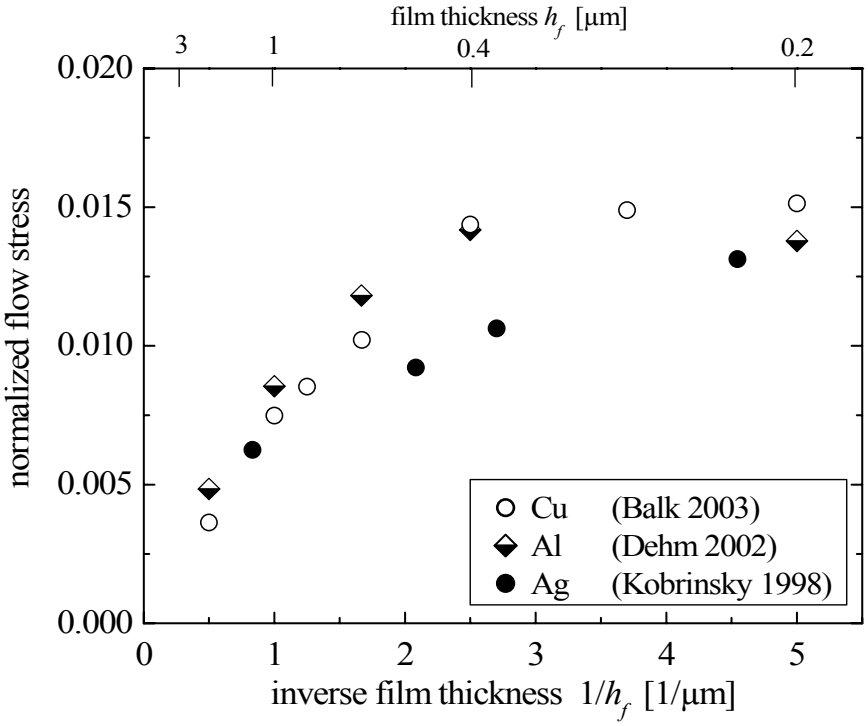

Figure 2-4 **The room temperature flow stresses of polycrystalline Cu [30], Al [31] and Ag [32] thin films are shown as a function of the inverse film thickness. For comparison, the flow stresses of Cu, Al and Ag where normalized to their shear moduli of μ_{Cu} = 42 MPa, μ_{Al} = 25 MPa and μ_{Ag} = 32 MPa, respectively. The Ag films were surface passivated with a 50 nm thick layer of SiO_x.**

Thermal processes determine thin film plastic behavior at elevated temperatures. Many authors suggest that thermally activated dislocation glide is a dominant mechanism for plastic deformation in thin metal films [37-40]. However, the small geometrical and microstructural dimensions in a thin film must be taken into account if common bulk deformation mechanisms are applied to thin film systems. As a result, diffusion plays a crucial role in thin film plasticity, since the diffusion paths are very small compared to common bulk dimensions. The model developed by Gao et al. [41] considers diffusional creep in a thin film under tension and confined by a substrate by assuming that surface atoms diffuse into grain boundaries and locally relax the tensile stress there. As a result, the average stress in the film is lowered, even though the stress in the grain interior may still be unchanged. Similarly, if compressive stresses are present, atoms near the grain boundaries diffuse to the surface and again locally reduce the film stress at the grain boundaries. Gao et al. [41] found, that the amount of stress relaxation due to constrained diffusional creep is a function of both film thickness and grain size. The stress relaxation

increases as the film thickness and the grain size decreases. Experimental observations on Cu thin films by Weiss et al. [40] revealed that the thermo-mechanical behavior of Cu thin films cannot be explained by dislocation-based plasticity alone but constrained diffusional creep strongly contributes to the stress relaxation at temperatures above 250 °C. In a transmission-electron-microscopy (TEM) study on ultra-thin Cu films, Balk et al. [30] found microscopic evidence for constrained diffusional creep: during thermal cycling they discovered the reversible motion of dislocations parallel to the surface. These dislocations had no resolved applied shear stress acting upon them, according to Schmid's law. It is believed that the motion of these so called "parallel glide" dislocations is a consequence of diffusion-induced shear stresses created by constrained diffusional creep close to the intersection of the grain boundaries with the substrate [30]. The nucleation of "parallel glide" dislocations in the vicinity of grain boundaries was postulated earlier by Gao et al. [41].

Thermo-mechanical behavior of thin metal films has mainly been studied in fcc metals. However, other metals and intermetallics are used for thin film applications. For instance, coatings based on the intermetallic phase NiAl are applied to turbine blades for protection against oxidation and corrosion at high temperatures. The influence of film thickness and grain size on the thermo-mechanical behavior of NiAl is not yet known. It is unclear whether thermo-mechanical phenomena found for fcc metal films exists in NiAl, since dislocation processes are altered by the CsCl-type lattice structure. The question arises whether geometrical and microstructural confinements have a similar impact on the plasticity as observed for fcc metal thin films. In other words: does the room temperature yield strength of NiAl thin films increase with decreasing film thickness and grain size? Investigations on bulk NiAl revealed that the yield strength of NiAl (48 at-% Al) under compression increases from 500 to 800 MPa with decreasing grain size from 500 to 10 µm [42]. However, it is unknown whether this trend is still present if the grain size is further decreased into the sub-micrometer range.

For thin polycrystalline NiAl films with thicknesses and grain sizes below a few micrometers, the brittle-to-ductile transition (BDT) may deviate from bulk NiAl. Indications for a size effect on the BDT were found by Schulson and Barker [43], who studied the ductility of bulk NiAl at 400 °C as a function of grain size. They measured a significant increase in ductility once the grain size was smaller than 20 µm.

A microstructural size effect of bulk NiAl at temperatures above 1000 °C was discovered by Arzt and Grahle [44]: While the stress dependence on strain rate for coarse

grained NiAl followed a power-law relation, it was linear for fine grained NiAl with a grain size of 20 μm for low creep rates. This indicates that the creep behavior of coarse grained NiAl is dominated by dislocation motion while diffusional creep plays a decisive role in fined grained NiAl. One may assume that diffusion controlled plasticity becomes even more pronounced for NiAl films with thicknesses and grain sizes in the range of a micrometer. However, this has not yet been experimentally proven.

Results reported in the literature on bulk NiAl indicate that size effects may play an important role in NiAl thin film plasticity. A major goal of the second part of this study is to elucidate the influence of film thickness, grain size, and chemical composition on the plasticity in NiAl thin films in the temperature range between room temperature and 700 °C.

3 Channel cracking of NiAl thin films on Si substrates

Abstract

Thin intermetallic films, which serve e.g. as protective coatings against oxidation, are prone to cracking due to thermal strains. In the present chapter, we report on the cracking behavior of thin polycrystalline NiAl films on Si substrates as a model system. The stress-temperature evolution and the cracking behavior of thermally-strained NiAl films was studied as a function of Al content (45 to 52 at-% Al) and film thickness (0.4 to 3.0 μm). Ni-rich NiAl films were found to sustain higher tensile stresses than Al-rich films. Al-rich NiAl films failed by the formation of intergranular cracks, which extended even into the Si substrates. The fracture toughness K_c of the Al-rich films was determined from the fracture stress, substrate crack depth and film thickness, revealing K_c values of 2.2 - 2.9 MPa $m^{1/2}$ independent of film thickness. Thus, the fracture toughness is smaller than for polycrystalline bulk NiAl of stoichiometric composition. It is speculated that this is caused by the high Al content of the Al-rich NiAl films. The fracture stress was found to increase with decreasing film thickness indicating that the film thickness corresponds to a critical crack length.

3.1 Introduction

Mechanical properties of thin films differ from their bulk counterparts due to geometrical constraints [29]. It is well established that flow stresses of metal thin films increase with decreasing film thickness [2, 31, 45-47] with flow stresses significantly exceeding those of the corresponding bulk material. However, it is unclear whether similar size effects are present in the cracking behavior of brittle thin films constrained by a substrate. Whereas theoretical models were developed [21-24, 27, 48], a conclusive experimental picture has not yet been obtained.

NiAl-based alloys are typical coating materials for the protection of turbine blades against high temperature oxidation and corrosion [1]. A major concern for such coatings in service is the low fracture toughness at temperatures below the brittle-to-ductile transition temperature, which is in the range of 400 to 600 °C [49, 50]. Although the fracture toughness of single-crystalline [10, 11, 51-56] and polycrystalline NiAl [9, 13, 14, 57, 58] is well studied, NiAl thin films with thicknesses below 10 μm have not been analyzed so far. The technological NiAl coatings that are investigated usually contain several alloying elements such as Cr, Pt, Ti, W and Ta [50, 59], which can alter the cracking behavior of NiAl. Furthermore, technological NiAl coatings predominantly exhibit an inhomogeneous Ni and Al concentration across the film thickness [60]. As a result, the dependence of the fracture behavior of NiAl coatings on the Al content and the coating thickness remains unclear.

This chapter aims to elucidate the cracking behavior of thin high-purity NiAl films with homogeneous Ni and Al contents. Especially the influence of the Al content and the film thickness on their cracking behavior was studied. Analogous to the technical application of NiAl-based high-temperature coatings, film stresses were induced by thermal straining and studied as a function of temperature. Based on the measurement of changes in stress due to film cracking, the fracture toughness of the films were determined similar to the suggestion by Vlassak [24]. In order to achieve thermal strains up to 0.88 % in NiAl, Si substrates were used because of the large difference in thermal expansion between NiAl and Si. The fracture stress and the fracture toughness of the NiAl films were correlated with the Al content, the film thickness and microstructure.

3.2 Experimental

3.2.1 Deposition of NiAl films

NiAl films with Al contents in the range of 45.0 - 52.4 at-% and film thicknesses between 0.4 - 3.0 µm were deposited[1] on 290 µm thick Si wafers with a diameter of 5.1 cm. The substrates were covered with 50 nm thick bilayers of amorphous SiO_2 followed by amorphous Si_3N_4 to prevent interdiffusion of Si and NiAl. Prior to the NiAl deposition, all substrates were heated in a pre-vacuum chamber at 120 °C for 2 h. Subsequently, the substrates were cleaned in the deposition chamber by Ar^+ ion bombardment using a 200 Volt Kauffmann ion source.

The actual deposition of the NiAl films was carried out by power regulated DC magnetron co-sputtering using two elemental targets of Ni (99.999 % purity) and Al (99.98 % purity). The base pressure of the deposition chamber was below 5×10^{-8} Pa. Ar served as sputter gas. Al contents of the NiAl films were varied by adjusting the sputter power of the Al target between 138 and 194 W and of the Ni target between 135 and 150 W. The NiAl deposition was conducted without additional heating at an Ar flow of 30 cm^3 per minute resulting in an Ar pressure of 1×10^{-1} Pa. The NiAl film thickness ranged between 0.4 and 3.0 µm with sputter times of 10 and 75 min, respectively. In order to obtain a homogeneous film thickness, the substrates were rotated during deposition at 100 revs/min.

Two sets of samples were investigated which differ only by their thermal treatment after deposition: The first set of NiAl films (*set I*) was used to study the influence of the chemical composition on the fracture toughness. They had Al contents between 45.0 and 51.5 at-% with nearly equal film thicknesses of 1.1 ± 0.2 µm. These films were annealed at 600 °C in UHV ($1 \cdot 10^{-6}$ Pa) for 1 h directly after deposition without breaking the vacuum. The second set of films (*set II*) was annealed *ex situ* in a protective N_2 atmosphere and then the stress evolution during thermal cycling was measured. Observed stress drops during cooling were indicative of film cracking. The films of *set II* were Al-rich with Al contents from 50.4 to 52.4 at-%. In order to study the effect of film thickness on fracture behavior, the film thickness of these samples was varied between 0.4 and 3.0 µm. Table 3-1 summarizes the chemical composition, film thickness, grain size and annealing conditions of all NiAl films investigated in this chapter.

[1] I thank Gerhard Adam for the support in sample preparation.

Table 3-1 **Overview of the samples investigated. The grain sizes are lognormally distributed. The error of the Al content, film thickness and the median grain size (standard deviation) are given in brackets. The median grain size increased with film thickness. However, a precise determination of median grain sizes smaller than 0.1 µm was not achieved experimentally.**

sample set	number of samples	Al content [at-%]	600 °C annealing	film thickness [µm]	median grain size [µm]
I	20	45.0 (± 0.5) to 51.5 (± 0.5)	*in situ* 1 h / UHV	1.1 (± 0.2)	0.5 to 0.9 (± 0.4)
II	2	50.4 (± 0.5)	*ex situ* 2 h / N_2	1.0 (± 0.1)	0.36 (± 0.13)
II	6	52.2 (± 0.5)	*ex situ* 1 h / N_2	0.6 to 3.0 (± 0.1)	< 0.1*
II	4	52.4 (± 0.5)	*ex situ* 2 h / N_2	0.4 to 1.0 (± 0.1)	0.1* to 0.3 (± 0.15)

* grain size estimate based on focused ion beam observations

3.2.2 Microstructural characterization

The chemical composition of the NiAl films was determined using wavelength-dispersive X-ray (WDX)[2] and optical emission spectroscopy (OES)[3]. Both methods yielded identical results with a maximum error in Al and Ni content of ± 0.5 at-%. However, the deviation of four individual measurements performed on one sample was less than 0.15 at-%. Phase and texture analysis were carried out by X-ray diffraction (XRD) measurements in Bragg-Brentano geometry (Siemens M18XHF-V operated at 40 kV) with a step size of $2\theta = 0.02°$ and measurement times of 1 s using Cu Kα radiation. In order to determine the texture of the NiAl films, the relative diffraction intensities of the individual texture components were compared to results of NiAl powder measurements [61].

The microstructural characterization was carried out by optical microscopy (Olympus BH2-UMA), scanning electron microscopy[4] (SEM - JEOL 6300F operated at 3 kV) and focused ion beam (FIB) microscopy (FEI 200xP operated at 30 kV). These

[2] I gratefully acknowledge the help of Siglinde Haug for the WDX measurements.
[3] I thank Albrecht Meyer for performing the OES measurements.
[4] I am grateful to Sabine Kuehnemann for her support with the SEM investigations.

techniques were also applied to investigate crack formation in the films after thermal cycling. In addition, the onset of cracking was investigated *in situ* in an SEM during thermal cycling of NiAl films with an Al content of 52.4 at-% and a thickness of 1.0 µm.

The film thickness was determined by FIB microscopy by milling cross-sections in the NiAl films and measuring the projected film thickness taking into account the imaging angle of 45°. The grain size distribution was determined by marking the grain boundaries of about 300 grains on FIB micrographs recorded at 0° tilt. In order to distinguish individual grains showing identical channeling contrast at 0° tilt, micrographs recorded at tilt angles of 10° and 20° were used for comparison. The size of the grains was quantitatively analyzed by measuring the area of the marked grains using a computer-based image processing system (Quantimet Q500/W, Leica). The grain size was defined as the diameter of a circle with equivalent area.

3.2.3 Stress measurements

The substrate curvature technique was applied to measure the residual stresses in the NiAl films. This technique takes advantage of the fact that residual film stresses result in bending of the film-substrate composite. Since the film thickness h_f is negligible compared to the substrate thickness h_s the stress σ_f in the film can be calculated according to [62]:

$$\sigma_f = \frac{M_s \, h_s^2}{6 \, h_f} C, \qquad (3\text{-}1)$$

based on the measurement of the curvature C of the sample, and the use of the biaxial elastic modulus M_s of the substrate. To obtain absolute stress values, the curvature of the bare substrates was measured prior to NiAl deposition and then subtracted from the curvature of the NiAl-coated sample. A detailed description of this technique is given by Flinn [63] and Keller et al. [46]. The average biaxial film stress can be determined with an accuracy of ± 5 % by the substrate curvature technique, with uncertainties in the film thickness determination and drift of the sample during thermal cycling as the major error sources.

The stresses in the films of sample *set I* were measured at room temperature after deposition and UHV annealing as a function of the Al content. The as-grown films of

sample *set II* were thermally cycled in a protective N_2 atmosphere. During thermal cycling stresses evolve in the film due to differences in the thermal expansion coefficient of the NiAl film and the Si substrate. The film stresses were measured during thermal cycling in 10 K intervals using the substrate curvature technique. The samples were heated at 6 K/min to 600 °C, then the temperature was held constant at 600 °C for 1 or 2 h in order to achieve grain growth. The longer annealing time of 2 h was intended to yield larger grain sizes than in the films annealed for 1 h. Before cooling, some samples were additionally heated to a maximum temperature of 650, 700 or 730 °C. An increase in maximum temperature increases the applied thermal strain. Subsequent cooling was performed at a constant cooling rate of 6 K/min down to 100 °C, and at less than 4 K/min below 100 °C. A heating / cooling rate of 6 K/min corresponds to a strain rate of $1.3 \times 10^{-6}\ s^{-1}$, assuming thermal expansion coefficients of $2.5 \times 10^{-6}\ K^{-1}$ for Si [64] and $15 \times 10^{-6}\ K^{-1}$ for NiAl [65]. Cooling from 730 °C to room temperature results in a thermal strain of $\varepsilon_{th} = 0.88$ % for NiAl films. Additionally, a few NiAl films were subjected to a second temperature cycle with a maximum temperature of 600 or 700 °C.

3.3 Results

3.3.1 Microstructure of NiAl films

The XRD measurements revealed that all films consisted solely of ordered β-NiAl with the CsCl-structure. The texture of the films depended on the chemical composition, as reported earlier [66], and varied from a {110} fiber texture for Ni-rich films to a {111} fiber texture for stoichiometric films to a mixed {111} and {211} texture for Al-rich NiAl films.

All films had equiaxed grains with a mean grain size smaller than the film thickness after annealing at 600 °C (see table 3-1 and figure 3-1). An increase in annealing time at 600 °C from 1 to 2 h increased the grain size of the NiAl films by a factor of about 3. A 1.0 µm film annealed for 2 h had a median grain size > 0.3 µm, while a film of similar Al content and film thickness, annealed for 1 h, had a median grain size < 0.1 µm. The grain size had a lognormal distribution independent of the Ni and Al content.

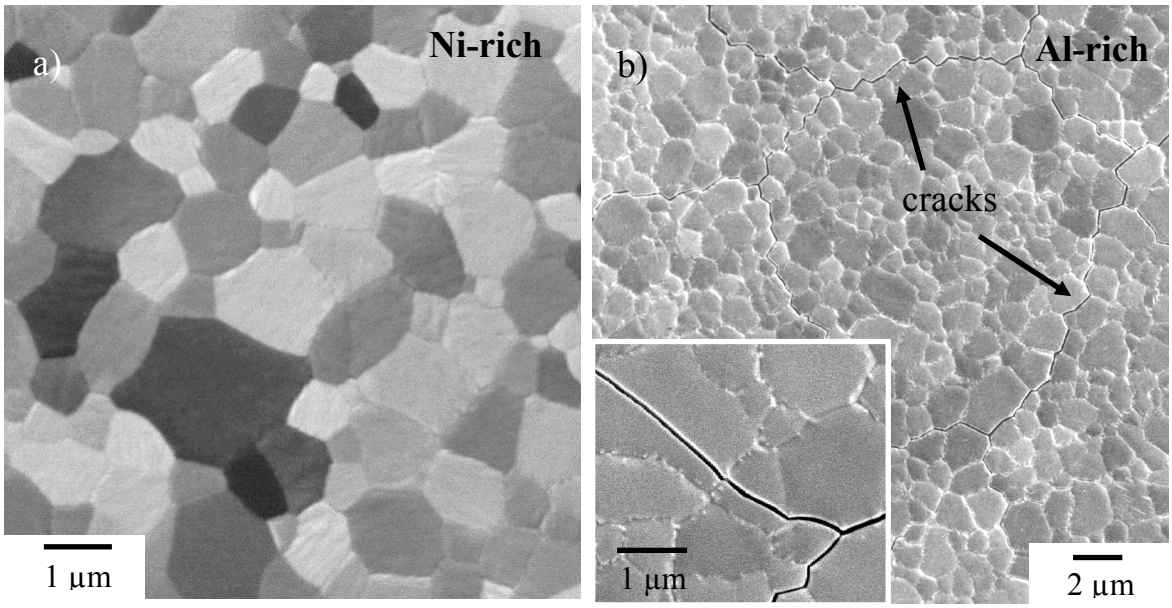

Figure 3-1 **Microstructure of (a) Ni-rich (46 at-% Al) and (b) Al-rich (51 at-% Al) NiAl films with film thicknesses of 1.3 and 1.1 µm, respectively, after annealing at 600 °C in vacuum. While the (a) Ni-rich film is devoid of cracks (FIB micrograph), the (b) Al-rich film exhibits a dense network of cracks (SEM micrograph). The cracks propagate predominantly in an intergranular manner, only a few transgranular cracks are present as shown in the inset of figure 3-1 b.**

After annealing at 600 °C, Ni-rich films remained devoid of cracks, whereas films with an Al content of more than 50 at-% developed a network of microcracks (figures 3-1, 3-2). Figure 3-1 b indicates that cracks propagated predominantly in an intergranular manner, only very few transgranular cracks were observed. On a larger scale, the crack patterns were often rectangular in shape with dimensions of up to 1 mm (figure 3-2). The orientation of these cracks was preferentially along <110> directions of the Si substrate. Frequently, the rectangular crack patterns were filled with a dense network of arbitrarily oriented cracks, while in some cases areas of up to 0.5 mm^2 were crack-free.

The microstructure of as-deposited Al-rich films of sample *set II* was extremely fine-grained with grain sizes below 50 nm. However, the subsequent annealing treatment at 600 °C in a protective N_2 atmosphere caused grain growth and, after cooling to room temperature, cracks spanning the entire sample were observed. The grain sizes of the *ex situ* annealed films were found to be smaller than in the UHV-annealed films (see table 3-1). With increasing film thickness, an increase in median grain size was observed for all films.

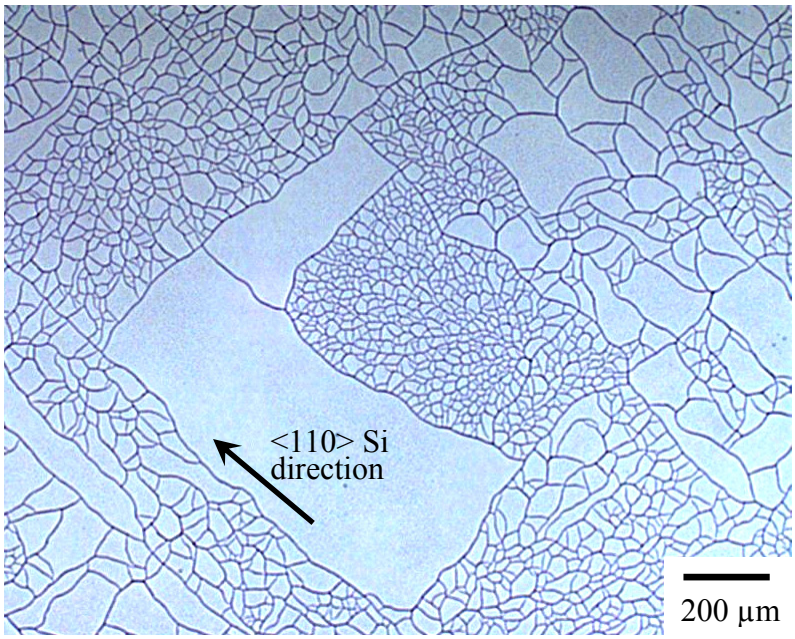

Figure 3-2 **Optical micrograph showing the crack pattern (dark lines) after thermal cycling of a 1.0 µm thick NiAl film with an Al content of 52.2 at-%. Rectangular areas bordered by well oriented cracks are visible. These cracks run parallel to <110> Si directions of the substrate. Additionally, arbitrarily oriented cracks form dense crack networks inside the rectangular areas. Some large rectangular areas remained devoid of cracks.**

3.3.2 Room temperature stress values of annealed NiAl films

In figure 3-3 the room temperature stress of UHV-annealed NiAl films with thicknesses of 1.1 ± 0.2 µm (sample *set I*) are shown as a function of Al content. Films with Al contents ranging from 45.0 to 50.2 at-% exhibited high biaxial tensile stresses of about 1100 MPa. A significant decrease in tensile film stress was observed when the Al content increased from 50.2 to 51.5 at-%. The stress values dropped from 1100 MPa to less than 600 MPa due to the formation of cracks spanning the entire films (see figures 3-1 b, 3-2). In contrast, NiAl films with an Al content $\leq$ 50.2 at-% were devoid of cracks.

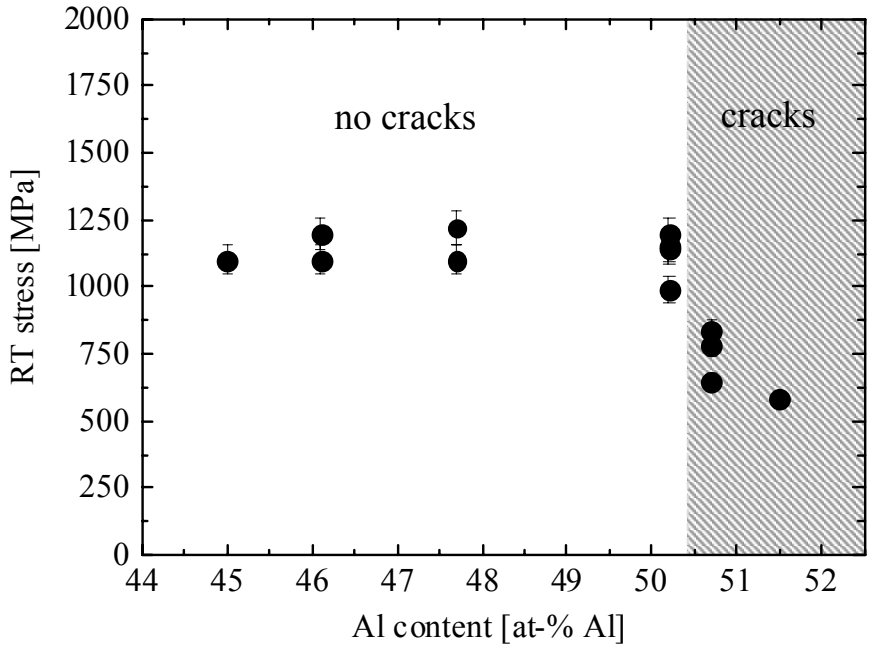

Figure 3-3 **Biaxial film stress as a function of Al content of NiAl films, measured at room temperature (RT) after annealing at 600 °C in UHV. The thickness of the films is 1.1 ± 0.2 µm. While the stresses in the Ni-rich films are independent of composition, a significant decrease in stress is observed for Al-rich films due to the formation of cracks (compare figure 3-1 a, b).**

3.3.3 Thermal stress evolution in brittle NiAl films

The stress evolution of as-deposited NiAl films with an Al content ≥ 50.4 at-% (sample *set II*) was measured during thermal cycling in order to gain information on the onset of cracking and to determine the fracture stress. Figure 3-4 shows the stresses as a function of temperature in a 1.0 µm thick as-deposited film with an Al content of 52.4 at-%. The as-grown film initially exhibited a compressive stress at room temperature, which increased from 600 to 1300 MPa as the temperature was raised to 350 °C. Upon further heating the compressive film stress relaxed and at 600 °C the film was almost stress-free. This strong stress relaxation was correlated with the observed grain growth, which typically occurred during heating of as-deposited metallic films. Annealing the film at 600 °C for 2 h did not noticeably change the stress. Upon subsequent cooling, the film stress became tensile and increased with decreasing temperature. However, at temperatures below 140 °C a significant stress drop occurred and the tensile stress values decreased upon further cooling to room temperature.

In order to find out whether the stress drop upon cooling was caused by the formation of cracks, an equivalent as-deposited film with the same thickness and Al content was cycled between room temperature and 600 °C *in situ* in an SEM. During cooling, cracks were observed to form at a temperature below 140 °C (see figure 3-4). Based on these observations, the maximum stress during cooling prior to the occurrence of a stress drop is defined as the fracture stress (as indicated in figure 3-4).

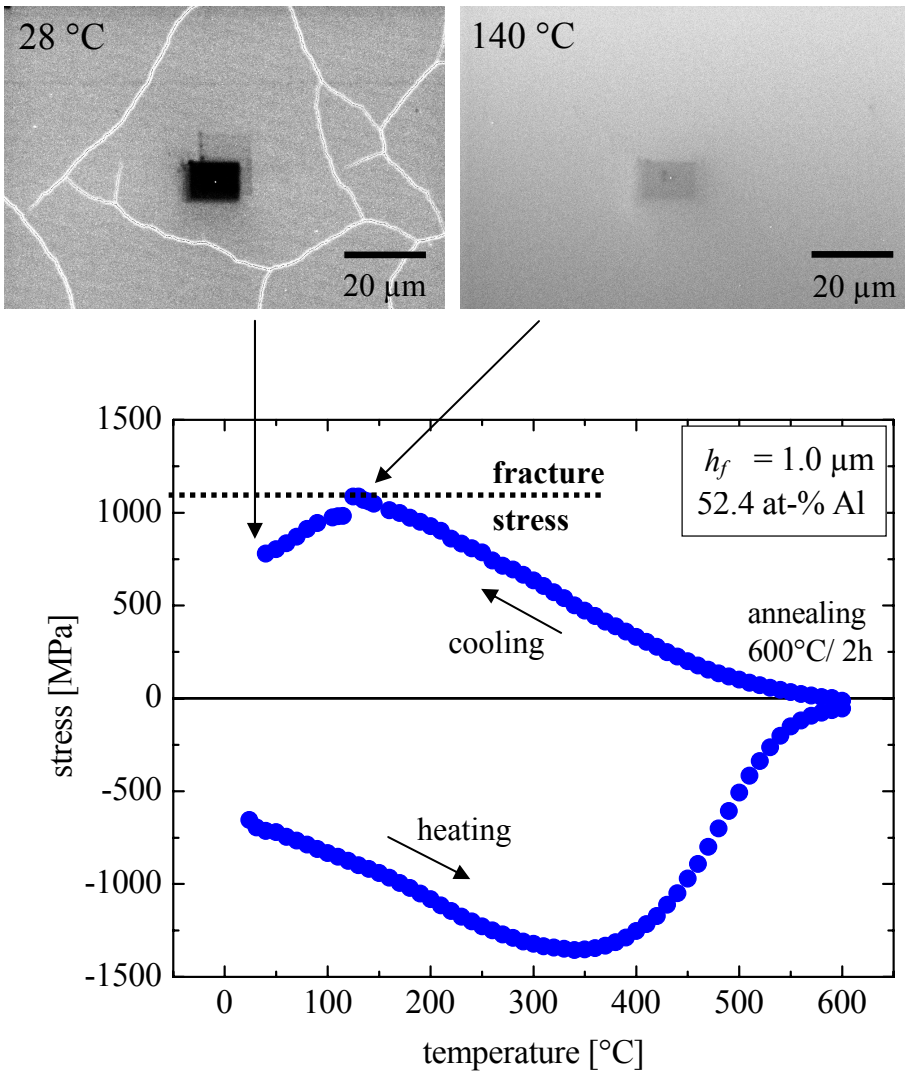

Figure 3-4 **Stress temperature cycle of an as-deposited NiAl film with an Al content of 52.4 at-% and a film thickness of h_f = 1.0 µm. The stress drop at a temperature of 120 °C during cooling can be associated with crack formation in the film as confirmed by *in situ* SEM: The film surface does not show any cracks at 140 °C while a typical crack pattern is observed at 28 °C. The *in situ* SEM images show the identical sample site, which was marked by the dark rectangular area in the center of the micrograph stemming from carbon contamination.**

Following this approach, the fracture stresses of Al-rich NiAl films were determined as a function of Al content and film thickness. The fracture stress of films with a thickness of 1.0 ± 0.1 µm was found to decrease slightly from 1160 to 1090 MPa with increasing the Al content from 50.4 to 52.4 at-% Al (figure 3-5). This corresponds to an increase in temperature at which fracture occurs from 90 to 125 °C. As a result, both the fracture stress and the room temperature stress decreased with increasing Al content for constant film thickness. This result is in agreement with the room temperature stress values of UHV-annealed NiAl films reported in figure 3-3 where a decrease in stress with increasing Al content was observed for Al-rich films.

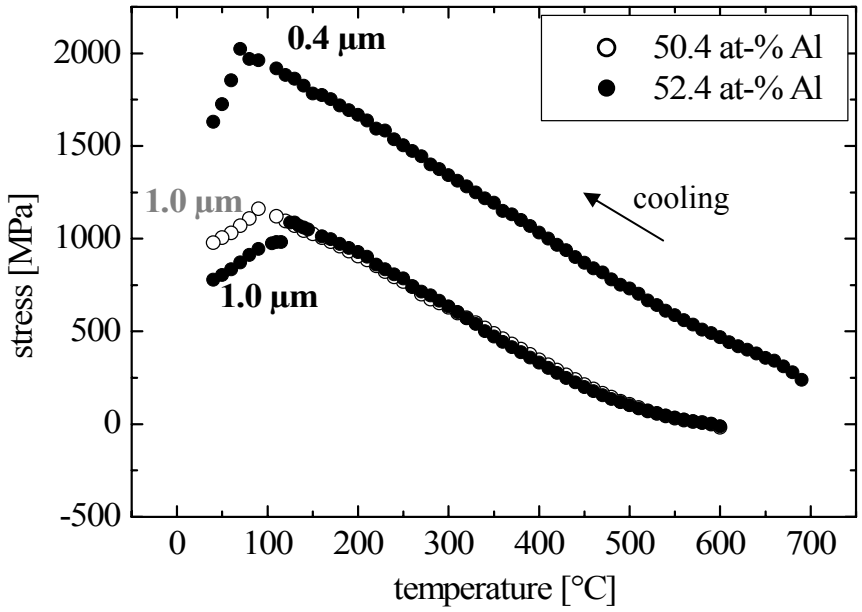

Figure 3-5 Stress evolution on cooling from 600 or 700 °C to room temperature for Al-rich NiAl films. For all films, stress drops occur between 125 and 70 °C indicating film fracture.

In comparison to the chemical composition, the film thickness was found to have a strong influence on the fracture stress of Al-rich NiAl films: A decrease in film thickness from 1.0 to 0.4 µm increased the fracture stress by a factor of about 2 from 1090 to 2020 MPa for films with an Al content of 52.4 at-% (figure 3-5). This dependence was confirmed for NiAl films with smaller grains and almost identical Al content of 52.2 at-% where the film thickness was varied between 0.6 and 3.0 µm (figure 3-6). As shown in figure 3-6, the fracture stress increased with decreasing film thickness, with a value of 600 MPa for a 3.0 µm thick film and more than 1500 MPa for a 0.6 µm thick film. In contrast, the fracture stress remained largely unaffected by the grain size. NiAl films with a thickness of 1.0 µm and an almost identical Al content of 52.2 and 52.4 at-% exhibited the same fracture stress of about 1100 MPa, even though the films differed in grain size by a factor of three due to the different annealing times.

As a result of the crack formation in Al-rich films during the first temperature cycle, the mechanical response of these films to subsequent thermal straining was changed. The second temperature cycle of an NiAl film with a network of cracks revealed a substantially smaller stress-temperature "hysteresis" than the first thermal cycle indicating a loss of film stiffness due to the formation of cracks (see figure 3-7). A maximum in tensile stress was no longer observed in the second cycle.

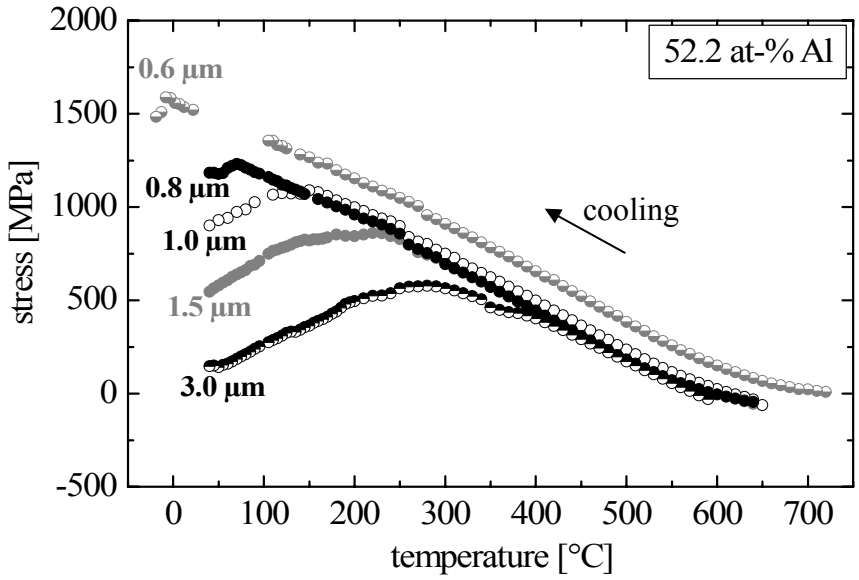

Figure 3-6 Stress evolution during cooling from 600, 650 or 730 °C to room temperature for NiAl films with an Al content of 52.2 at-% and film thicknesses between 0.6 and 3.0 µm. The 0.6 µm thick film was cooled to -25 °C in order to achieve the formation of cracks. Note that a decrease in film thickness increases the fracture stress defined as the maximum stress prior to the occurrence of a stress drop.

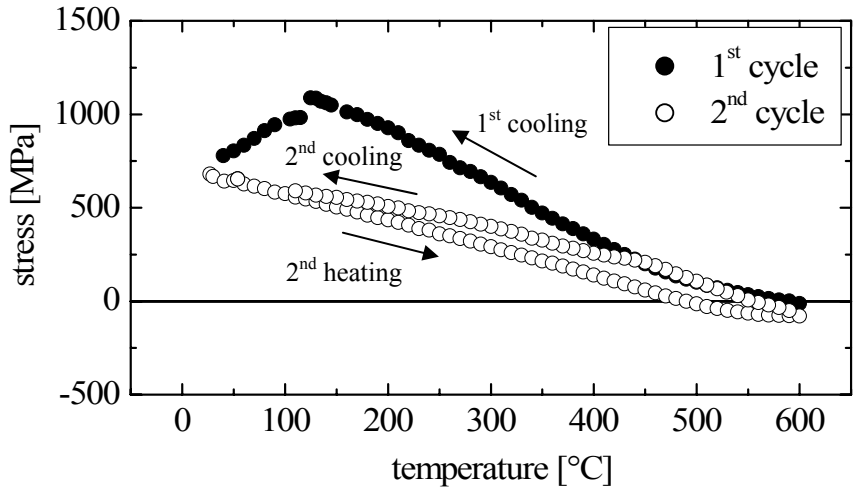

Figure 3-7 **First and second stress temperature cycle of a 1.0 µm thick NiAl film with an Al content of 52.4 at-%. The first cycle (closed symbols) was carried out in the as-deposited state and shows a stress drop on cooling at 125 °C. The second cycle (open symbols) exhibits lower stress values and a much smaller slope during cooling compared to the first cycle, but no stress maximum.**

Cross-sectional FIB studies revealed that cracks extended over the entire film thickness and penetrated into the Si substrate (see figure 3-8). In most cases, the substrate cracks followed a different propagation path compared to the film; in the film the crack was normal to the film plane while in the substrate the crack deviated from this direction. In single crystal Si the {111} planes crack preferentially [67], which may explain this deviation for the (100) oriented Si substrates. Furthermore, fracture along Si {111} planes agreed with the observed preferential crack paths in the NiAl films along $<01\bar{1}>$ Si directions (see figure 3-2), since the Si {111} fracture planes and the Si (100) surface plane contain the $<01\bar{1}>$ direction. The orientation of channeling cracks seems to be influenced on a large scale by the orientation of the substrate. Debonding of the films at the film / substrate interface was never observed indicating a strong adhesion between the NiAl films and the amorphous Si_3N_4-coated Si substrates.

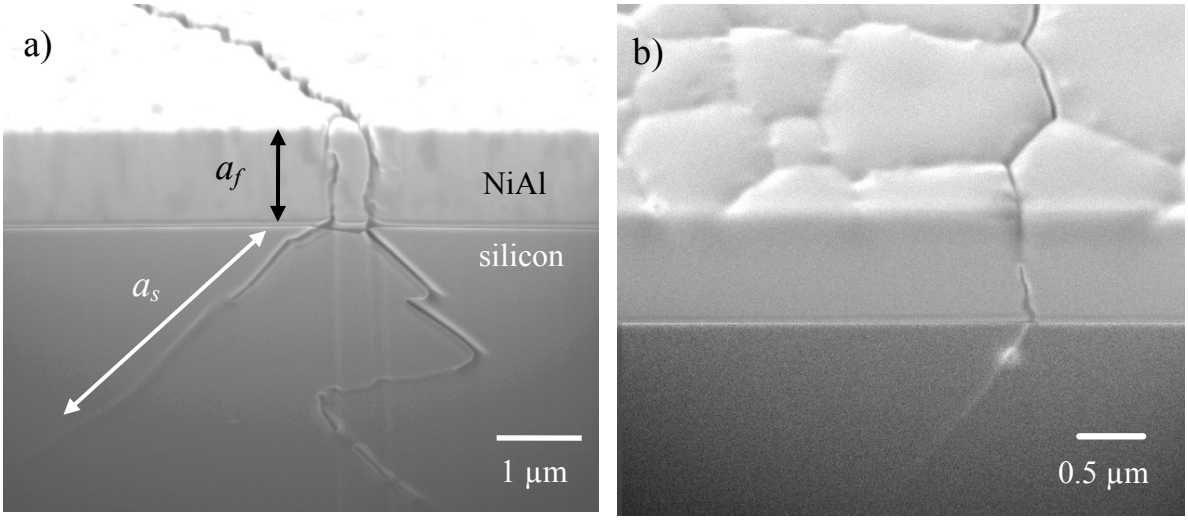

Figure 3-8 **FIB micrographs of cross-sections in an NiAl film with (a) an Al content of 52.2 at-% and a thickness of 1.5 µm after thermal cycling in N_2 atmosphere, and (b) an NiAl film with an Al content of 51.5 at-% and a thickness of 1.0 µm after UHV annealing. In both samples cracks propagated in the film along grain boundaries and extended from the surface to the film / substrate interface. Furthermore, the cracks penetrated into the Si substrate. The crack lengths a_f and a_s are marked in (a). For better visualization, the contrast of the substrate area was enhanced by commercial image processing software.**

3.4 Fracture toughness determination

The aim of this section is to determine the fracture toughness of the Al-rich NiAl films based on the experimental results reported in section 3.3. For this purpose, a model developed by Beuth [21] and Ye et al. [27] is adopted to account for the observed crack geometry in our NiAl films.

3.4.1 Channel cracking in thin films on substrates

The propagation of cracks in a thin film on a substrate differs significantly from bulk behavior because the constraining effect of the substrate limits the elastic energy released by the crack propagation as summarized by Hutchinson and Suo [20]. Computational results by Nakamura and Kamath [68] revealed that steady-state condition, i.e. constant energy release rate, for channel cracking is reached once the crack length parallel to the surface exceeds a few times the film thickness. Based on this result, the energy release rate for channel cracking can be obtained from a two-dimensional plane strain analysis by

comparing the elastic energy far behind and far ahead of the crack front. The thickness h_f of the film is considered as a critical crack length a_f as shown in figure 3-8. The energy release rate G, defined as the reduction of the elastic energy associated with the crack advancing by unit area, is given by:

$$G = Z\frac{\sigma_{fr}^2 h_f}{E_f^*}, \tag{3-2}$$

where σ_{fr} is the fracture stress and E_f^* represents the plane strain elastic modulus of the film given by:

$$E_f^* = \frac{E_f}{1-\nu_f^2}, \tag{3-3}$$

where E_f and ν_f are the Young's Modulus and the Poisson's ratio of the film. The dimensionless parameter Z in equation (3-2) depends on the elastic mismatch between film and substrate, and on the crack geometry. Crack propagation will occur if the critical energy release rate G_c for crack propagation equals the fracture energy Γ per unit area:

$$G_c = \Gamma \ . \tag{3-4}$$

To evaluate the fracture toughness of the cracked NiAl films, the accurate determination of Z in equation (3-2) is essential. For this, channeling cracks (figure 3-1 b) and substrate cracks of length a_s (figure 3-8) have to be taken into account. This is supported by the observation that the crack patterns follow the orientation of the Si substrate (see figure 3-2). The determination of the Z values for the Al-rich NiAl films of this work is the subject of the appendix in section 3.7.

3.4.2 Fracture toughness of the NiAl films

For all Al-rich films, values of $Z = 6.0 \pm 1.4$ were calculated (see appendix section 3.7). The large error of Z is due to experimental uncertainties in the determination of substrate crack lengths (see section 3.7 and table 3-2). If the parameter Z is known, the total energy release rate G_c in equation (3-2) can be calculated from the film thickness, fracture stress and plane-strain elastic modulus of the film (table 3-2). Due to the substrate cracking, the total energy release rate is a function of both the fracture energy of the film Γ_f and of the substrate Γ_s and is given by:

$$G_c = \Gamma_f + \frac{a_s}{h_f}\Gamma_s \ , \qquad (3\text{-}5)$$

The fracture energy of the Si substrate was taken as $\Gamma_s = 2.4$ J/m^2 for fracture along {111} Si planes [69]. Solving equation (3-5) for Γ_f and inserting the ratio of substrate crack length to film thickness and the total energy release rate as determined according to equation (3-2) yields the fracture energy of the NiAl films. Finally, the critical stress intensity factor K_c of the films can be calculated using the well-established Griffith equation:

$$K_c = \left(E_f^* \Gamma_f\right)^{0.5} \ . \qquad (3\text{-}6)$$

Following this approach, the fracture toughness of brittle NiAl films was determined as $K_c = 2.2$ to 2.9 MPa m$^{1/2}$. The corresponding fracture stress, fracture energy and fracture toughness are summarized in table 3-2 as a function of film thicknesses and Al contents. Experimental errors were considered in the calculations, resulting in an absolute error for the fracture toughness of less than 15 % (see table 3-2). As a result, large uncertainties in the measured substrate crack lengths did not strongly affect the calculated fracture toughness values.

Table 3-2 **Evaluation of the fracture toughness of Al-rich NiAl films as a function of Al content and film thickness h_f. The error of the fracture toughness K_c arises from the uncertainty of the substrate crack length a_s and the error of the measured fracture stress σ_{fr}. See text for further details.**

Al content [at-%]	h_f [µm]	σ_{fr} [MPa]	a_s / h_f	Z	G [J/m^2]	Γ_f [J/m^2]	K_c [MPa m$^{1/2}$]
50.4	1.0	1160 ± 60	2.5 ± 1.5	6.0 ± 1.4	35 ± 11	29 ± 7	2.6 ± 0.3
52.2	0.6	1590 ± 90	2.5 ± 1.5	6.0 ± 1.4	39 ± 13	33 ± 8	2.8 ± 0.4
52.2	0.8	1230 ± 60	2.5 ± 1.5	6.0 ± 1.4	31 ± 10	25 ± 6	2.4 ± 0.3
52.2	1.0	1075 ± 55	2.5 ± 1.5	6.0 ± 1.4	30 ± 10	24 ± 5	2.4 ± 0.3
52.2	1.5	860 ± 45	2.5 ± 1.5	6.0 ± 1.4	29 ± 9	23 ± 5	2.3 ± 0.3
52.2	3.0	580 ± 30	2.5 ± 1.5	6.0 ± 1.4	26 ± 8	20 ± 4	2.2 ± 0.2
52.4	0.4	2020 ± 100	2.5 ± 1.5	6.0 ± 1.4	42 ± 13	36 ± 9	2.9 ± 0.4
52.4	1.0	1090 ± 55	2.5 ± 1.5	6.0 ± 1.4	31 ± 10	25 ± 6	2.4 ± 0.3

Although the fracture stress increases significantly with decreasing film thickness, the fracture toughness K_c remains independent of the film thickness (see table 3-2). It may be speculated from the present results that fracture toughness increases slightly with decreasing film thickness. However, this tendency is within the accuracy of the measured K_c values. Furthermore, the fracture toughness of the brittle, Al-rich NiAl films remains independent of the Al content: variations between 50.4 and 52.4 at-% Al in 1.0 ± 0.1 µm thick films resulted in K_c values between 2.4 and 2.6 MPa m$^{1/2}$. For the Ni-rich NiAl films no fracture occurred during thermal cycling.

3.5 Discussion

Our results indicate that NiAl thin films respond to thermal stresses in different ways depending on the chemical composition. In addition, the film thickness affects the cracking behavior in films with excess Al. Both findings will now be discussed.

3.5.1 Influence of chemical composition on fracture

The stoichiometric and Ni-rich NiAl films (with Al contents of 45.0 to 50.2 at-%) deformed plastically and did not fracture in our experiments, whereas the Al-rich films (with Al contents of 50.4 to 52.4 at-%) exhibited pronounced cracking. Brittle fracture in general occurs if the flow stress required for plastic yielding exceeds the fracture stress. In previous studies on bulk NiAl the yield strength was found to increase with deviations from stoichiometry to the Ni-rich and to the Al-rich side [6, 42, 70, 71]. However, the increase in yield strength on the Al-rich side was more pronounced than on the Ni-rich side [6, 71]. An excess of 3 at-% Al is reported to enhance the yield strength of stoichiometric NiAl at room temperature by a factor of about 8 [6]. A deviation from stoichiometry to the Al-rich side is accompanied by constitutional vacancies on Ni sites while in Ni-rich NiAl the Al atoms are replaced by Ni atoms [5]. The constitutional vacancies in Al-rich NiAl are stronger obstacles to the dislocation motion than Ni anti-site atoms [72], which promotes the susceptibility to brittle fracture.

The Al-rich NiAl films exhibited predominantly intergranular fracture indicating that grain boundaries in these films are more vulnerable to cracking than cleavage planes. A simple criterion for the transition between cleavage and boundary fracture is given by Cottrell [73]:

$$R = \frac{\gamma_{coh}}{2\gamma_{sc}} \ , \qquad (3\text{-}7)$$

where γ_{coh} is the cohesive energy of the grain boundary and γ_{sc} is the energy of the surface exposed by cleavage. For $R < 1$ boundary fracture is favored while for $R > 1$ cleavage is expected. It is reasonable to take γ_{sc} as the minimum free surface energy which is 1.71 J/m^2 for the NiAl {110} surface planes [74]. The cohesive energy of the grain

boundary was calculated by Mutasa and Farkas [75] for $\Sigma = 5$ boundaries as a function of chemical composition. They found a decrease with increasing Al content from $\gamma_{coh} = 3.4$ J/m^2 for Ni-rich to 1.6 J/m^2 for Al-rich grain boundaries illustrating the weakness of Al-rich grain boundaries (no absolute Al concentrations are reported in reference [75]).

Applying the values of γ_{sc} and γ_{coh} to equation (3-7) gives $R < 1$ for Al-rich grain boundaries, predicting intergranular fracture. In contrast, for Ni-rich grain boundaries a value of $R = 1$ is obtained where a transition to cleavage is expected. This agrees with experimental results on bulk polycrystalline NiAl, where a transition from intergranular to transgranular fracture was observed by increasing the Ni content [9, 57]. The low fracture toughness of Al-rich grain boundaries was also confirmed by experimental studies on NiAl bicrystals [56].

3.5.2 Influence of film thickness on fracture

The Al-rich NiAl films showed a strong increase in fracture stress with decreasing film thickness (see table 3-2). This finding is in qualitative agreement with the applied model, which assumes that the film thickness corresponds to a critical crack length (see section 3.4). In contrast to bulk materials, where brittle fracture is typically caused by a single defect with a critical size, the fracture stress in a thin film is reached simultaneously at various sites, since the film thickness corresponds to a critical crack length and is constant over the entire film.

In figure 3-9 the fracture stress of NiAl films with Al contents of 52.2 and 52.4 at-% is shown in a double-logarithmic plot as a function of the inverse film thickness. If the fracture toughness and, thus, the energy release rate is independent of the film thickness, a linear dependence according to equation (3-2) with a slope of 0.5 is expected. This assumes that the ratio of film crack length to substrate crack length is constant for all films (which corresponds to a constant parameter Z in equation (3-2)). As shown in figure 3-9, the slope of 0.5 fits well to the reported data of the NiAl films. Only NiAl films with a thickness of 0.6 and 0.4 µm fracture at higher stresses of 1590 and 2020 GPa, respectively, which is 250 MPa (0.6 µm thick film) and 350 MPa (0.4 µm thick film) larger than predicted by equation (3-2). As a consequence, the fracture toughness values determined (see table 3-2) increase slightly with decreasing film thickness.

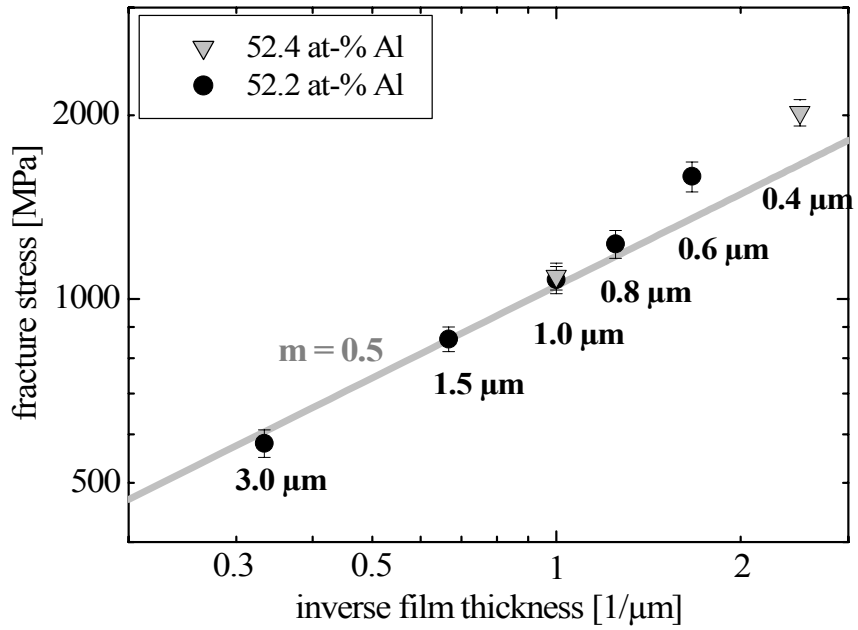

Figure 3-9 **The measured fracture stress values of NiAl films with Al contents of 52.2 and 52.4 at-% are shown as a function of the inverse film thickness (double logarithmic plot). The fracture stress increases with decreasing film thickness. Note that the fracture stress of films with a thickness below 0.8 µm are slightly larger than predicted by the inserted line with a slope of 0.5.**

A possible complication is that thinner films fractured at lower temperatures during thermal straining than thicker films. For example, a 3.0 µm thick NiAl film cracked at 280 °C while a 0.6 µm thick film fractured at temperatures below 0 °C (see figure 3-6). A decrease in temperature may lower the fracture toughness of NiAl even at temperatures below the brittle-to-ductile transition temperature of about 400 °C [9-12]. However, this is in contrast to the experimental results, which show an increase rather than a decrease in fracture toughness for the thinner films.

It is known that freestanding thin metal foils under uniaxial loading with foil thicknesses comparable to the size of a plastic zone in the vicinity of the crack tip reveal a significant increase in "apparent" fracture toughness with decreasing foil thickness. This is usually related to the plane stress state near the two surfaces which result in a larger plastic zone compared to plane strain. In contrast, the opposite behavior is expected if the film thickness becomes smaller than the theoretical size of the plastic zone and the extension of the plastic zone is limited by the substrate [76]. Due to the constraint a plane strain state with a constant energy release rate is maintained [21]. A decrease in film thickness would

then progressively confine the plastic zone, which would result in a lower fracture toughness. Again, this is opposite to the observed experimental trend. This may indicate that the size of the plastic zones in our films was smaller than the smallest film thickness of 0.4 μm.

The relatively large fracture toughness values of 2.8 and 2.9 MPa $m^{1/2}$ for the thinnest NiAl films, 0.4 and 0.6 μm thick, could be caused by overestimating the substrate crack length. Based on our experimental observations, an average value of 2.5 times the film thickness was chosen. A decrease in the evaluated fracture toughness of the 0.4 μm thick film from 2.9 to 2.5 MPa $m^{1/2}$ is obtained if the ratio of substrate crack length to film thickness is decreased from 2.5 to 0.5 (see section 3.4). Such a trend can be seen in the cross sectional SEM and FIB observations. However, due to the lack of contrast a more precise analysis of substrate crack lengths was not possible.

3.5.3 Cracking behavior during cooling

The stress measurements during cooling showed that, once cracking occurred, the film stress continuously decreased with decreasing temperature (see figures 3-4, 3-5 and 3-6). This implies that the film stiffness is continuously lowered by further crack propagation. FIB investigations revealed that regions with both a dense network of cracks and almost crack-free areas with dimensions of up to several hundred microns are present at room temperature (see figures 3-2 and 3-10 a). Since already existing cracks tend to deflect propagating cracks, it is argued that in the crack-free areas the nucleation of cracks is inhibited. This was confirmed by introducing a small cavity by FIB machining in a crack-free region of a 1.5 μm thick thermally-cycled NiAl film. As shown in figure 3-10, cracks nucleated at the cavity and a crack network spans throughout the former crack free region. Therefore, it can be concluded that once fracture occurred in the films the crack density increases during further cooling, since a decrease in temperature increases the driving force for crack nucleation. As a result, the stiffness of the film decreases continuously resulting in a further decrease in film stress with decreasing temperature although the thermal strain still increases.

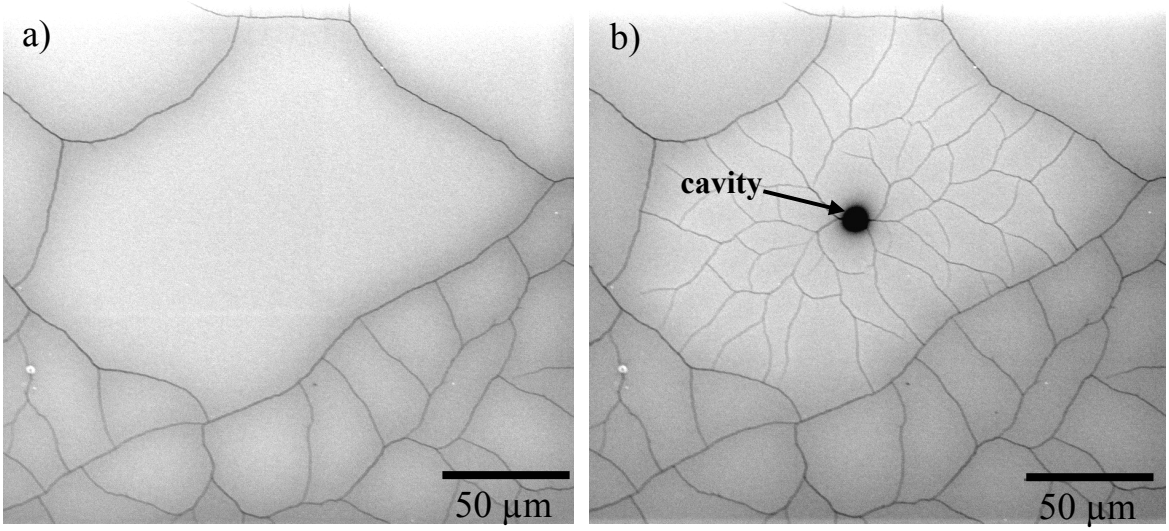

Figure 3-10 FIB micrographs of a 1.5 µm thick NiAl film with an Al content of 52.2 at-% taken at room temperature after a thermal cycle to 650 °C. In (a) crack-free regions and regions with a dense network of cracks are present. (b) Introducing a small cavity in the crack-free region by FIB, crack nucleation occurs introducing a new crack network.

3.5.4 Comparison to bulk fracture toughness

The fracture toughness of the Al-rich NiAl films was determined to be in the range of 2.2 to 2.9 MPa $m^{1/2}$. Although the cracks penetrated into the Si substrate, the evaluated fracture toughness of the NiAl films should remain unaffected by the substrate, as the fracture energy and the crack length of the substrate are considered in the present model (see section 4.3). Crack penetration into the Si substrate is expected since the fracture toughness of Si is low compared to NiAl and the NiAl films are stiffer than the Si substrates.

The Al-rich NiAl films exhibited lower fracture toughness values compared to polycrystalline bulk NiAl where values in the range of 4 to 12 MPa $m^{1/2}$ were found [9, 13, 14]. However, all fracture toughness values reported for polycrystalline bulk NiAl correspond to stoichiometric or Ni-rich NiAl. This is in agreement with the enhanced fracture toughness observed for stoichiometric and Ni-rich NiAl films in this work, in which no fracture occurred although they were subjected to the same thermal straining as the Al-rich films.

Besides the chemical composition, a major difference to bulk NiAl are the very small grain sizes of less than 1 µm. With respect to the intergranular fracture mode, small grains are known to inhibit crack nucleation but promote crack propagation since plastic yielding is confined by the small grains. However, once a crack is nucleated and

propagates along grain boundaries, the crack deflection at triple junctions decelerates the crack velocity. The smaller the grains, the more often cracks are deflected while channeling through the film. Therefore, a decrease in grain size is actually expected to increase the fracture toughness, which was confirmed experimentally for intergranular fracture in stoichiometric bulk NiAl with grain sizes of 9 and 84 μm [9]. However, an increase in grain size from 0.1 to 0.3 μm for 1.0 μm thick NiAl films with almost identical Al contents of 52.2 and 52.4 at-%, respectively, did not affect the fracture toughness of the NiAl films. It can be concluded that the excess of Al rather than the small film thicknesses and grain sizes accounts for the lower fracture toughness of NiAl films in comparison to bulk NiAl.

3.6 Summary and conclusion

The cracking behavior of NiAl films on Si substrates was studied as a function of the Al content (45.0 to 52.4 at-%) and film thickness (0.4 to 3.0 μm). The films were thermally cycled to maximum temperatures of 600 - 730 °C resulting in thermal strains of 0.71 - 0.88 %. The findings can be summarized as follows:

- Stoichiometric and Ni-rich NiAl films (45.0 to 50.2 at-% Al) accommodated thermal strain by plastic deformation and remained free of cracks.
- Al-rich films (50.4 to 52.4 at-% Al) subjected to a thermal strain of 0.71 % showed extensive cracking.
- The channeling cracks observed in Al-rich films propagated predominantly in an intergranular manner and extended into the Si substrate. For a given film thickness the crack density increased with thermal strain.
- The fracture stress of Al-rich NiAl films increased with decreasing film thickness. Good agreement is found with existing models of thin film fracture in which the film thickness corresponds to a critical defect size. In contrast, differences in the grain size in the range of 0.1 to 0.3 μm did not affect the fracture stress.
- The fracture toughness K_c of Al-rich NiAl films was determined to be in the range of 2.2 to 2.9 MPa $m^{1/2}$. Contrary to the fracture stress, the fracture toughness showed no distinct dependence on the film thickness. The fracture toughness values of the Al-rich NiAl films were found to be lower than those of polycrystalline bulk NiAl with stoichiometric composition.

3.7 Appendix

To obtain the critical energy release rate G_c for crack propagation, the parameter Z as given in equation (3-2) has to be determined.

Optical microscopy as well as FIB and SEM observations of the Al-rich NiAl films after thermal cycling revealed channeling cracks with a mean crack distance of 15 - 35 times the film thickness (see figures 3-1 b and 3-2). Relying on the decrease of stress upon cooling after the occurrence of cracking (see figures 3-4, 3-5 and 3-6), it is reasonable to assume that the crack density at the point of first cracking is even lower. Thouless [48] found that the interaction of a propagating crack with existing cracks of a crack pattern is negligibly small if the mean crack distance exceeds about 8 times the film thickness. This is the case for all NiAl films investigated in this chapter and therefore crack interactions were neglected in the following. In order to determine the parameter Z for the brittle NiAl films, channeling cracks (figure 3-1 b) and substrate cracks (figure 3-8) have to be taken into account. As pointed out by Ye et al. [27], it is convenient to define non-dimensional energy release rates ω_f and ω_s for film and substrate, respectively, which are normalized to the fracture stress, film thickness and elastic modulus of the film. The parameter Z in equation (3-2) can than be expressed as [27]:

$$Z = \int_0^1 \omega_f \, d\eta_f + \int_1^{(a_s+h_f)/h_f} \omega_s \, d\eta_s \,, \qquad (3\text{-}8)$$

$$\text{with} \qquad \eta_f = \frac{a_f}{h_f} \qquad \text{and} \qquad \eta_s = \frac{a_s + h_f}{h_f},$$

where a_f is the film crack length and a_s is the substrate crack length as indicated in figure 3-8 a. The substrate crack lengths a_s were determined by cross-sectional FIB microscopy (see figure 3-8). Due to the weak contrast of the Si substrate in the FIB micrographs, the substrate crack length a_s, with values in the range of 1 to 4 times the film thickness, contains a large error. Therefore a mean value for the ratio of substrate crack length to film thickness of 2.5 ± 1.5 was assumed (see table 3-2).

3.7.1 Energy release rate of the film

The non-dimensional energy release rate ω_f for a crack tip in the film was numerically evaluated by Beuth [21] as:

$$\omega_f = g\,\pi\,\eta_f\left(1-\eta_f\right)^{1-2s}\left(1+\lambda_1\eta_f\right)^2. \qquad (3\text{-}9)$$

Where the pre-factor g, the parameter λ_1 and the exponent s depend on the elastic mismatch between film and substrate only and are a function of the two Dundurs' parameters α und β. Beuth showed that for $0 \le \alpha \le 0.5$ the influence of the parameter β is weak [21]. The pre-factor g is a non-dimensional integral of the crack opening displacement and was quantitatively determined by Beuth [21]. The parameter λ_1 was fitted by Ye et al. [27] to achieve agreement to the full numerical solution of the problem. λ_1 is tabulated as a function of α by Ye et al. [27]. Values for the stress singularity exponent s as a function of α are given by Beuth [21]. The Dundurs parameter α characterizes the elastic mismatch of film and substrate:

$$\alpha = \frac{E_f^* - E_s^*}{E_f^* + E_s^*}\ , \qquad (3\text{-}10)$$

where E_s^* = 154 GPa [77] is the plane strain modulus of the (100) oriented Si substrate. The plane-strain modulus E_f^* of the NiAl films was calculated taking the texture of the films into account by applying the elastic constants of NiAl [78]. In the mixed {111} and {211} texture of Al-rich NiAl films, {111} oriented grains are elastically isotropic, but {211} grains are anisotropic. The plane strain modulus of the {211} texture component was calculated by averaging the plane strain modulus along $<0\bar{1}1>$ and $<1\bar{1}\bar{1}>$ directions. It turned out that the plane strain moduli of {111} and {211} orientations have similar values with 235 GPa for {111} and 231 GPa for {211} oriented grains. Consequently, the texture and thus the chemical composition of the Al-rich films have a negligible influence on the plane strain modulus of the Al-rich NiAl films. Therefore, the elastic mismatch between the brittle NiAl films and the Si substrates was assumed to be independent of the Al content. The parameters g, λ_1 and s in equation (3-9) can be

calculated based on the elastic properties of the NiAl films and the Si substrate. The corresponding values are summarized in table 3-3.

3.7.2 Energy release rate of the substrate

Crack penetration into the substrate was theoretically studied by Ye et al. for substrate cracks normal to the film surface [27]. Although the substrate cracks in our samples are inclined to the normal of the film surface (see figure 3-8), the model of Ye et al. is used to evaluate the energy release rate of the Si substrate. Due to the large uncertainty in the determination of the substrate crack length as reported above, it is of minor importance whether the total or the projected substrate crack length normal to the surface is chosen. By finite element simulations Ye et al. obtained the normalized energy release rate ω_s of the substrate as:

$$\omega_s = \frac{4\pi}{\pi^2 - 4}\left(\frac{E_f^*}{E_s^*}\right)\eta_s\left[\sin^{-1}\left(\frac{1}{\eta_s}\right)\left(1-\frac{1}{\eta_s}\right)^{0.5-s}\left(1+\frac{\lambda_2}{\eta_s}\right)\right]^2. \qquad (3\text{-}11)$$

In analogy to λ_1 in equation (3-9), the fitting parameter λ_2 was fitted to a full numerical solution of the problem. The value of λ_2 for the Al-rich NiAl films on Si substrates is listed in table 3-3 according to Ye et al. [27].

Finally, the parameter Z is obtained by inserting equations (3-9) and (3-11) into equation (3-8). Applying the values for the Al rich NiAl films as given in table 3-3, values of $Z = 6.0 \pm 1.4$ were calculated for all brittle NiAl films of this work.

Table 3-3 **Summary of the plane strain moduli for the film, E_f^*, and the substrate, E_s^*, and parameters α, g, s, λ_1 and λ_2 of equation (3-9), (3-10) and (3-11). See text for further details.**

	E_f^* [GPa]	E_s^* [GPa]	α	g	s	λ_1	λ_2
Al-rich NiAl films	233	154	0.204	1.44	0.543	0.00219	-0.300

4 Size effects on the plasticity of NiAl thin films

Abstract

Thin NiAl films, which can be used as protective coatings against oxidation at elevated temperatures, may fail as a result of high thermal stresses. Therefore, the influence of geometrical and microstructural constraints on the plasticity of NiAl films was studied for different Al contents (45 to 50 at-% Al) and film thicknesses (0.2 to 3.1 μm). The films were deposited on Si substrates and subjected to temperature changes resulting in thermal strains of up to 0.84 %. The stress evolution in the films was measured by the substrate curvature method. The residual stress at room temperature of near-stoichiometric NiAl films significantly increased with decreasing film thickness indicating an increase of the film strength. At temperatures above 400 °C strong stress relaxation was found, which was more pronounced in thinner films suggesting the contribution of diffusional creep processes. The existence of a critical film thickness is suggested at which a transition from diffusion controlled to dislocation controlled plasticity occurs.

4.1 Introduction

The intermetallic alloy β-NiAl combines many properties advantageous for the application as a structural material: high thermal conductivity, low density and excellent resistance against oxidation and corrosion [65]. However, lack of ductility below 400 °C and insufficient creep strength at high temperatures are its major drawbacks. Nevertheless, NiAl is technically used as a high-temperature coating for turbine blades [1]. Although NiAl has been studied extensively as a bulk material, little is known about its mechanical behavior in a confined volume, e.g. a thin film.

The mechanical properties of metals are known to significantly change if sample dimensions and / or grain sizes are in the range of a micrometer [2, 29]. For instance, the yield strength of thin metallic films strongly increases with decreasing film thickness as summarized by Kraft et al. [79]. Studies on bulk NiAl also indicate size effects: The maximum tensile elongation at 400 °C was found to dramatically increase once the grain size was below 20 μm [43]. Furthermore, in NiAl with a grain size of 20 μm, a transition from power-law creep to diffusional creep with decreasing strain rate was reported, while the creep behavior of coarse grained NiAl was always governed by power-law creep [44]. It is not yet known whether such size effects become even more significant under further dimensional and microstructural confinement reaching into the sub-micrometer regime.

This chapter aims to elucidate size effects on the plasticity of thin NiAl films over the temperature range from 20 to 700 °C. The chemical composition (45 to 50 at-% Al) as well as the film thickness (0.2 to 3.1 μm) of polycrystalline NiAl films were varied and the mechanical response to thermal straining was measured using a laser-optical substrate-curvature system. The large thermal mismatch between the NiAl films and the Si substrate enabled a thermal strain of 0.84 % on thermal cycling from room temperature to 700 °C. The deformation behavior of the NiAl films was characterized on the basis of stress-temperature curves and correlated with geometrical and microstructural size effects.

4.2 Experimental

4.2.1 Deposition of NiAl films

NiAl thin films were deposited onto (001) Si substrates using a magnetron co-sputtering process[5]. The Si substrates, which were 50 mm in diameter and 280 ± 10 µm in thickness, were coated on both sides with 50 nm thick amorphous layers of SiO_2 and Si_3N_4 in order to prevent interdiffusion of Si and NiAl. Prior to the NiAl deposition, the substrates were heated in a pre-vacuum chamber (base pressure of 1 x 10^{-6} Pa) at 120 °C for 1 h in order to clean off adsorbents from the substrate surface. Additionally, the substrates were cleaned in the ultrahigh vacuum (UHV) deposition chamber (base pressure of 5 x 10^{-8} Pa) by Ar^+ ion bombardment using a 200 V Kauffmann ion source. The deposition of NiAl was carried out in the UHV chamber at an Ar flow of 30 cm^3 per minute resulting in an Ar pressure of 1 x 10^{-1} Pa. During deposition, the samples were rotated at 100 revs/min in order to achieve a homogeneous film thickness.

For the sputtering process elemental targets of Ni (99.999 % purity) and Al (99.98 % purity) were used. In order to obtain NiAl films with Al contents between 45 and 50 at-%, the sputter power of the Al target was varied between 138 and 162 W while the power of the Ni target was kept at 150 W for all film depositions. NiAl film thicknesses in the range of 0.2 to 3.1 µm were obtained by varying the sputter time between 5 and 85 min. After deposition, the samples were annealed in UHV at 600 °C for 1 h without breaking vacuum. The cooling to room temperature after annealing was performed as fast as possible to minimize time-dependent relaxation processes during cooling. A cooling rate of approximately 3 K/s was achieved upon cooling from 600 to 200 °C by turning off the heating power.

[5] I thank Gerhard Adam for his support in film deposition.

4.2.2 Microstructural investigations

The chemical composition of the NiAl films was measured using wavelength-dispersive X-ray (WDX)[6] as well as optical emission spectroscopy (OES)[7]. In order to determine the crystallographic structure and the texture of the NiAl films, X-ray diffraction (XRD) measurements in Bragg-Brentano geometry (using a Siemens M18XHF-V operated at 40 kV using Cu Kα radiation) were carried out with a step size of $2\theta = 0.02°$ and measurement times of 1 s. The texture of the NiAl films was determined by comparing the relative diffraction intensities of the individual texture components with results of NiAl powder measurements [61].

The chemical composition at the surface and in the NiAl films were investigated by Auger electron spectroscopy (AES)[8] depth profile analysis (JOEL-JAMP 7830F operated at 10 kV). Ar^+ ions were used as sputter gas achieving a sputter rate of 27 nm/min for NiAl. Individual AES measurements were performed after sputtering times of 25 to 30 s. To investigate the influence of thermal cycling on the chemical composition, AES measurements were carried out on films after UHV annealing and after *ex situ* thermal cycling in N_2 atmosphere to a maximum temperature of 700 °C (for details see section 4.2.3).

The microstructure of the NiAl films was investigated by focused ion beam (FIB) microscopy (FEI 200xP operated at 30 kV) as well as transmission electron microscopy (TEM) using a JOEL 2000FX operated at 200 kV. The film thickness was determined by ion milling cross-sections in the NiAl films using the FIB microscope and measuring the projected film thickness at an angle of 45°. The grain size distributions were measured by marking at least 300 grains on FIB or TEM micrographs observed at 0° tilt. The marked grains were quantitatively analyzed using a computer-based image processing system (Quantimet Q500/W, Leica). The grain size was defined as the diameter of a circle of equivalent area.

The TEM investigations[9] were mainly carried out on plan-view samples in order to search for dislocations in 0.2 and 3.0 μm thick films with an Al content of 48.5 at-%. For plan-view TEM sample preparation, the NiAl coated Si wafers were cut with an ultrasonic disc cutter, ground and subsequently dimpled from the uncoated side to a total thickness of

[6] I gratefully acknowledge the help of Siglinde Haug for the WDX measurements.
[7] I thank Albrecht Meyer for performing the OES measurements.
[8] I am grateful to Bernhard Siegle for performing the AES measurements.
[9] I thank Gerhard Dehm for the support with the TEM investigations.

about 20 µm. Finally, the samples were thinned to electron transparency by Ar^+ ion milling.

4.2.3 Stress measurements

The biaxial stresses of the NiAl films were measured using the substrate-curvature technique [2, 63]. Residual stresses in the film lead to a bending of the film / substrate composite which is measured with an optical system and analyzed as described by Keller et al. [46]. Measuring the curvature C and using the biaxial elastic modulus of the substrate M_s and the thicknesses of the film h_f and the substrate h_s, the film stress σ_f can be calculated according to [62]:

$$\sigma_f = \frac{M_s\, h_s^2}{6\, h_f} C\,. \qquad (4\text{-}1)$$

The curvature of the bare substrates was always measured prior to NiAl deposition and was then subtracted from the curvature of the NiAl coated sample. Therefore, all reported stress values are absolute stresses. This procedure allowed the absolute film stress to be determined with an accuracy of ± 5 % and ensured the reproducible measurement of stress-temperature curves. The major error sources are uncertainties in the film thickness determination and sample drift during thermal cycling. A detailed description of the substrate-curvature technique is given by Flinn [63].

The residual film stresses were measured at room temperature (RT) after UHV annealing and during thermal cycling to maximum temperatures between 200 and 700 °C in a protective N_2 atmosphere. During thermal cycling, stresses are generated in the film due to the thermal mismatch between film and substrate. The film stresses were measured every 10 K. The samples were heated and cooled at a constant rate of 6 K/min, while below 100 °C the achievable cooling rate was 4 K/min. The heating and cooling rates of 4 and 6 K/min correspond to strain rates of $0.9\text{x}10^{-6}\ s^{-1}$ and $1.3\text{x}10^{-6}\ s^{-1}$, respectively, assuming thermal expansion coefficients of $2.5\text{x}10^{-6}\ K^{-1}$ for Si [64] and $15\text{x}10^{-6}\ K^{-1}$ for NiAl [65]. Thus, a temperature increase from RT to 700 °C resulted in a thermal strain of $\varepsilon_{th} = 0.84$ %.

4.3 Results

4.3.1 Composition and microstructure of the NiAl films

After UHV annealing, all NiAl films revealed a polycrystalline microstructure following a lognormal grain size distribution, independent of the Ni and the Al content. The median grain size was often smaller than the film thickness and increased with film thickness (table 4-1, figures 4-1 a, b). The grains were equiaxed, with only a few grains extending over the entire film thickness for films thicker than 0.2 µm (figure 4-1 c). A thermal cycle in N_2 atmosphere to 700 °C of UHV-annealed films did not lead to a noticeable change in the grain size as was quantitatively analyzed for a 0.8 µm thick film with an Al content of 48.5 at-% and a median grain size of 0.46 µm.

Table 4-1 Summary of Al content, film thickness, grain size and texture of the NiAl films investigated. Prior to the microstructural analyses, all films were annealed at 600 °C in UHV for 1 h. The error of the Al content, film thickness and the median grain size (standard deviation) is given in brackets.

Al content [at-%]	number of samples	film thickness [µm]	median grain size [µm]	texture
50.2 (± 0.5)	7	1.1 (± 0.05)	0.6 (± 0.3)	strong {111} weak {211}
49.0 (± 0.5)	1 3	1.1 (± 0.05) 3.1 (± 0.05)	0.5 (± 0.3) 0.8 (± 0.4)	strong {111} weak {211}
48.5 (± 0.5)	2 2 2 2 2 2	0.2 (± 0.05) 0.4 (± 0.05) 0.6 (± 0.05) 0.8 (± 0.05) 1.0 (± 0.05) 3.0 (± 0.05)	0.2 (± 0.1) 0.4 (± 0.2) 0.5 (± 0.2) 0.5 (± 0.2) 0.5 (± 0.3) 0.8 (± 0.4)	strong {111} weak {211}
47.7 (± 0.5)	2	1.2 (± 0.05)	0.5 (± 0.3)	predominant {111} additional {211}
46.1 (± 0.5)	3	1.3 (± 0.05)	0.7 (± 0.4)	mixed {111}&{211}
45.0 (± 0.5)	2	1.2 (± 0.05)	0.6 (± 0.4)	strong {110}

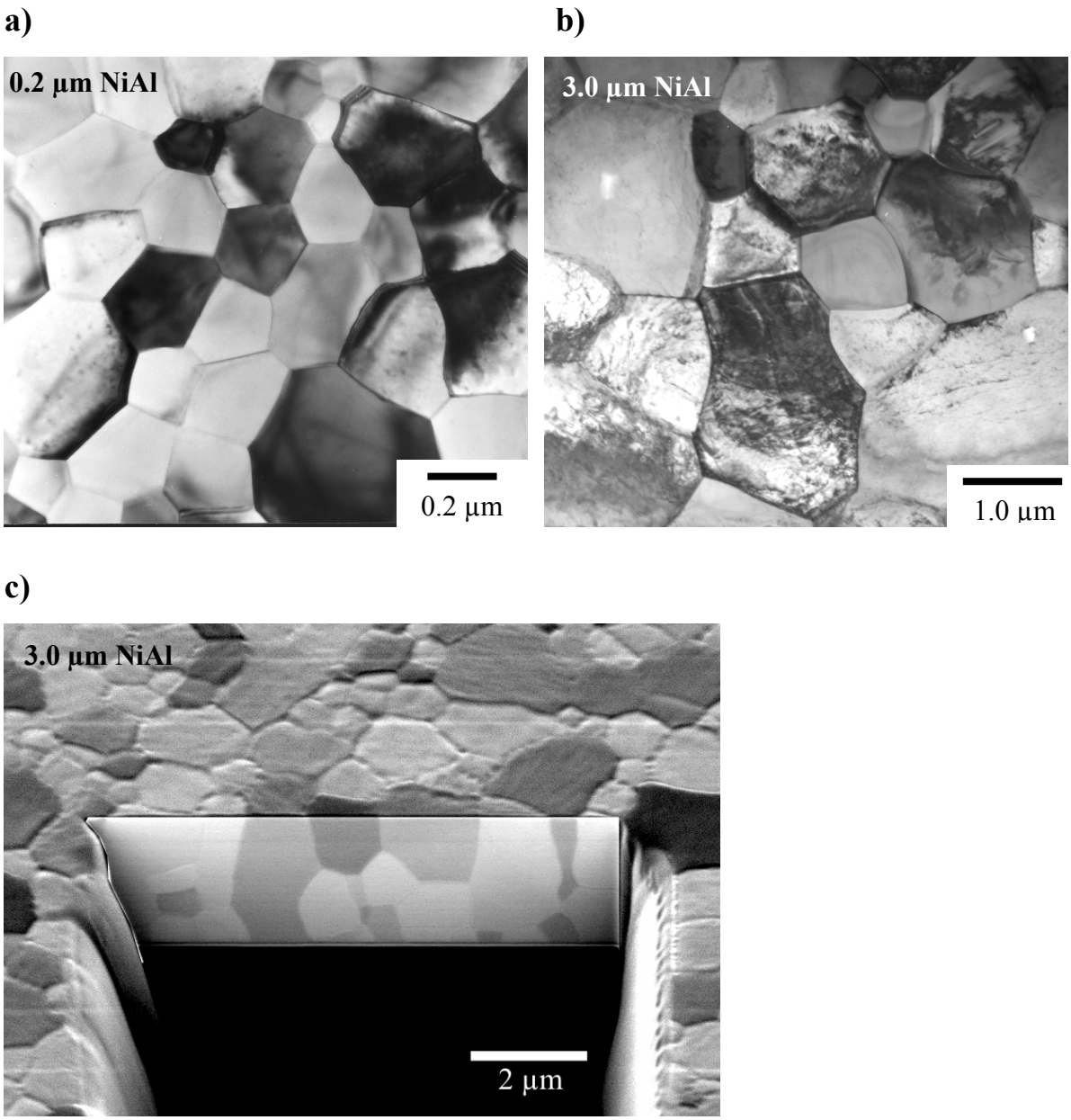

Figure 4-1 **TEM micrographs of (a) a 0.2 µm and (b) a 3.0 µm thick NiAl film with an Al content of 48.5 at-%. (c) FIB micrograph of a cross section of a 3.0 µm thick film (48.5 at-% Al). The grains are equiaxed and grain boundaries parallel to the surface are present. For better visualization, the contrast of the cross-section was enhanced by image processing.**

The analysis of the chemical composition of the films using WDX and OES showed good agreement and is summarized in table 4-1. The deviation of at least four individual measurements performed on one sample was less than 0.15 at-% for both techniques. The XRD measurements revealed that all films consisted solely of β–NiAl. The texture of the UHV-annealed films was found to depend on the chemical composition [66]. The near-stoichiometric films with Al contents of 48.5 to 50.2 at-% showed a strong {111} fiber texture with a small amount of {211} grains. With decreasing Al content the

amount of {211} grains increased so that NiAl films with an Al content of 46.1 at-% exhibited a mixed {111} and {211} texture. However, the NiAl films with the smallest Al content (45.0 at-% Al) were strongly {110} textured. In contrast to the Al content, the film thickness had no pronounced influence on the texture (see table 4-1). Thermal cycling in N_2 atmosphere did not affect the texture of the films.

TEM investigations of 3.0 and 0.2 µm thick films (48.5 at-% Al) after thermal cycling to 700 °C revealed dislocations in the thicker film, predominantly in the larger grains (figure 4-2), while the thinner film was devoid of dislocations.

AES depth profile analyses showed a homogeneous distribution of Al and Ni throughout the entire film thickness, which was unaffected by thermal cycling (figures 4-3 a, b). However, the composition near the surface changed significantly during thermal cycling in the N_2 atmosphere: While almost no oxygen was detected at the surface of the UHV-annealed films (figure 4-3 a), an Al oxide layer with a thickness of about 20 nm was present after thermal cycling to 700 °C (figure 4-3 b). This indicates the N_2 atmosphere did not completely suppress oxidation.

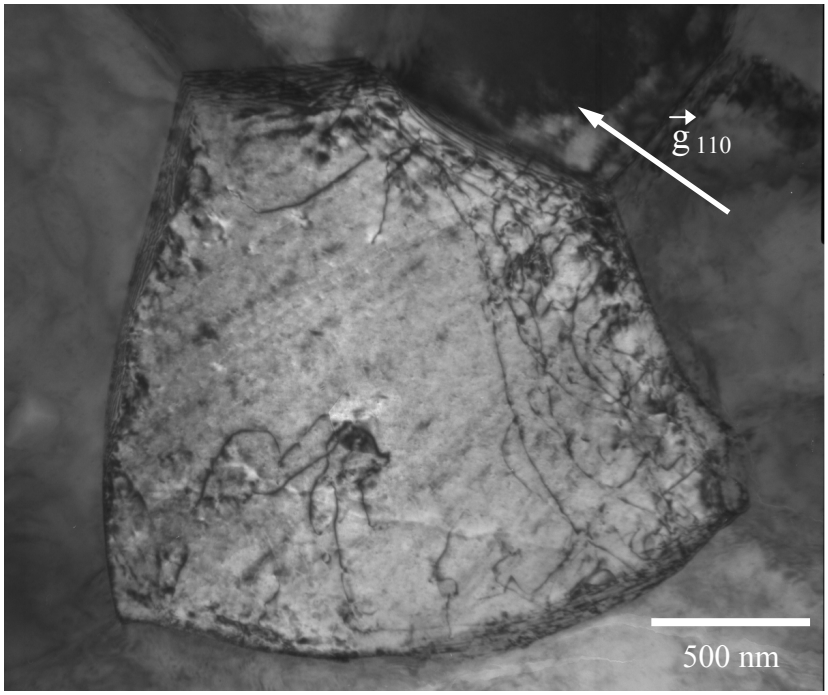

Figure 4-2 Bright-field TEM micrograph of a 3.0 µm thick NiAl film with an Al content of 48.5 at-%. The plan-view image reveals dislocations after thermal straining to 700 °C in an N_2 atmosphere prior to TEM sample preparation.

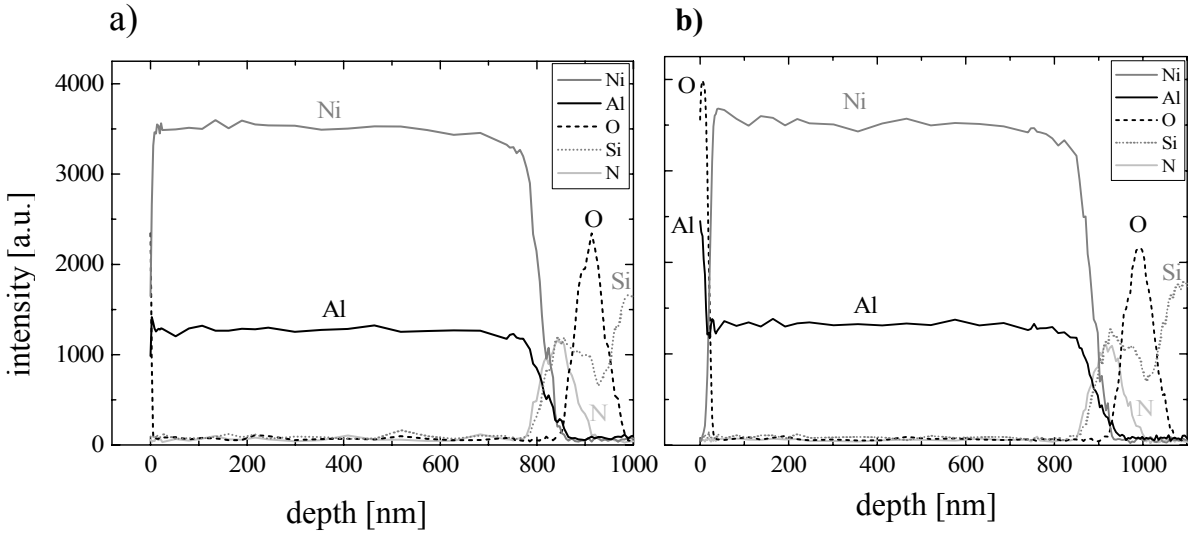

Figure 4-3 **AES depth profile of a 0.8 µm thick NiAl film with an Al content of 48.5 at-%. While the NiAl film after UHV annealing (a) is free of an oxide layer at the surface, (b) a 20 nm thick surface layer of aluminum oxide is revealed after thermal cycling of the film to 700 °C in N_2 atmosphere. In contrast, the chemical composition close to the film/substrate interface remained unchanged by the thermal cycling.**

4.3.2 Thickness effect on the RT stress of UHV-annealed films

The influence of the film thickness on the RT stress after UHV annealing at 600 °C was studied on NiAl films with Al contents between 48.5 and 50.2 at-%. Due to differences in the thermal expansion between film and substrate large tensile stresses of up to 2 GPa were induced in the film upon cooling from 600 °C. Furthermore, the film stress strongly increased with decreasing film thickness (figure 4-4). While the RT stress values of 3.0 µm thick films were about 550 MPa, films with a thickness of 0.4 µm showed RT stresses of about 1800 MPa. A further decrease in film thickness, however, did not lead to higher RT stresses after annealing at 600 °C (figure 4-4). For this reason, a 0.2 µm and a 0.4 µm thick film were additionally annealed at 800 °C for 1 h in UHV. While the RT stress of the 0.4 µm film did not significantly change compared to 600 °C annealing, the 0.2 µm film exhibited an increase in RT stress from 1.8 ± 0.2 to 2.2 ± 0.2 GPa (figure 4-4). These values correspond to the values for purely elastic deformation of 1.7 and 2.3 GPa for cooling from 600 °C and 800 °C, respectively, assuming a linear increase in stress with decreasing temperature with a rate of 3.0 MPa/K as observed experimentally (see section 4.3.4). This indicates that the yield strength of the 0.2 µm thick film was not yet reached.

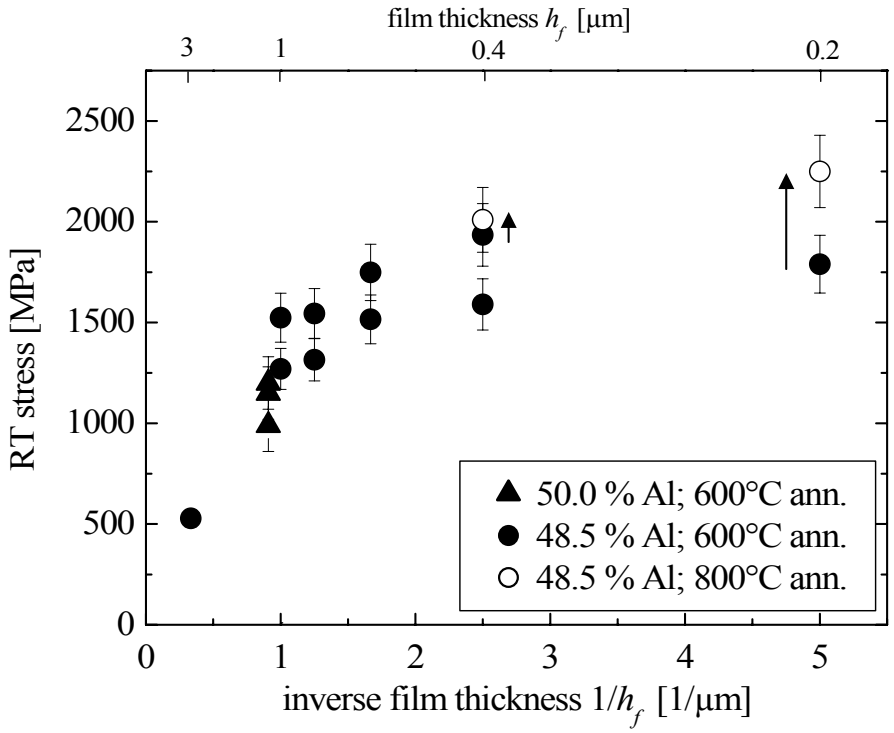

Figure 4-4 **Room temperature (RT) film stress after annealing at 600 °C versus the inverse film thickness (closed symbols). The room temperature stress of the thinnest films increase further after cooling from a higher maximum temperature of 800 °C in a subsequent cycle (open symbols) as indicated by the arrows. Minor changes in the chemical composition do not have a significant impact on the RT stress.**

4.3.3 Stress evolution during first and subsequent temperature cycles

In addition to the RT stress measurements, the stress evolution of UHV-annealed films was studied during thermal cycling to 700 °C. In figure 4-5 the stress-temperature curves of the first and the second cycle of a 0.4 µm thick film (Al content of 48.5 at-%) are shown. Upon first heating from RT, the initially large tensile stress of 1500 MPa decreased linearly with increasing temperature at a rate of 2.6 MPa/K up to about 400 °C and a biaxial tensile stress of 600 MPa (see figure 4-5). On further heating, an accelerated stress relaxation with an increased rate of up to 5.5 MPa/K occurred resulting in a deviation from the linear stress-temperature behavior. Above 500 °C the film stress became compressive and eventually reached compressive stress values up to 400 MPa, which then relaxed to about 250 MPa. During cooling the film stress became tensile again and increased linearly with decreasing temperature at a rate of 2.8 MPa/K. At RT the initial tensile stress of 1500 MPa before thermal cycling was regained.

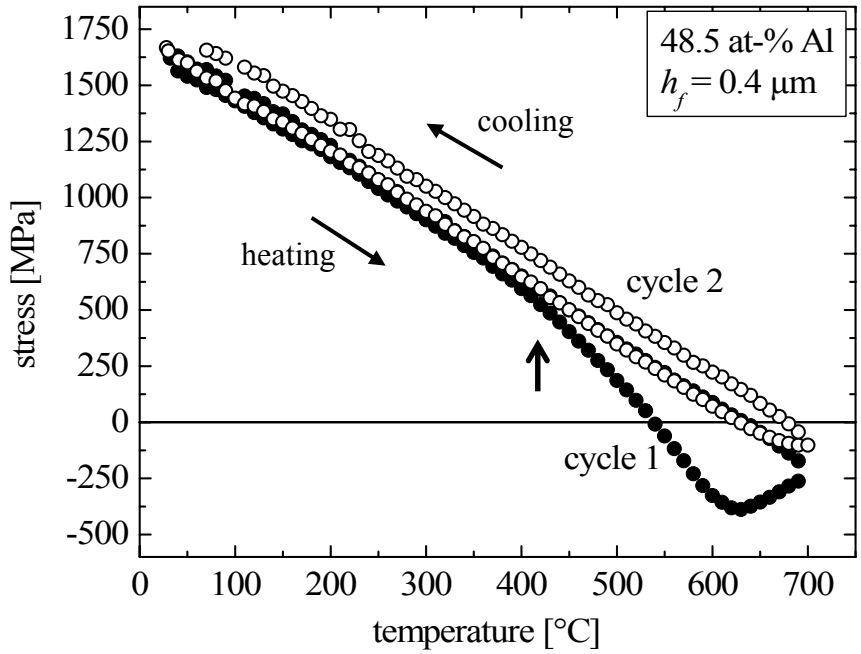

Figure 4-5 **First stress-temperature cycle of a 0.4 µm thick NiAl film with an Al content of 48.5 at-% (closed symbols). An accelerated stress relaxation during heating above 400 °C was observed as marked by the arrow. Upon further heating the film stress became compressive and started to relax above 630 °C. In contrast, the second heating cycle (open symbols) showed an almost linear behavior with no increase in stress relaxation rate at 400 °C. The cooling curves from 700 °C to 40 °C are linear for the first and second temperature cycle.**

The second temperature cycle of the 0.4 µm thick film coincided with the first cycle during heating to 400 °C (see figure 4-5). However, above 400 °C the second cycle continued at a rate of 2.8 MPa/ K until compressive stresses and temperatures above 600 °C were reached (figure 4-5). In contrast to the heating cycle, the cooling curve of the second cycle coincided with the first cycle. Subsequent stress-temperature cycles were almost identical.

The differences between first and second temperature cycles upon heating were found only for films thinner than 1.0 µm. Films with thicknesses larger than 1.0 µm did not show the accelerated stress relaxation in the tensile regime and gave almost identical first, second and subsequent stress-temperature cycles.

4.3.4 Effect of thickness on the stress evolution

The effect of film thickness on the stress evolution for second and higher temperature cycles is shown in figure 4-6 for 0.2, 0.8, and 3.0 µm thick NiAl films with Al contents of 48.5 at-%. It is clearly seen that the RT stresses increase for thinner films. Upon heating from RT, the tensile film stresses decreased linearly with increasing temperature. As the film stresses became compressive, a deviation from the linear behavior was observed, indicating plastic deformation of the films. The temperature where the transition occurred increased from 350 to 680 °C with decreasing film thickness of 3.0 to 0.2 µm. Upon cooling from 700 °C, the film stresses became tensile and increased with decreasing temperature resulting in almost symmetrical heating and cooling curves. The slopes of the linear regimes in the stress-temperature curves were similar for heating and cooling cycles. While a clear "hysteresis" was observed for 3.0 µm thick films, the stress-temperature "hysteresis" became narrower for thinner films.

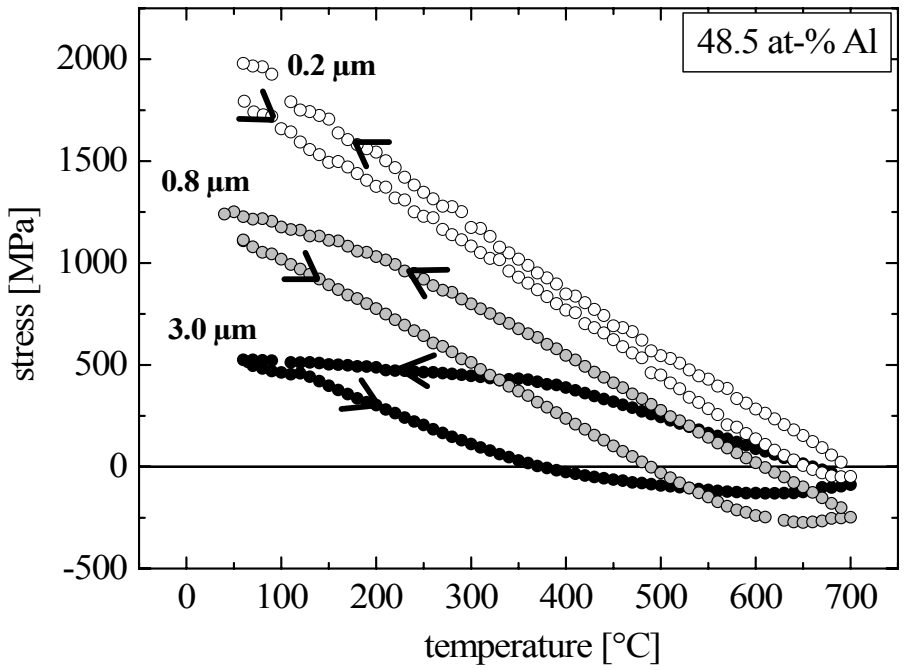

Figure 4-6 Stress evolution during temperature cycles to 700° C in NiAl films with an Al content of 48.5 at-% and film thicknesses of 0.2, 0.8 and 3.0 µm. All stress-temperature cycles correspond to the second or higher cycles. Thinner films exhibit higher tensile stresses and a narrower stress-temperature "hysteresis".

The slopes of the linear regimes during cooling are shown in figure 4-7. NiAl films with a thickness of 0.2 µm exhibited a slope of 2.8 ± 0.1 MPa/K, compared to values of only 1.5 ± 0.2 MPa/K for 3.0 µm thick films. To gain more insight into the effect that determines the slope of the linear regimes, 3.0 µm thick films were thermally cycled to different maximum temperatures between T_{max} = 200 and 700 °C. For instance, cooling from T_{max} = 400 °C resulted in a significantly higher slope of 3.0 MPa/K (figure 4-8). As summarized in figure 4-9, the slope in the linear regime during cooling increased from about 2.5 to about 3.1 MPa/K with increasing T_{max} from 200 to 400 °C, but decreased from 3.1 to 1.6 MPa/K when T_{max} was further increased to 700 °C. The slope of 3.1 ± 0.2 MPa/K obtained for a 3.0 µm film in a temperature cycle to 400 °C is even higher than the value observed for a 0.2 µm thick film cycled between RT and 700 °C (see figure 4-7). The reported slopes were reproducibly measured and are almost independent of the previous temperature cycle.

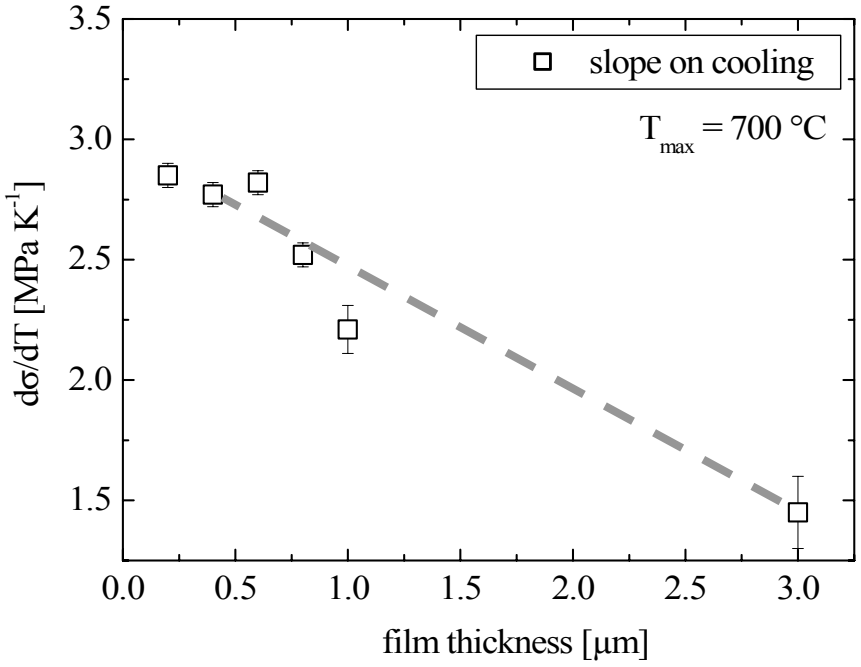

Figure 4-7 Slopes dσ/dT of the linear stress-temperature regimes as a function of film thickness. The slopes were determined upon cooling in the temperature interval from 680 to 400 °C from stress-temperature cycles to T_{max} = 700 °C. The Al content was 48.5 at-% for all films.

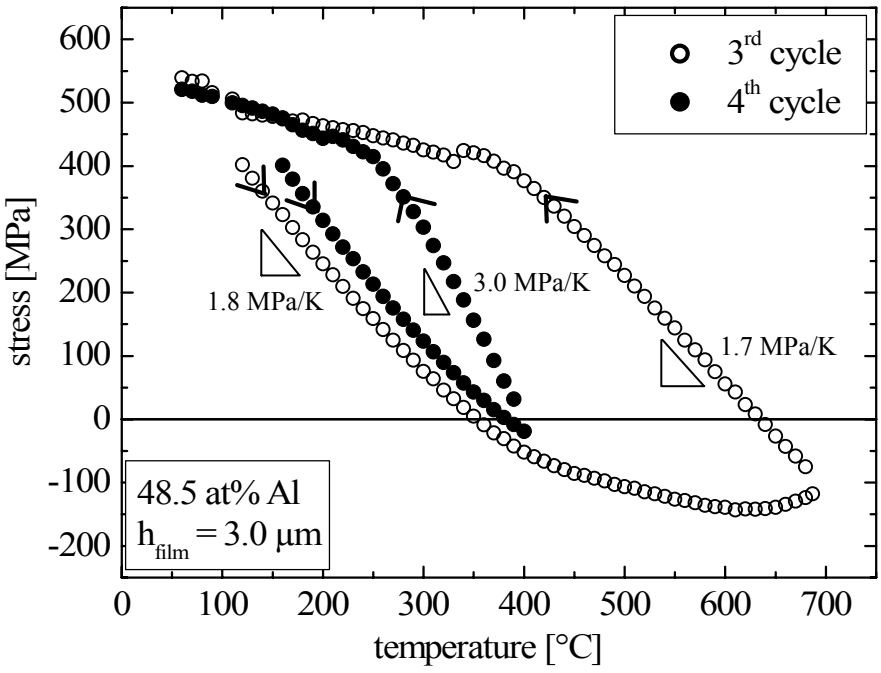

Figure 4-8 **Stress temperature cycles with different maximum temperatures (T_{max}) of a 3.0 µm thick NiAl film. Thermal cycling to T_{max} = 700 °C yielded a slope of 1.7 ± 0.1 MPa/K during both heating and cooling. However, for T_{max} = 400 °C the slope upon cooling increased to 3.0 ± 0.1 MPa/K.**

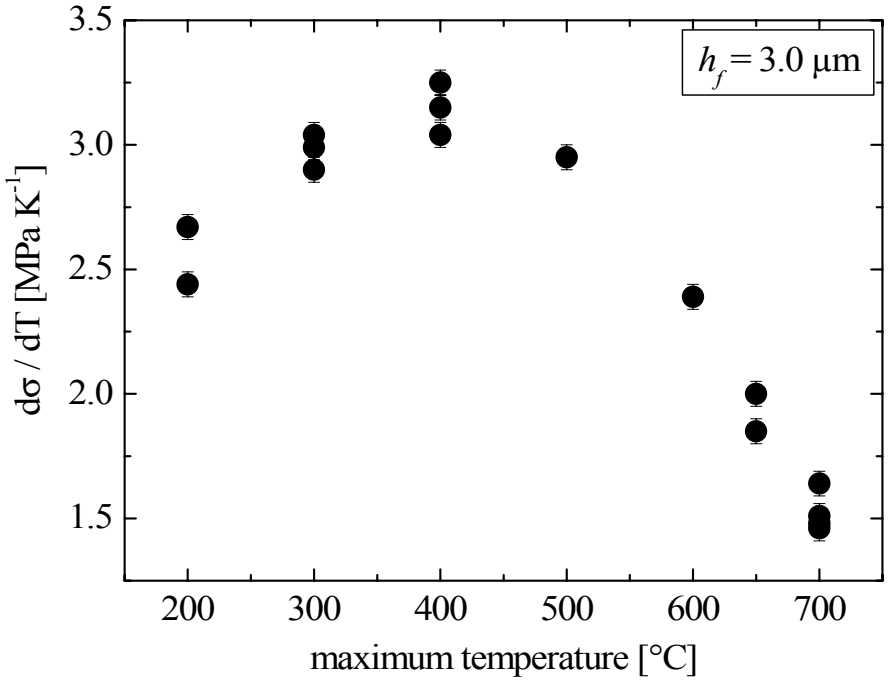

Figure 4-9 **Slopes dσ/dT upon cooling of stress-temperature curves of 3.0 µm thick films (48.5 at-% Al) as a function of maximum temperature. A slope of 3.2 MPa/K was observed upon cooling from 400 °C. However, the slopes decreased if the maximum temperature deviated from 400 °C to both lower and higher temperatures.**

Another important influence of film thickness on the stress evolution in NiAl films (48.5 at-% Al) is observed in the temperature regime of 600 to 700 °C (see figure 4-6). In this temperature regime maximum compressive stresses evolved. To compare the compressive film stresses, all stress values are taken at a temperature of 690 °C. While the compressive stress at 690 °C increased from 50 to 250 MPa with increasing film thickness from 0.2 to 0.8 µm, the opposite behavior was observed for thicker films where the compressive stresses fell from 250 to 100 MPa. This behavior is summarized in figure 4-10 for film thicknesses between 0.2 and 3.0 µm.

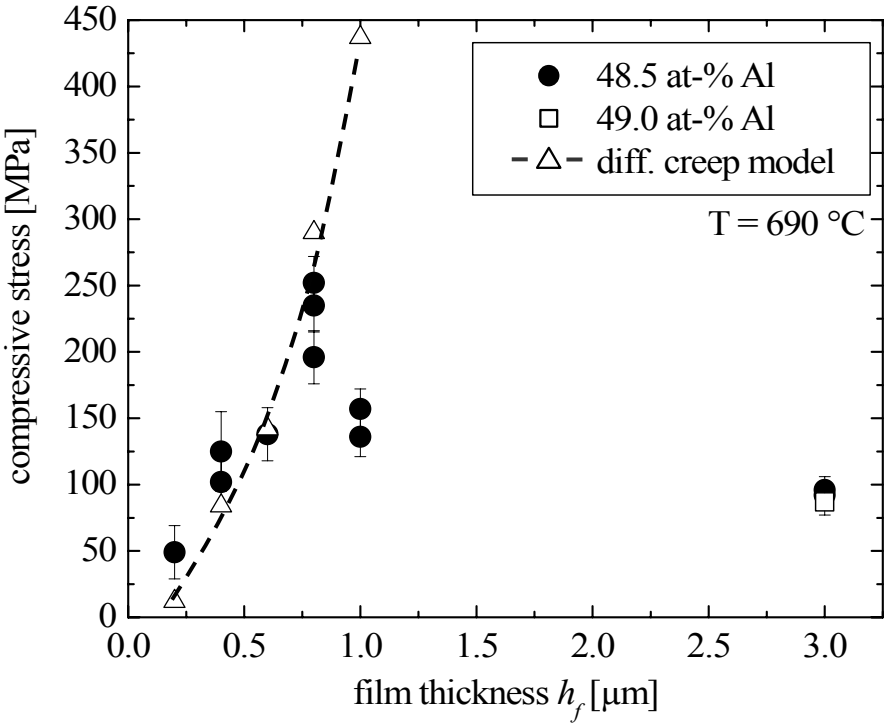

Figure 4-10 Measured compressive stress at 690 °C of NiAl films with an Al content of 48.5 at-% as a function of film thickness. The stress values were obtained from temperature cycles to 700 °C. In addition, calculated stress values were added, which are based on the constrained diffusional creep model derived by Gao et al. [41]. The activation energy was assumed to Q_{gb} = 210 kJ/mol. See section 4.4.2 for further details.

4.3.5 Influence of Al content on the stress evolution

In figure 4-11 the stress-temperature cycles of two 1.1 ± 0.1 µm thick NiAl films with median grain sizes of 0.55 ± 0.05 µm, but Al contents of 47.7 at-% (Ni-rich) and 50.2 at-% (stoichiometric) are compared. The curves coincide in the temperature regime between 200 and 500 °C. However, differences in stress, which are far beyond the error in absolute stress determination, were observed at lower and higher temperatures: The stoichiometric film sustained smaller tensile stresses at RT, but significantly exceeded the compressive stresses of the Ni-rich film above 550 °C (figure 4-11). The compressive stresses at temperatures above 650 °C of films with thicknesses of 1.1 ± 0.2 µm and Al contents between 45.0 and 50.2 at-% confirm this behavior (figure 4-12). The stresses decreased with increasing deviation from stoichiometry from about 225 MPa for stoichiometric to about 75 MPa for Ni-rich films with an Al content of 45.0 at-%. The compressive stress values presented in figure 4-12 were obtained from temperature cycles to T_{max} = 700 °C. In order to compare films of different Al contents, only the maximum compressive stress values which occurred either at approximately 650 °C or 690 °C were considered. For example, a 1.2 µm thick film with an Al content of 47.7 at-% reached the maximum compressive stress of 145 ± 15 MPa at 650 °C (see figure 4-11).

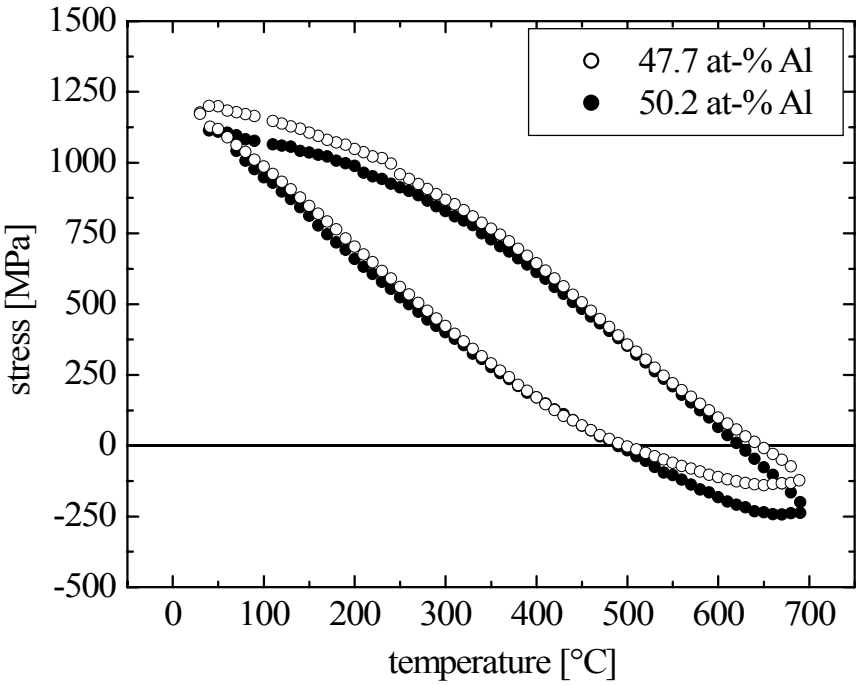

Figure 4-11 Effect of the chemical composition (47.7 and 50.2 at-% Al) on the stress evolution during a temperature cycle to 700 °C of 1.1 ± 0.1 µm thick NiAl films. Both films were already cycled previously. While the stoichiometric NiAl film (50.2 at-% Al) shows lower film stresses at room temperature compared to the Ni rich film (47.7 at-% Al), higher compressive stresses are present at temperatures above 500 °C.

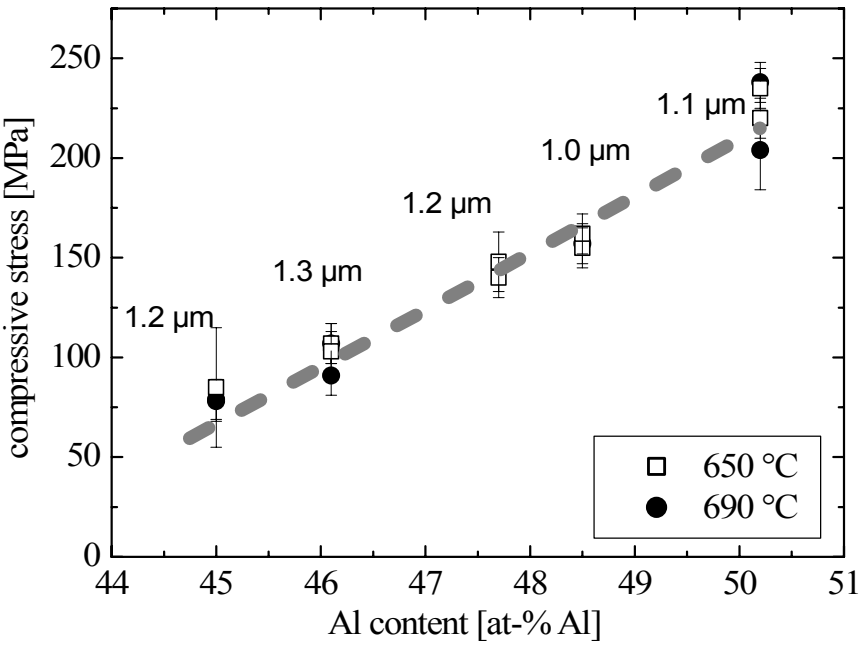

Figure 4-12 Compressive stress for 1.0 to 1.3 µm thick NiAl films recorded at either 650 °C or 690 °C as a function of Al content. The reported stresses are the maximum compressive stresses reached in a temperature cycle to 700 °C. For this reason, stresses for two different temperatures are reported depending on the temperature where the maximum stresses were reached. The film thicknesses are given next to the corresponding data points.

4.4 Discussion

To understand the thermo-mechanical behavior of NiAl thin films, it is necessary to consider both general thin film deformation mechanisms and the characteristics of the intermetallic phase NiAl. Therefore, in a first section, thin film plasticity and the relevant mechanical properties of bulk NiAl shall be briefly reviewed. In the light of these phenomena, the results of our work will be discussed in a second section. In a third section, the microstructure and the mechanical behavior of the NiAl films are compared with Cu and Al films.

4.4.1 Background

Plasticity of metal thin films

Thin metallic films commonly show a significant increase in yield strength with decreasing film thickness. This behavior has been observed for various metal thin films with face-centered cubic (fcc) lattice structure, for example for Cu [30, 46, 47], Al [31, 45], and Ag [32]. Several models were developed to account for the increase in yield strength with decreasing film thickness [2, 33, 34]. The models mainly consider constraints on the motion of dislocations imposed by the small grain size or film thickness. Freund [33] and Nix [2] have considered the motion of a single dislocation in a thin film. Their "channeling mechanism" leads to an inverse relationship between yield strength σ_y and thickness h_f:

$$\sigma_y = s^{-1}\left(\tau_p + \frac{b\,\mu_{eff}}{4\pi(1-\nu_f)}\frac{\sin\varphi}{h_f}\right), \qquad (4\text{-}2)$$

where s is the Schmid factor, τ_p the Peierls stress, b the Burgers' vector, ν_f the Poisson's ratio of the film and φ the angle between glide plane normal and film normal. The effective shear modulus μ_{eff} takes into account that dislocation segments deposited at interfaces "feel" the stiffness of both adjacent materials.

On the basis of this model, the overall dependence of yield strength on film thickness of fcc metal thin films can be understood, and for epitaxial, quasi-single-crystalline films the model is even in quantitative agreement with experimental observations [31]. However, it generally underestimates the absolute values of the yield strength of polycrystalline films for which it was not designed. Several authors have

pointed out that the high strength of thin fcc films is related to strong strain hardening which occurs even at very small plastic strains [47, 80, 81]. Another approach for describing the dependence of yield strength on film thickness considers the repeated activation of dislocation sources rather than the motion of dislocations [36]. Following this approach a better quantitative agreement between theory and experiment for the thickness effect on the yield strength of polycrystalline fcc metal thin films was found [36].

At elevated temperatures plasticity in thin films is governed by thermally activated processes. The major mechanisms discussed in the literature are (1) thermally activated dislocation glide and (2) constrained diffusional creep:

(1) Thermally activated dislocation glide in thin films is mainly adopted from the derivations obtained for bulk materials and is discussed by several authors as the dominant deformation mechanism in thin metal films at elevated temperatures [37-40, 82].

(2) Constrained diffusional creep in thin films on substrates was computationally studied by Gao et al. [41]. They considered stress-induced diffusion of atoms from the film surface into the grain boundaries and vice versa depending on the stress state in the film. The stress in the vicinity of the grain boundary is lowered by the diffusion, which in turn lowers the mean stress of the film.

Assuming elastic behavior, the thermally-induced stress σ_{el} during a temperature change from T_0 to T_1 can be calculated according to:

$$\sigma_{el} = \sigma_0 + \frac{d\sigma}{dT}(T_1 - T_0), \tag{4-3}$$

where σ_0 is the film stress at the temperature T_0 and $d\sigma/dT$ is the thermo-elastic slope determined by the elastic modulus of the film and the thermal mismatch between film and substrate. Assuming constrained diffusional creep as the only deformation mechanism, the average film stress σ_f can be described according to Gao et al. [41] and Weiss et al. [40] as follows:

$$\sigma_f = \sigma_{el} - \left(\sigma_{el} - \sigma_{gb}\right)\left(\frac{4h_f}{d}\tanh\left[\frac{d}{4h_f}\right]\right), \tag{4-4}$$

where d is the grain size and σ_{gb} is the grain boundary traction, averaged in the film thickness direction. The grain boundary traction is given by [41]:

$$\sigma_{gb} = \sigma_{el} \exp\left(-\frac{\lambda t}{t_0}\right), \tag{4-5}$$

where t is the time, and t_0 is a characteristic time which can by expressed by:

$$t_0 = \frac{4\pi k_B T h_f^{\,3}}{E_f^* \delta D_{gb} \Omega}. \tag{4-6}$$

Here, E_f^* is the plane-strain elastic modulus of the film, k_B is Boltzmann's constant, δ is the grain boundary width, Ω is the atomic volume and D_{gb} is the grain boundary diffusivity. The parameter λ in equation (4-5) is a geometry-dependent constant and is a function of the film thickness to grain size ratio. Temperature and time are linked by the heating / cooling rate. It is assumed that the stress at the grain boundary before the onset of diffusion corresponds to the stress in the grain interior. At low temperatures σ_{gb} is equal to σ_{el} and the average film stress σ_f is determined by the linear stress-temperature behavior according to equation (4-3). However, if the temperature rises and diffusion becomes active, the stresses close to the grain boundaries start to relax leading to a decrease in σ_{gb} and, thus, a decrease in average film stress σ_f. A detailed description for the simulation of stress-temperature curves based on constrained diffusional creep is given by Weiss et al. [40]. They successfully applied this concept combined with thermally activated dislocation motion in the grain interior to a thermally strained Cu thin film on Si substrate.

Mechanical behavior of NiAl

The intermetallic phase NiAl has a CsCl-type lattice structure and a melting point of 1638 °C [3]. NiAl is thermodynamically stable in a wide range of chemical composition ranging from 45 to 60 at-% Al below 400 °C [3]. Plasticity in NiAl at RT is limited because only three independent slip systems of the type {110}<001> are active in NiAl [15]. However, at temperatures above 400 °C, NiAl shows a brittle-to-ductile transition (BDT) [9-12] which is attributed to either the activation of additional slip systems or the climb of <001> dislocations. The yield strength of NiAl depends only weakly on temperature between RT and 400 °C, but decreases significantly above 400 °C [6]. At

room temperature, the yield strength increases strongly with deviation from the stoichiometric composition to both the Al-rich and the Ni-rich side [6, 83]. For instance, the yield strength of NiAl was found to increase from σ_y < 200 MPa to σ_y > 600 MPa with a change in composition from stoichiometric to 45 at-% Al [83]. In contrast, the creep resistance at high temperatures shows the opposite dependency on the chemical composition where a deviation from stoichiometry decreases the creep strength of NiAl [8]. This is mainly explained by an increase in diffusivity [7] as a consequence of an increase in point defects accounting for the deviation in stoichiometry [5].

4.4.2 Discussion of experimental results

Influence of film thickness on plastic yielding

The tensile stresses at RT after UHV annealing at 600 °C of NiAl films with near-stoichiometric composition strongly increased with decreasing film thickness (see figure 4-4). This dependency has already been observed for fcc thin films but has not yet been reported for intermetallic films.

The film stress at RT after thermal cycling of thin metallic films on rigid substrates is commonly identified as the RT flow stress of the film. This requires that plastic yielding occurred upon cooling and the RT stress is independent of the maximum temperature of the preceding thermal cycle. While this is generally believed to be the case for fcc metals, it is not applicable for NiAl films where the brittle to ductile transition inhibits plasticity below 400 °C [11, 84]. The RT stress was found to depend on T_{max}: For example, the RT stress of a 0.8 μm thick NiAl film with an Al content of 48.5 at-% increased from 1100 to 1300 MPa with increasing T_{max} from 650 to 750 °C.

Therefore, we define the yield strength of the NiAl films as the stress during cooling from 700 °C at which the stress-temperature curve deviates from linear behavior. Although the temperature at which yielding occurs is different, the definition of yield strength is reasonable since the measured yield strength for all NiAl films was reached upon cooling in the temperature regime between RT and 400 °C in which the temperature does not influence the yield strength strongly [6]. In figure 4-13, the measured yield strengths of the NiAl films were normalized to the shear modulus μ_{NiAl} = 69 GPa [65] and compared with the normalized RT flow stresses of Cu [30] and Al films [31] from the

literature. While the normalized flow stresses of Cu and Al films are almost equal, the increase in stress with decreasing film thickness is more distinct in NiAl.

The measured yield strengths of the NiAl films are compared to the yield strengths predicted by the Nix-Freund model according to equation (4-2). For the NiAl films a {110}<001> slip system was assumed based on observations in polycrystalline NiAl reported in literature [15, 65]. For a {111} textured film this results in an angle $\varphi = 35°$ and a Schmid factor of $s = 0.47$. The Burgers' vector b, the Poisson's ratio ν_f and the Peierls stress τ_p were assumed as $b = 2.89$Å [65], $\nu_f = 0.31$ [65] and $\tau_p = 125$ MPa [72]. Furthermore, a 20 nm thick surface layer of aluminum oxide was taken into account as experimentally observed after the first temperature cycle in N_2 atmosphere (see figure 4-3). As shown in figure 4-13, the model predicts a relatively weak increase in yield strength with decreasing film thickness and strongly underestimates the measured yield strengths of the NiAl films with film thicknesses below 3 µm.

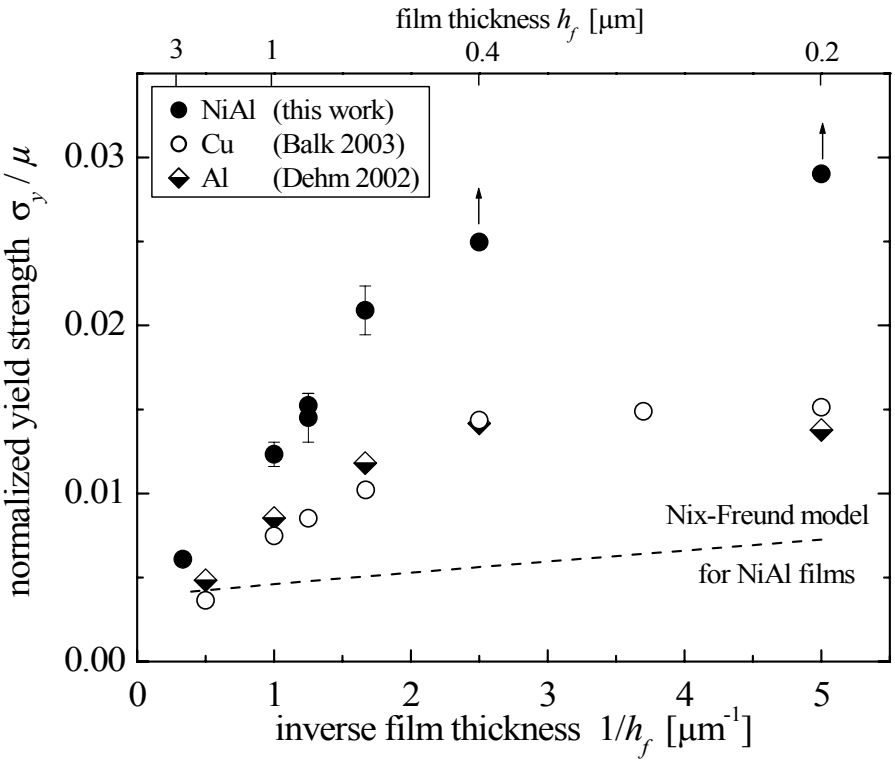

Figure 4-13 The measured yield strengths of NiAl thin films are shown together with literature data for the RT flow stresses of Cu films by Balk et al. [30] and Al films by Dehm et al. [31] as a function of film thickness. For comparison, the values of NiAl, Cu and Al are normalized to their shear moduli $\mu_{NiAl} = 69$ GPa, $\mu_{Cu} = 42$ GPa, $\mu_{Al} = 25$ GPa. The increase in yield strength with decreasing film thickness is more pronounced for NiAl than for the flow stresses of Cu and Al and cannot be described by the Nix-Freund model [2, 33]. Note, that the yield strengths of the NiAl films with a thickness $h_f \leq 0.4$ µm were not reached as indicated by the arrows.

Microstructural size effects on yield strength were studied in bulk materials with grain sizes in the range of 10 to 500 µm for Cu [85], Al [86] and NiAl [42]. All three bulk materials exhibit the well known Hall-Petch behavior, which predicts a dependence of yield strength, $\sigma_{y,}$ on grain size, *d,* according to $\sigma_y \propto k\, d^{-0.5}$. The parameter *k* determines the magnitude of yield strength enhancement due to grain refinement and contains a critical stress needed to activate a dislocation source. Baker et al. [42] found that for bulk NiAl the parameter *k* strongly depends on the chemical composition and ranges from 0.15 MPa $m^{1/2}$ for stoichiometric to 1.4 MPa $m^{1/2}$ for Ni-rich NiAl with an Al content of 45 at-%. Baker et al. [42] argued that this increase in the parameter *k* with deviation from stoichiometry is correlated with the increasing Peierls stress [72], because the activation of a dislocation source becomes more difficult with an increase in friction stress. For bulk NiAl with a chemical composition of 48.5 at-% Al *k* is about 1.0 MPa $m^{1/2}$ [42] which is significantly higher than reported for bulk Cu and bulk Al with *k*-values of 0.16 MPa $m^{1/2}$ [85] and 0.07 MPa $m^{1/2}$ [86], respectively. In accordance, the Peierls stress of NiAl with values higher than 100 MPa [72] also greatly exceeds the Peierls stress of Cu and Al which is very low for fcc metals. This may explain why the increase in yield strength with decreasing film thickness and grain size is more pronounced in the NiAl films compared to Cu and Al films. This increase is even more pronounced for NiAl films which would give a *k*-value of more than 2 MPa $m^{1/2}$ in this study as compared to bulk NiAl with a *k*-value of 1.0 MPa $m^{1/2}$.

It is speculated that the initial nucleation of dislocations plays a decisive role in NiAl film plasticity. Lack of dislocations strongly limits plasticity. With decreasing grain size and film thickness, activating dislocation sources may become increasingly difficult, as proposed in the simulations by von Blanckenhagen et al. [36]. This was qualitatively confirmed by plan-view TEM investigations, where dislocations were observed in a 3.0 µm thick NiAl film (figure 4-2) while a 0.2 µm film of the same chemical composition showed almost no dislocations (see figure 4-1 a), even during thermal straining in the TEM. The high NiAl Peierls stress may exaggerate this effect, in comparison to Cu and Al films, as discussed above.

Effect of diffusional creep on the stress evolution

The first stress-temperature curves of films with a thickness smaller than 1.0 µm showed an accelerated stress relaxation behavior in the tensile stress regime at about 400 °C during heating while the second and higher cycles exhibited a linear stress-temperature behavior until compressive stresses and temperatures above 550 °C were reached (see figure 4-5). Two mechanisms for the observed stress relaxation are possible: The brittle to ductile transition or the onset of diffusional creep processes. The brittle to ductile transition, which is indeed reported at about 400 °C (see section 4.4.1), is commonly explained by increasing thermal activation of dislocation motion. However, dislocation plasticity is very likely not responsible for the observed stress relaxation because this relaxation is more pronounced in thinner films, which are more devoid of dislocations. Instead it is argued that at temperatures above 400 °C a diffusional creep process became active which caused the stress relaxation upon heating. This conclusion is supported by the following calculations.

The constrained diffusional creep model of Gao et al. [41] was applied to the first *ex situ* temperature cycle of an NiAl film with an Al content of 48.5 at-% and a film thickness of 0.4 µm. No reliable data for grain boundary diffusion in NiAl are reported in the literature. For this reason, the activation energy Q_{gb} for grain boundary diffusion was varied between 170 and 210 kJ/mol which is 0.55 to 0.7 times the activation energy for volume diffusion in bulk NiAl of comparable chemical composition were values of about 300 kJ/mol have been measured [7, 87]. The pre-exponential term of the diffusion coefficient was assumed to be $D_0 = 4*10^{-4}$ m^2s^{-1} which is of the same order of magnitude as reported for volume diffusion in NiAl bulk material [7]. All parameters which were inserted in equations (4-3) to (4-6) for the modeling of the stress-temperature curves are summarized in table 4-2.

Table 4-2 Parameters used for the modeling of stress-temperature curves assuming constrained diffusional creep where *dT/dt* is the heating rate, *dσ/dT* the heating slope, Ω the atomic volume, λ a numerical constant, and *δ* the grain boundary width. E_f^* is the plane-strain elastic modulus assuming a {111} film texture. See text for further information.

h_f [µm]	d [µm]	E_f^* [GPa]	σ_0 (40°C) [MPa]	dT/dt [K/min]	$d\sigma/dT$ [MPa/K]	Ω [m^3]	δ [m]	λ	D_0 [m^2/s]	Q_{gb} [kJ/mol]
0.4	0.36	235	1610	6	2.75	$1.2*10^{-29}$	$5*10^{-10}$	42.2	$4*10^{-4}$	170 to 210
1.0	0.52	235	1420	6	2.67	$1.2*10^{-29}$	$5*10^{-10}$	67.0	$4*10^{-4}$	170 to 210

With the constrained diffusional creep model it is possible to describe an accelerated stress relaxation in the tensile stress regime upon heating as observed experimentally (figure 4-14 a)[10]. The onset as well as the magnitude of the stress relaxation are sensitive to the activation energy for grain boundary diffusion: Taking a value of Q_{gb} = 190 kJ/mol yields a higher stress relaxation rate for a 0.4 µm thick film in the tensile regime starting at 430 °C, which agrees with the experimental findings. In contrast, for an activation energy of Q_{gb} = 210 kJ/mol, the stress relaxation is delayed while it starts at a lower temperature for Q_{gb} = 170 kJ/mol.

The model curves for the 0.4 µm thick film quickly reach a stress-free state and maintain that upon further heating, whereas the experimental stress-temperature curve develops compressive stresses of up to 350 MPa (figure 4-14 a). This discrepancy may be related to the fact, that for an ongoing stress relaxation in compression the diffusional creep process has to be reversed compared to tension. In a new approach by Hartmaier et al. [88] constrained diffusional creep is described by the nucleation and climb of dislocations in grain boundaries rather than the diffusion of atoms. In their discrete dislocation dynamics simulations they obtained a critical stress for the nucleation of climb dislocations. This may be the reason why the stress relaxation in compression does only occur once a critical stress is reached. However, a full understanding of this phenomena is still lacking.

Diffusional creep is strongly influenced by the length of the diffusion paths. Small film thicknesses and grain sizes are expected to promote diffusional creep. This is in agreement with the observation that the first temperature cycles of NiAl films with thicknesses larger than 1.0 µm did not show a stress relaxation in the tensile regime as it was observed for thinner films. This behavior is also predicted by the constrained diffusional creep model assuming an activation energy of Q_{gb} = 190 kJ/mol as shown in figure 4-14 b for a 1.0 µm thick film.

[10] Mathematica4.1 software was used for the model calculations.

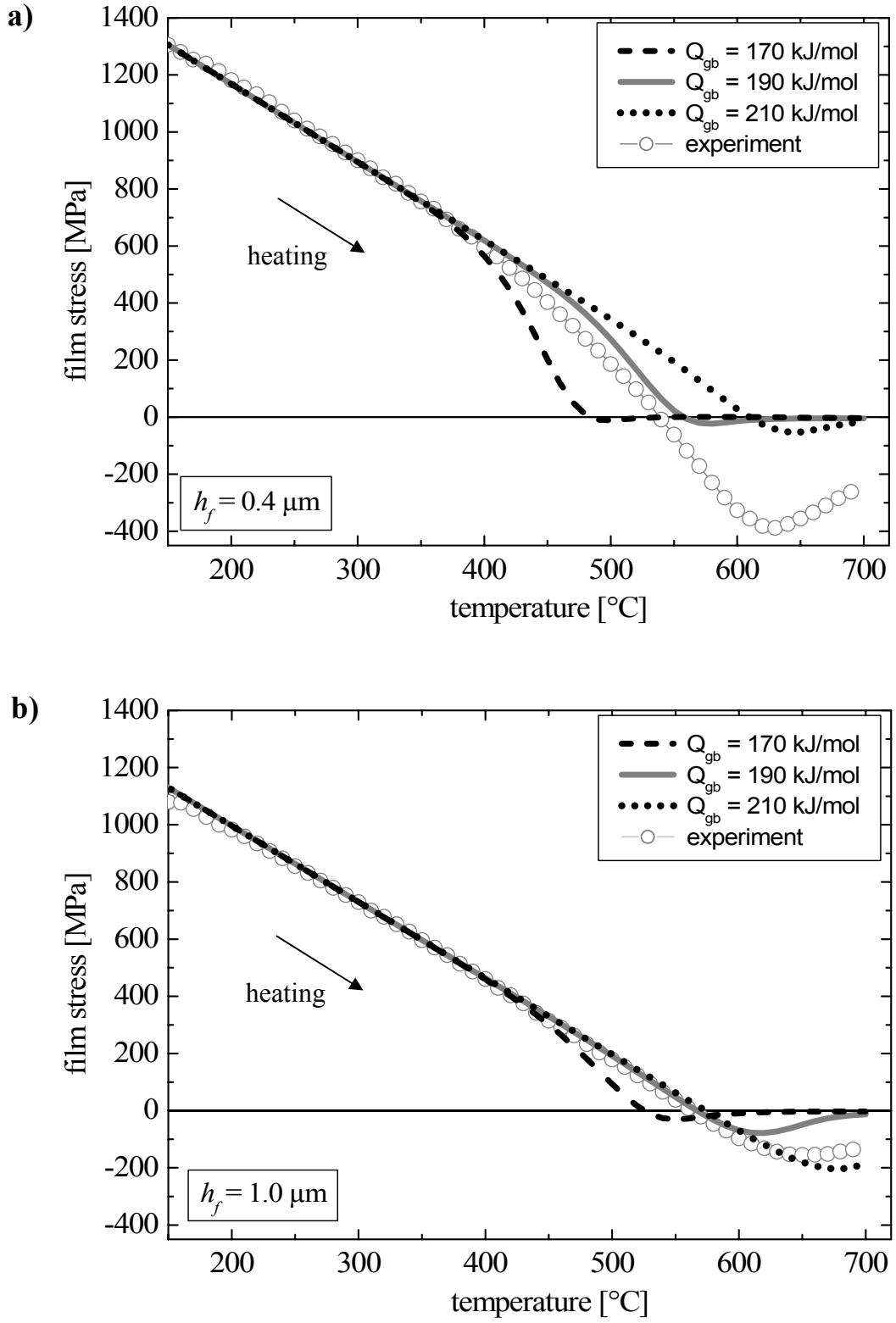

Figure 4-14 Model calculations of the stress relaxation during the first heating cycle in (a) a 0.4 µm and (b) a 1.0 µm thick NiAl film with Al contents of 48.5 at-% in comparison to the experimental data. The activation energy Q_{gb} for grain boundary diffusion determines the onset and magnitude of stress relaxation. For the simulation, the experimental findings were used. See text for further details.

At the end of the first temperature cycle, an oxide layer had formed on the surface which obstructed diffusion along the surface in subsequent cycles. A diffusional creep process may still be active because NiAl forms below 1000 °C meta-stable oxides which are not perfectly dense [89]. As a result, diffusion along the interfaces between film/oxide or along grain boundaries parallel to the surface (see figure 4-1c) might be maintained leading to stress relaxation by diffusional creep. Owing to the limited surface diffusion, the diffusivity under these conditions is expected to be lower in the second and subsequent temperature cycles compared to the first cycle. In analogy to the first stress-temperature curves, the constrained diffusional creep model was also applied to second heating cycles. Due to the presence of the surface oxide layer, a higher activation energy of $Q_{gb} = 210$ kJ/mol and a lower pre-exponential factor of $D_0 = 2*10^{-4}$ m^2s^{-1} were used for modeling. The stress at RT and the slope of the linear regime of the stress-temperature curves were adjusted to the experimental data. While the heating curves of NiAl films with a thickness smaller than 0.6 µm can be described in this way, significant deviations occurred for thicker films. The calculated stresses at 690 °C for films thinner than 1.0 µm are compared in figure 4-10 to the experimental values. While the measured compressive stresses for films thinner than 0.8 µm are roughly predicted by the model, the stress for a 1.0 µm thick film was overestimated by 280 MPa. The difference between predicted and experimental value is even more pronounced for the 3.0 µm thick film where the measured compressive stress at 690 °C is only about 100 MPa in contrast to a calculated stress of 630 MPa. It can be concluded that constrained diffusional creep is dominant for films with a thickness smaller than 0.8 µm but is not the major relaxation process for the 3.0 µm thick films. Instead, the decrease in compressive stress at 690 °C for films thicker than 0.8 µm may indicate the action of thermally-activated dislocation processes which are more pronounced in thicker films with larger grains. Therefore, it is postulated that, for the NiAl films with an Al content of 48.5 at-% at a thickness of 0.8 to 1.5 µm, a transition from diffusion controlled to dislocation controlled plasticity occurred. For films with a thickness of 1.1 ± 0.2 µm, which is in the postulated transition zone, the contribution of diffusional creep to plastic deformation at high temperatures is accentuated by the variation of the Al content from 45 to 50 at-%: the stress at 690 °C was found to be lower for the off-stoichiometric composition (figure 4-12) which agrees with creep results on bulk NiAl [8]. This supports the contribution of a diffusional process, since the diffusivity in NiAl increases with deviation from stoichiometry [7].

Cyclic deformation

Another important result of this work is the finding that the slope of the linear regimes in stress-temperature curves increased with decreasing film thickness (figures 4-6 and 4-7). The texture and thus the elastic properties did not depend on film thickness indicating that the change in slopes is not an elastic effect. It is also not expected that constrained diffusional creep caused the differences in slope because the slopes in the linear regimes were similar during both heating and cooling, although the temperature regimes were very different. The following tentative explanation for this experimental finding is proposed.

It is assumed that dislocation plasticity during thermal cycling induced a kinematic strain hardening effect which lowered the stress-temperature slopes during heating and cooling. The degree of dislocation-based plasticity seems to be proportional to the descent in slope with respect to the "ideal" elastic slope. In a temperature cycle to 700 °C strong plastic deformation occurred in 3.0 µm thick films, while films with a thickness less than 0.8 µm showed only a small amount of plasticity with an increasing contribution of diffusional creep as discussed above. As a consequence, cooling from 700 °C yielded a larger slope for thinner films due to a smaller amount of plastic strain introduced upon heating. This is confirmed by the stress-temperature cycles of the 3.0 µm thick films which were heated to different maximum temperatures in the range of 200 to 700 °C. Above 400 °C, the stress-temperature curves of the 3.0 µm films deviated from the linear line indicating the onset of plastic yielding (see figure 4-8). As a result, pure elastic behavior and, thus, the highest slope is expected upon cooling from about 400 °C as it is observed experimentally (figure 4-9). If the temperature exceeded 400 °C, plastic deformation occurred on heating which subsequently lowered the slope upon cooling. This became more pronounced with increasing T_{max} (figure 4-9) which is associated with an increase in plastic deformation. A similar behavior was observed during heating. The slope upon heating from 40 °C also decreased with increasing plastic strain introduced during cooling in the preceding cycle. The smaller slopes observed upon cooling from temperatures below 400 °C (figure 4-9) can also be correlated to plastic deformation during cooling in the preceding temperature cycle. As a consequence, the linear slope comprises an elastic and an inelastic proportion, the latter depending on the plastic strain history. The inelastic proportion p_{in} of the slope is calculated as:

$$p_{in} = \frac{m_{el} - m_{\exp}}{m_{el}}, \qquad (4\text{-}7)$$

where m_{exp} is the experimentally determined slope and m_{el} is the pure elastic slope which was assumed to 3.25 MPa/K as measured for a 3.0 µm film upon cooling from 400 °C. The amount of plastic strain during heating was determined from the stress-temperature curves of films with a thickness of 0.8 to 3.0 µm heated to 700 °C and of 3.0 µm films heated to a maximum temperatures between 400 and 700 °C. Films thinner than 0.8 µm were not considered, since plastic deformation upon heating was very small and, as discussed above, believed to be dominated by constrained diffusional creep which would not contribute to the inelastic effect. The elastic ΔT_{el}, inelastic ΔT_{in} and plastic proportion ΔT_{pl} of a stress-temperature cycle is shown in figure 4-15 a for a 3.0 µm thick film. For plastic strain determination, two lines with the pure elastic slope of 3.25 MPa/K were applied to the curves (figure 4-15 a). One line intercepted the heating curve at the point where it deviates from the linear line which indicates the onset of plastic yielding. Another line was applied to the data point at T_{max}. The plastic strain ε_{pl} was calculated from the distance ΔT_{pl} between the two lines according to:

$$\varepsilon_{pl} = \Delta T_{pl} * (\alpha_{NiAl} - \alpha_{Si}), \qquad (4\text{-}8)$$

where α_{NiAl} and α_{Si} are the thermal expansion coefficients of the NiAl films and the Si substrate, respectively, as given in section 4.2.3. Figure 4-15 b shows that the inelastic proportion increases linearly with plastic strain independent of whether variations in film thickness or in T_{max} were considered. This dependency confirms, that the linear slope upon cooling can be directly correlated to the amount of plastic deformation introduced in the film upon heating.

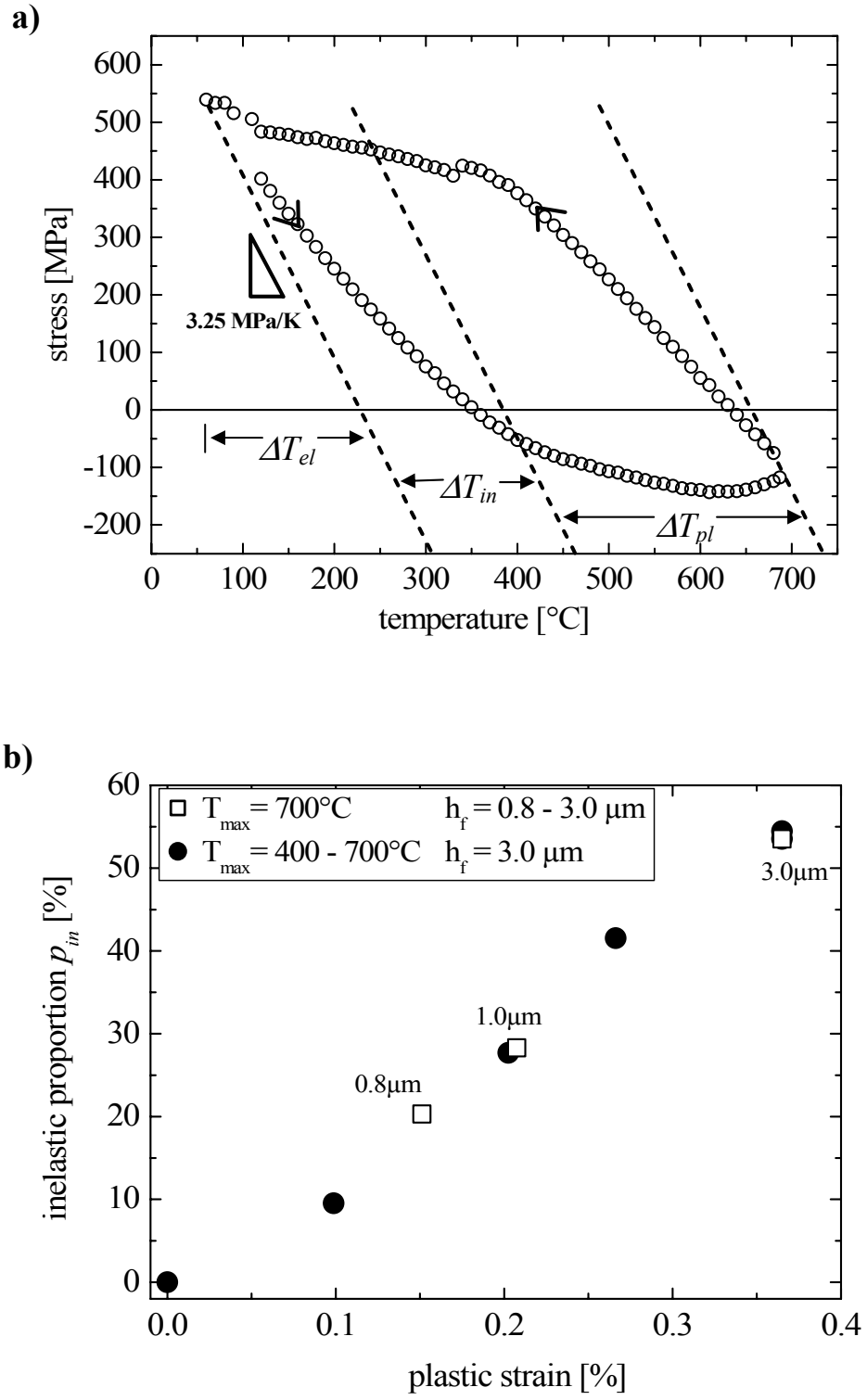

Figure 4-15 **(a) The elastic ΔT_{el}, inelastic ΔT_{in} and plastic proportion ΔT_{pl} of a stress-temperature cycle to 700 °C are shown for a 3.0 µm thick film. For the determination, linear lines with the elastic slope of 3.25 MPa/K were applied to the stress temperature curve. The plastic strain was calculated from ΔT_{pl} according to equation (4-8) (see text). (b) The inelastic proportion of the slope increases with increasing amount of plastic strain introduced in the film. Different plastic strains were achieved by thickness variations of films cycled to T_{max} = 700 °C and variations in T_{max} for 3.0 µm thick films. The individual film thicknesses are given next to the data points.**

On the microscopic level, the following mechanism is proposed to account for the kinematic strain hardening effect. In thicker films plastic deformation is most likely governed by the motion of dislocations (see e.g. figure 4-2). The relatively small grain sizes of the NiAl films could result in dislocation pile-ups upon heating especially for thicker films due to the higher amount of plastic strain (see figure 4-6). During cooling from the maximum temperature, the thermal stresses are reduced which may result in a piecemeal dissolving of the dislocation pile-ups. It is speculated that the slope upon cooling is smaller because of the backward motion of dislocations from pile-ups even though the stress is lower than the yield strength. On further cooling, however, the tensile yield strength is reached leading to macroscopic yielding and the formation of new dislocation pile-ups. The plastic deformation upon cooling in turn affects the slope upon subsequent heating. As a consequence, the elastic behavior is superimposed by a kinematic hardening effect which may be caused by the "reversible" motion of dislocations. TEM observations on 3.0 μm thick films revealed dislocations in larger grains whereas smaller grains were mainly devoid of dislocations. This is a hint for strong dislocation activity in individual grains which may result in dislocation pile-ups. However, a clear microscopic evidence for the discussed kinematic strain hardening mechanism is still lacking.

4.4.3 Comparison with Cu and Al thin films

The microstructure of NiAl thin films does not follow the trends commonly observed for polycrystalline Cu and Al films. The NiAl median grain size is smaller than the film thickness, while typical grain size values found for polycrystalline Cu and Al films clearly exceed the film thickness [30, 31, 40, 46]. Furthermore, the NiAl film texture depends on the chemical composition, revealing {111}, {211} and {110} oriented grains, whereas Cu and Al films are predominantly {111}-textured [30, 31, 40, 90].

The thermo-mechanical behavior of the NiAl thin films can be compared to literature values for Cu and Al films. For Cu [30, 45-47], Al [31] and NiAl films (this work) the flow stresses increase with decreasing film thickness and grain size. This behavior is much more pronounced in the NiAl films where flow stresses of more than 2 GPa for 0.2 μm thick films were measured. The higher flow stress of NiAl films compared to Cu and Al films is thought to be caused by a higher Peierls stress and the lack of dislocations.

Constrained diffusional creep as a dominant deformation mechanism at elevated temperatures was postulated for both Cu [40, 91] and NiAl films. However, constrained diffusional creep upon heating was observed in Cu under compression [40, 91], while NiAl films showed diffusional stress relaxation in the tensile stress regime. This is related to the increased room temperature stresses of NiAl films. Diffusional creep begins at a higher temperature for NiAl than for Cu, since the grain boundary diffusivity is lower in NiAl. An oxide passivation layer inhibits constrained diffusional creep for both NiAl and Cu [40, 91].

The slope of the linear stress-temperature regime for the NiAl films depended on the degree of prior plastic strain. While this behavior has recently been observed for Cu thin films [92], it has not been systematically investigated.

4.5 Summary

This section describes the influence of film thickness (0.2 to 3.1 μm), grain size (0.2 to 0.8 μm) and chemical composition (45 to 50 at-% Al) on the plasticity of NiAl thin films in the temperature range of 20 to 700 °C. The NiAl films were sputter-deposited on Si substrates and subjected to a maximum thermal strain of 0.84 %. The stress evolution during thermal cycling was measured using the substrate-curvature technique. The findings can be summarized as follows:

- Independent of chemical composition, all films showed equiaxed grains which were usually smaller in diameter than the film thickness. The grain size was found to increase from 0.2 to 0.8 μm with increasing film thickness from 0.2 to 3.1 μm.
- The tensile yield strength of NiAl films (48.5 at-% Al) was determined from the stress-temperature curves during cooling and increased significantly with decreasing film thickness. This effect is more pronounced than for the room temperature flow stresses of Cu and Al thin films.
- An accelerated tensile stress relaxation was observed in unpassivated NiAl films above 400 °C which was attributed to constrained diffusional creep. The formation of an oxide layer during thermal straining suppressed this effect during the second and subsequent heating cycles.
- The stress relaxation of NiAl films (48.5 at-% Al) at temperatures above 650 °C depends on film thickness: While films thinner than 0.8 μm showed a stronger stress relaxation with decreasing film thickness, the opposite behavior was found for thicker films. It is argued that diffusional creep is dominant in films thinner than 0.8 μm while plastic deformation in 3.0 μm thick films is governed by dislocation plasticity. The transition occurs at a film thickness of approximately 1 μm.
- Variations in the chemical composition of the films affect the stress relaxation above 600 °C: NiAl films with a thickness of about 1 μm revealed an increase in stress relaxation when deviating from stoichiometry to an Al content of 45 at-%. A deviation from stoichiometry increases the diffusivity and favors the contribution of constrained diffusional creep over the plastic deformation.
- The amount of plastic strain during the cyclic deformation influences the slope of the linear stress-temperature regime during heating and cooling. For instance, a

plastic strain of 0.36 % on heating leads to a decrease in the slope from 3.1 to 1.6 MPa/K on subsequent cooling. This behavior was tentatively explained by a kinematic strain hardening effect caused by the motion of dislocations.

5 Summary of the thermo-mechanical behavior of NiAl thin films

NiAl thin films with Al contents of 45 to 52 at-% and film thicknesses of 0.2 to 3.1 μm were studied in order to analyze the influence of chemical composition and geometrical and microstructural size effects on the yield strength, fracture stress and fracture toughness of polycrystalline NiAl thin films. The films were deposited via magnetron co-sputtering onto Si substrates with a thin amorphous Si_3N_4 diffusion barrier. The thermo-mechanical behavior was determined by thermal straining of the films between room temperature and 700 °C. The difference in thermal expansion coefficients between NiAl and the Si substrate induced biaxial stresses in the film during thermal cycling.

All NiAl films were found to be polycrystalline and consisted solely of the intermetallic phase β–NiAl. The mean grain size, which was slightly smaller than the film thickness, increased with film thickness. The results on the mechanical behavior of the NiAl films can be divided into two parts: (1) the cracking behavior of Al-rich films and (2) plastic deformation of stoichiometric and Ni-rich films.

Cracking behavior

The cracking behavior of the NiAl films depends on the chemical composition. NiAl films with a surplus of Al (Al content > 50 at-%) were found to have a lower fracture toughness than stoichiometric and Ni-rich films. While all stoichiometric and Ni-rich films remained devoid of cracks during thermal cycling, Al-rich films exhibited crack formation upon cooling from temperatures above 600 °C. The cracks in the Al-rich films formed crack networks with a characteristic pattern. The cracks extended throughout the entire film thickness and even reached into the Si substrate. The fracture stress measured during cooling from temperatures above 600 °C was found to increase with decreasing film thickness, indicating that the film thickness corresponds to a critical crack length. The fracture toughness was found to be almost independent of film thickness with values ranging from 2.2 to 2.9 MPa $m^{1/2}$. The fracture toughness of the Al-rich films was calculated from the fracture stress, with consideration of the crack geometry based on a model developed by Beuth [21] and Ye et al. [27].

Plastic deformation

Size effects on the deformation behavior were studied using stoichiometric and Ni-rich films. The tensile yield strength of Ni-rich films (48.5 at-% Al) was determined during cooling below 400 °C and was found to increase strongly with decreasing film thickness. While 3.0 µm thick films exhibited yield strength values of less than 500 MPa, a yield strength of more than 2000 MPa was measured for a 0.2 µm thick film of identical chemical composition. This behavior has not yet been reported for intermetallic films and is even more pronounced than reported for the room temperature flow stress of fcc metal films like Cu and Al. The higher yield strengths of the NiAl films compared to Cu and Al films were correlated to a higher Peierls stress and an increasing lack of dislocations with decreasing film thickness.

At elevated temperatures above 400 °C, a strong tensile stress relaxation was observed during heating in Ni-rich films thinner than 1.0 µm. This effect, attributed to constrained diffusional creep, is more pronounced in thinner NiAl films due to the smaller grain sizes. Constrained diffusional creep has also been postulated for the relaxation of compressive stresses of thin Cu films upon heating [30, 40]. The major differences to the Cu films are the higher temperature and the tensile stress state for the occurrence of stress relaxation in the NiAl films. The formation of a native oxide after the first temperature cycle is suggested to obstruct the relaxation of tensile stresses at 400 °C, so that diffusional creep only occurred above 600 °C in later cycles. Variations in the Al content accentuated the contribution of constrained diffusional creep: the creep strength of 1 µm thick NiAl films above 600 °C decreased with increasing deviation from stoichiometry, due to enhanced diffusivity. However, the deformation mechanism seems to change with increasing film thickness: films thinner than 1.0 µm agree with stress predictions based on constrained diffusional creep, while films thicker than 1.0 µm exhibit stresses that are lower than predicted. In this case dislocation plasticity is believed to be dominant based on TEM studies of a 3.0 µm thick film.

The linear regimes of stress-temperature curves of Ni-rich films revealed significantly different slopes. This unexpected behavior is more pronounced in thicker films and is tentatively explained with kinematic strain hardening. It is demonstrated that the amount of plastic strain introduced in the film determines the slope of the stress-temperature curves.

6 Appendix A: Sample overview

This appendix summarizes the processing parameters and characterization techniques used for the NiAl films of this study. The power P_{Ni} and P_{Al} for the Ni and the Al target during the co-sputter process determined the chemical composition. Note that slight changes in the sputter geometries affected the adjustment of the Al content of the films. For this reason, a new batch of samples with similar power values for Ni and Al led to slightly different Al contents.

The chemical analysis was carried out either by microprobe analysis (WDX) or optical emission spectroscopy (OES). The microstructural analysis comprise techniques like FIB, SEM and / or TEM. The last column describes the number of stress-temperature cycles carried out in N_2 atmosphere.

Table A-1 Overview of the investigated NiAl films with a surplus of Al (Al content > 50.2 at-%) used for the study of the cracking behavior of NiAl films. See text for details.

Al content [at-%]	h_f [µm]	sample number	P_{Ni} [W]	P_{Al} [W]	UHV annealed 600°C	chemical analysis	micro-structural analysis	XRD analysis	stress-temperature cycles
50.4	1.0	[55]	150	182			√	√	1
50.4	4.0	[12an]	150	178		√			
50.7	1.0	[09]	150	170	√	√	√	√	
50.7	1.0	[10]	150	170	√	√		√	
50.7	1.0	[36]	150	170	√		√		1
50.7	1.1	[18]	150	170	√		√	√	x
50.7	1.1	[25]	150	170	√		√	√	1
51.5	1.0	[23]	150	178	√	√	√	√	
51.5	1.0	[26]	150	178	√		√		x
51.5	1.0	[27]	150	178	√		√	√	
52.2	0.6	[69]	135	194			√		3
52.2	0.6	[72]	135	194		√			
52.2	0.8	[67]	135	194			√		1
52.2	1.0	[64]	135	194			√	√	1
52.2	1.5	[66]	135	194			√	√	1
52.2	3.0	[68]	135	194			√		1
52.4	0.4	[57]	150	194			√	√	2
52.4	1.0	[53]	150	194			√	√	2
52.4	1.0	[54]	150	194			√	√	
52.4	4.0	[13an]	150	194		√			

x: only stress measurement at room temperature after UHV annealing.

Table A-2 Overview of the investigated NiAl films which are of stoichiometric or Ni-rich composition (Al content ≤ 50.2 at-%) mainly used for the study of plasticity in the NiAl films. See text for details.

Al content [at-%]	h_f [µm]	sample number	P_{Ni} [W]	P_{Al} [W]	UHV annealed 600°C	chemical analysis	micro-structural analysis	XRD analysis	stress-temperature cycles
50.2	1.1	[01an]	150	162		√		√	
50.2	1.1	[02an]	150	162			√	√	
50.2	1.1	[02]	150	162	√	√	√	√	3
50.2	1.1	[03]	150	162	√		√	√	
50.2	1.1	[07]	150	162	√		√		3
50.2	1.1	[12]	150	162	√		√	√	2
50.2	1.1	[16]	150	162	√		√		7
49.0	0.4	[37]	150	162	√		√	√	2
49.0	0.4	[39]	150	162	√		√		x
49.0	1.1	[38]	150	162	√	√	√	√	
49.0	3.1	[31]	150	162	√		√		12
49.0	3.1	[32]	150	162	√		√		
49.0	3.1	[34]	150	162	√		√	√	1
48.5	0.2	[45]	150	162	√				2
48.5	0.2	[45dw]	150	162	√		√	√	
48.5	0.4	[42]	150	162	√			√	5
48.5	0.4	[48]	150	162	√		√		2
48.5	0.6	[43]	150	162	√				1
48.5	0.6	[49]	150	162	√		√	√	3
48.5	0.8	[44]	150	162	√		√		1
48.5	0.8	[44dw]	150	162	√	√	√	√	
48.5	0.8	[50]	150	162	√		(√)		9
48.5	1.0	[40]	150	162	√				x
48.5	1.0	[47]	150	162	√		√	√	2
48.5	3.0	[41]	150	162	√		√	√	
48.5	3.0	[46]	150	162	√		√		8
48.5	4.0	[11an]	150	162		√		√	
47.7	1.2	[15]	150	154	√		√	√	1
47.7	1.2	[17]	150	154	√		√		3
47.7	1.3	[22]	150	154	√			√	
47.7	3.0	[20]	150	154		√	√	√	
46.1	1.3	[21]	150	146	√			√	2
46.1	1.3	[24]	150	146	√		√	√	1
46.1	3.0	[19]	150	146		√	√	√	
45.0	1.2	[28]	150	138	√	√	√	√	
45.0	1.2	[29]	150	138	√		√	√	7

x: only stress measurement at RT after UHV annealing.
(√): only optical microscopy investigations.

Appendix B: X-ray diffraction profiles

XRD measurements in Bragg-Brentano geometry (θ - 2θ measurements) were carried out on various films, in order to check that the films were single-phase NiAl and to determine the texture of the films. In the following, the XRD profiles of 1.1 ± 0.2 µm thick NiAl films with Al contents of 45.0 to 51.5 at-% Al after UHV annealing are shown. The peaks at 2θ = 62° and at 2θ = 69° are the K_β and the K_α reflections of the Si (400) planes. The other peaks refer to β-NiAl. The corresponding NiAl planes are given next to the peaks.

Figure B-1 XRD profiles (θ-2θ measurements) of 1.1 ± 0.2 µm thick NiAl films with Al contents ranging from 51.5 to 45.0 at-% Al. The peaks at 2θ = 62° and at 2θ = 69° refer to the Si (400) planes of the substrate.

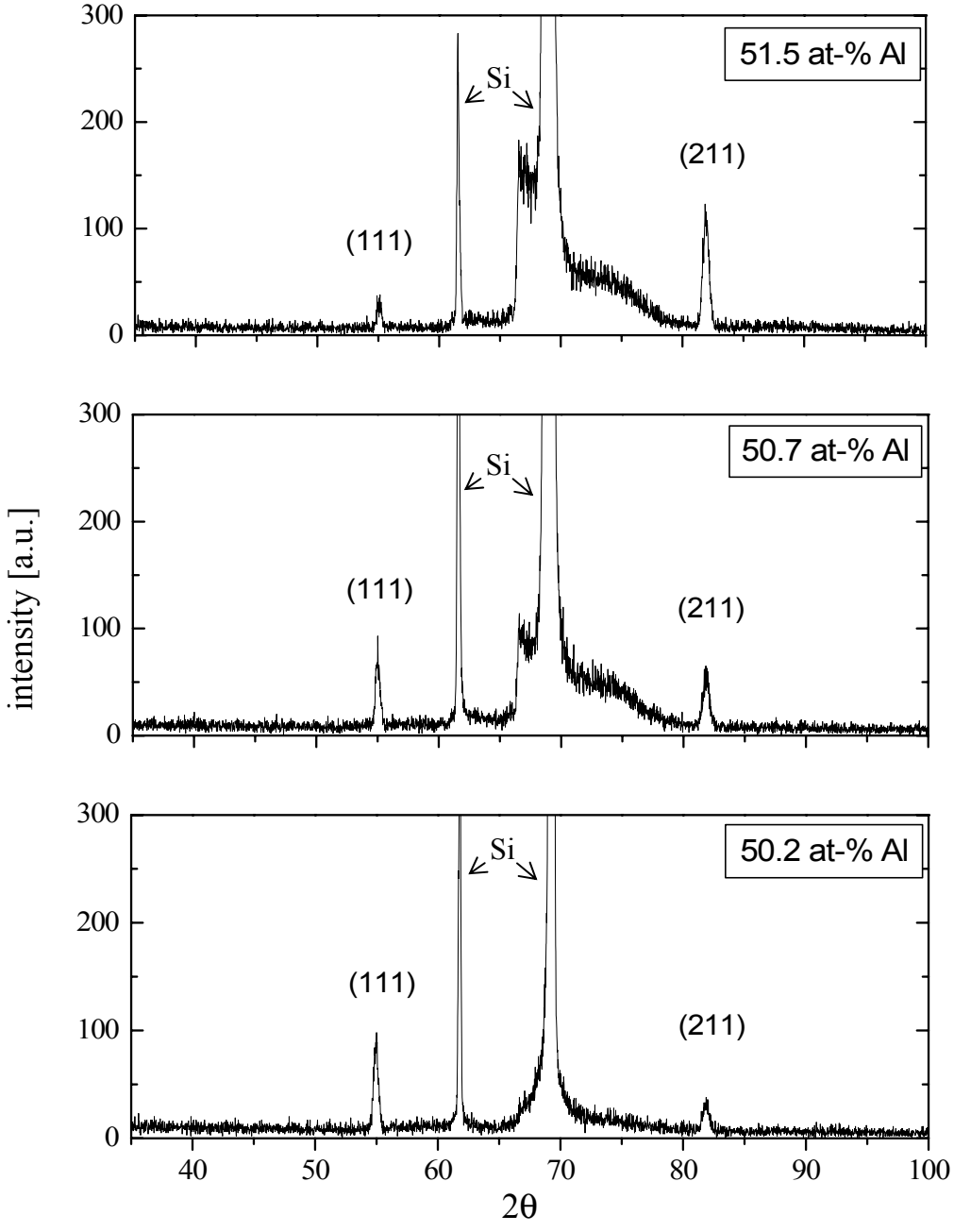

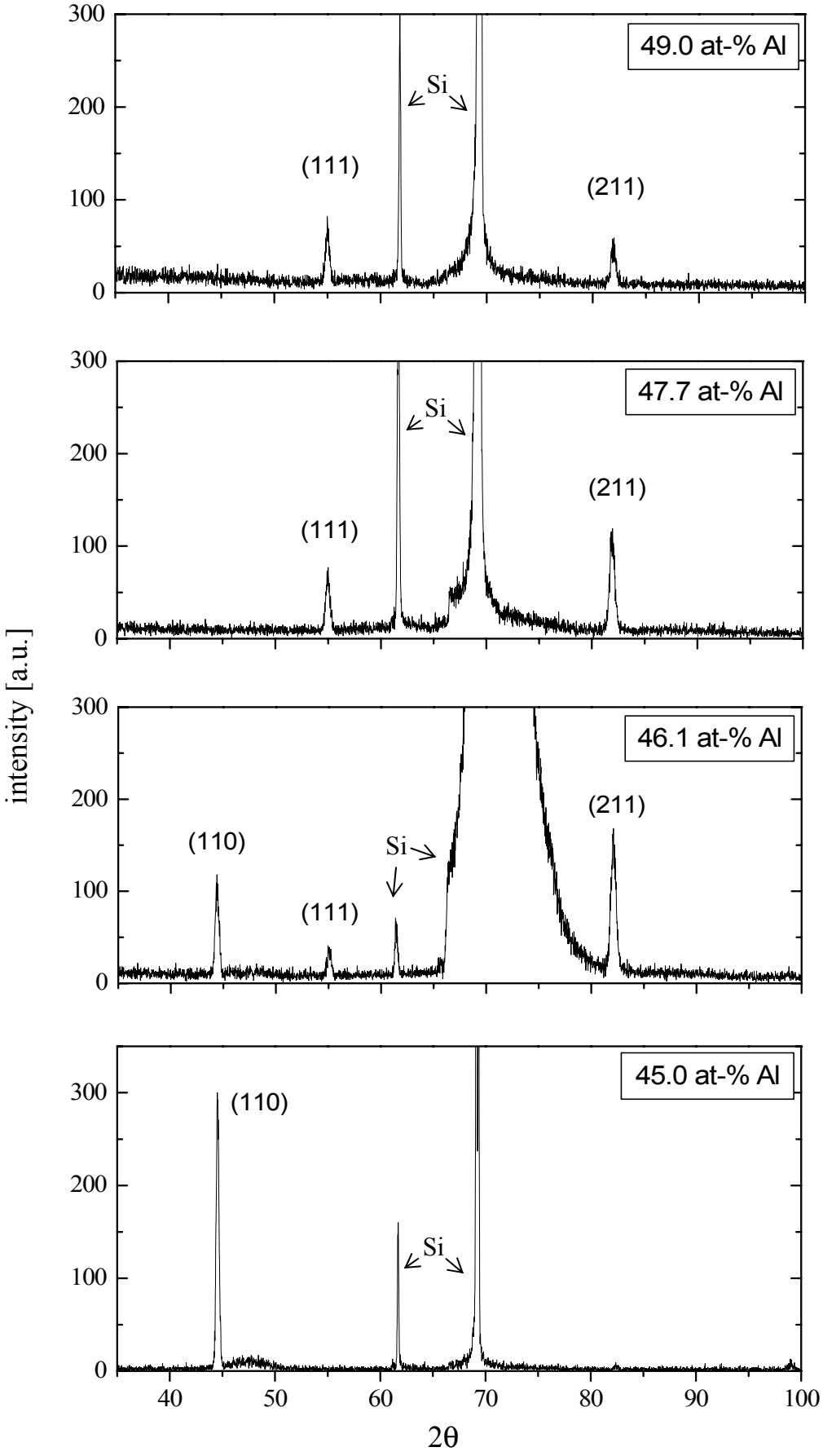
49.0 at-% Al
47.7 at-% Al
46.1 at-% Al
45.0 at-% Al
(111)
(211)
(110)
Si
intensity [a.u.]
2θ
0
100
200
300
40
50
60
70
80
90
100

7 Kurzfassung der Dissertation in deutscher Sprache

Einleitung

Die Lebensdauer von Turbinenschaufeln, die z.B. in Flugzeugturbinen Anwendung finden, wird technisch durch eine Beschichtung der Schaufeln deutlich erhöht. Turbinen-Werkstoffe auf der Basis von Nickel werden durch eine NiAl-Beschichtung gegenüber Oxidation und Korrosion geschützt und ermöglichen so Betriebstemperaturen von über 1000 °C. Neben der chemischen Schutzwirkung ist allerdings auch das mechanische Verhalten dieser NiAl-Beschichtungen für den technischen Betrieb von größter Bedeutung.

Obwohl technische NiAl-Beschichtungen auf ihre Zuverlässigkeit getestet werden, ist der Einfluss von Schichtdicke, chemischer Zusammensetzung und Mikrostruktur auf das mechanische Verhalten nur unzureichend bekannt. Dabei stehen zwei Aspekte im Vordergrund: Erstens müssen die Schichten im Betrieb bei hohen Temperaturen einen guten Widerstand gegenüber plastischer Verformung aufweisen. Zweitens ist eine ausreichende Bruchzähigkeit bei niedrigen Temperaturen notwendig, da beim Abkühlen thermische Spannungen in der Schicht auftreten.

Untersuchungen an dünnen Metallschichten wie z.B. an Cu und Al haben gezeigt, dass sich Metalle mit geometrischen und mikrostrukturellen Dimensionen von wenigen Mikrometern deutlich anders verhalten als das entsprechende Massivmaterial. Die Fließspannung von dünnen Metallschichten überschreitet die des Massivmaterials um ein Vielfaches und steigt mit abnehmender Schichtdicke weiter an [2]. Von NiAl als Massivmaterial ist bereits bekannt, dass es mikrostrukturelle Größeneffekte gibt, die sich auf die mechanischen Eigenschaften auswirken. So wurde beobachtet, dass sich die Verformbarkeit von polykristallinem NiAl bei 400 °C stark erhöht, wenn die Korngröße einen Wert von 20 µm unterschreitet [43]. Außerdem ergaben Kriechversuche, dass in feinkristallinem NiAl mit einer Korngröße von 20 µm diffusionskontrollierte Verformungsprozesse stattfinden, während grobkristallines NiAl sich vorwiegend durch Versetzungsprozesse plastisch verformt [44]. Es ist jedoch bisher nicht bekannt, ob sich diese Größeneffekte weiter verstärken, wenn die Korngröße und die geometrischen

Abmessungen im Bereich von wenigen Mikrometern oder sogar darunter liegen, wie es typischerweise bei dünnen Schichten der Fall ist.

In dieser Arbeit wurde der Einfluss von Schichtdicke, Korngröße und chemischer Zusammensetzung auf das thermo-mechanische Verhalten von NiAl-Schichten anhand eines Modellsystems untersucht. Dabei wurde sowohl die Bruchzähigkeit als auch die plastische Verformbarkeit von polykristallinen NiAl-Schichten mit Schichtdicken zwischen 0.2 und 3.1 μm charakterisiert.

Experimentelles Vorgehen

NiAl Schichten wurden mittels eines Magnetron-Co-Sputter-Verfahrens auf Si-Substrate abgeschieden. Die unbeschichteten Si-Substrate wurden vor der NiAl-Abscheidung auf beiden Seiten mit einer je 50 nm dicken Diffusionsbarriere aus SiO_2 und Si_3N_4 beschichtet und durch Ionenbeschuss gereinigt. Für die anschließende Beschichtung mit NiAl wurden Targets aus reinem Al und reinem Ni verwendet. Durch Variation der Sputterzeit und der Sputterleistung der Targets wurden Schichtdicken von 0.2 bis 3.1 μm und chemische Zusammensetzungen von 45 bis 52 at-% Al erreicht. Nach der Abscheidung wurde ein Teil der Schichten direkt in der Sputterkammer im Ultrahochvakuum (UHV) für eine Stunde bei 600 °C ausgelagert.

Die chemische Zusammensetzung der NiAl-Schichten wurde mittels optischer Emissionsspektroskopie (OES), Auger-Elektronen Spektroskopie (AES) und wellenlängen-dispersiver Röntgenspektroskopie (WDX) bestimmt. Zur Charakterisierung der Mikrostruktur wurde die fokussierte Ionenstrahl- (FIB), die Rasterelektronen- (REM) und die Transmissionselektronenmikroskopie (TEM) verwendet. Mit dem FIB-Mikroskop wurde an Querschnittsproben die Dicke der NiAl Schichten bestimmt. Die Textur der NiAl-Schichten wurde mittels Röntgenbeugungsexperimenten (XRD) untersucht.

Zur Charakterisierung des mechanischen Verhaltens der NiAl-Schichten wurden Temperatur-Zyklen in einer schützenden N_2-Atmosphäre durchgeführt. Dabei machte man sich zunutze, dass bei Temperaturänderungen aufgrund der unterschiedlichen Wärmeausdehnung von Schicht und Substrat biaxiale Spannungen in der Schicht entstehen. Dies führt zu einer elastischen Krümmung des Substrates. Die Krümmung wurde mit Hilfe eines optischen Systems gemessen und daraus die Schichtspannung bestimmt. Anhand der gemessenen Spannungs-Temperatur-Kurven konnte das

mechanische Verhalten der Schichten charakterisiert werden. Zum besseren Verständnis der Spannungsentwicklung in den NiAl-Schichten wurden gezielte mikrostrukturelle Untersuchungen vor und nach den Temperaturzyklen durchgeführt. Zusätzlich wurden ausgewählte Schichten *in situ* im REM und im TEM thermisch zykliert, um mikrostrukturelle Veränderungen während des Temperaturzyklus zu untersuchen.

Ergebnisse

Alle NiAl-Schichten bestanden nach der Auslagerung bei 600 °C aus einphasigem β-NiAl mit CsCl-Struktur und hatten eine polykristalline Mikrostruktur mit mittleren Korngrößen die zumeist kleiner als die Schichtdicke waren (Abbildung C-1). Die Schichten zeigten eine Fasertextur, wobei die Texturanteile mit der chemischen Zusammensetzung variierten. Für Schichten mit einer chemischen Zusammensetzung nahe der Stöchiometrie wurden vor allem {111} und {211} Texturanteile gefunden. Sehr Ni-reiche Schichten (Al-Gehalt ≤ 46 at-%) zeigten auch {110} Texturanteile.

Die Ergebnisse zum thermo-mechanischen Verhalten der NiAl-Schichten lassen sich in zwei Teile untergliedern. Der erste Teil beschreibt das Rissverhalten, während im zweiten Teil Ergebnisse zum plastischen Verhalten der Schichten vorgestellt werden.

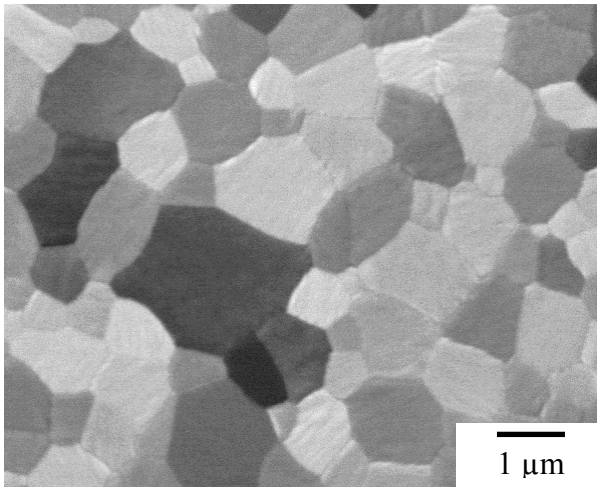

Abbildung C-1 FIB Aufnahme einer 1.3 µm dicken polykristallinen NiAl-Schicht (46 at-% Al) nach einer Auslagerung im UHV bei 600 °C. Die mittlere Korngröße der Schichten ist zumeist kleiner als die Schichtdicke.

Rissverhalten der NiAl-Schichten

Beim Abkühlen von der Auslagerungstemperatur von 600 °C auf Raumtemperatur (RT) wurden aufgrund des größeren thermischen Ausdehnungskoeffizienten von NiAl im Vergleich zu Si Zugspannungen in den NiAl-Schichten erzeugt. Dabei wurde an 1 µm dicken NiAl-Schichten ein deutlicher Einfluss der chemischen Zusammensetzung auf die Bruchzähigkeit beobachtet: Während Schichten mit einer Al-Konzentration von 45 bis 50 at-% nach dem Abkühlen auf RT keine Risse aufwiesen, bildeten sich in NiAl-Schichten mit einem Überschuss von Al (51 bis 52 at-% Al) bei der identischen thermischen Beanspruchung Rissnetzwerke aus (Abbildung C-2). Mikroskopische Untersuchungen zeigten, dass sich die Risse hauptsächlich entlang von Korngrenzen ausbreiteten. Des weiteren erstreckten sich die Risse über die gesamte Dicke der Schicht und breiteten sich auch in das Substrat aus.

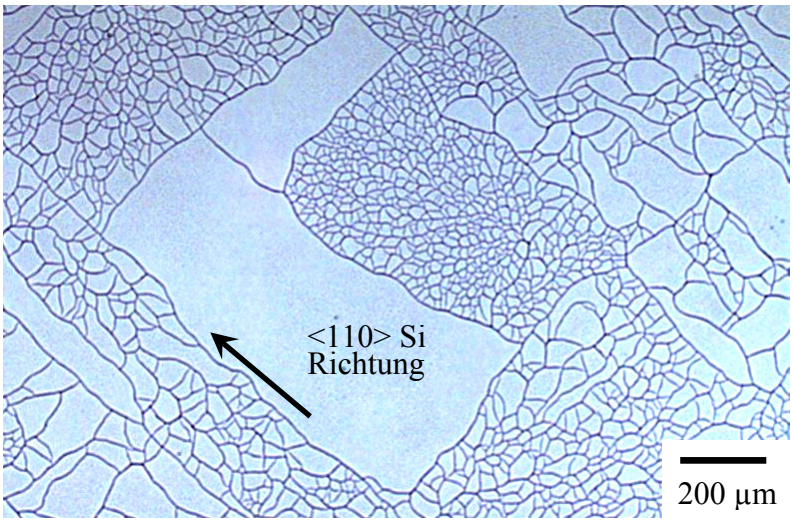

Abbildung C-2 Lichtmikroskopische Aufnahme einer 1.0 µm dicken NiAl-Schicht (52 at-% Al) nach einem Temperaturzyklus bis 600 °C. Beim Abkühlen ist ein charakteristisches Netzwerk aus Rissen entstanden, dass teilweise von der kristallographischen Orientierung des Si-Substrates bestimmt wurde.

Zur Bestimmung der Bruchspannung wurden nicht ausgelagerte, Al-reiche NiAl-Schichten bis zu einer Maximaltemperatur T_{max} = 700 °C thermisch zykliert und der Spannungsverlauf als Funktion der Temperatur experimentell ermittelt. Beim Abkühlen von T_{max} bildeten sich Zugspannungen in der Schicht, die mit abnehmender Temperatur kontinuierlich zunahmen. Bei Temperaturen unterhalb 400 °C wurde dann in den Al-reichen Schichten ein Abfall der Spannung gemessen. Anhand von Temperaturzyklen, die *in situ* im REM erfolgten, konnte dieser Spannungsabfall mit der Bildung von Rissen korreliert werden. Die erreichte Maximalspannung vor der Spannungsreduzierung wurde als Bruchspannung definiert. Durch Variation der Schichtdicke bei nahezu konstantem Al-Gehalt von 52 at-% wurde gefunden, dass dünnere Schichten einer höheren Zugspannung standhielten als dickere Schichten. Während 3.0 µm dicke Schichten Bruchspannungen von weniger als 600 MPa aufweisen, beträgt die Bruchspannung in einer 0.4 µm dicken Schichten 2000 MPa (Abbildung C-3). Im Gegensatz zur Schichtdicke ändert sich die Bruchspannung bei einer Variation der Korngröße nur unwesentlich. So zeigen 1 µm dicke NiAl-Schichten mit einer mittleren Korngröße von 0.1 und 0.3 µm eine nahezu identische Bruchspannung von 1100 MPa.

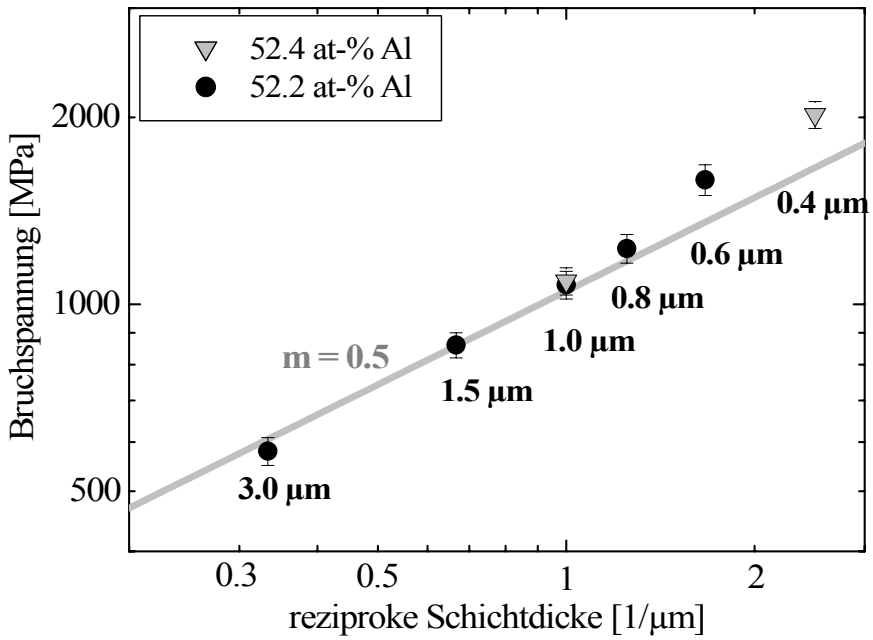

Abbildung C-3 Die Bruchspannung von NiAl-Schichten mit einem Al-Gehalt von ca. 52 at-% steigt mit abnehmender Schichtdicke stark an. Die Schichtdicke ist bei den jeweiligen Datenpunkten mit angegeben.

Plastisches Verhalten der NiAl-Schichten

Aufgrund der Rissbildung in den Al-reichen Schichten beim thermischen Zyklieren wurde das plastische Verhalten an stöchiometrischen und Ni-reichen Schichten untersucht, die bei thermischen Behandlungen stets rissfrei blieben.

Nach der Auslagerung bei 600 °C wurden bei RT in NiAl-Schichten mit einem Al-Gehalt von 48.5 at-% in dünneren Schichten wesentlich höhere Spannungen als in dickeren Schichten gemessen. In 0.2 µm dicken Schichten erreichten die Spannungen Werte von über 2000 MPa, während in 3.0 µm Schichten lediglich Spannungen von ungefähr 500 MPa gemessen wurden. Dabei liegt die Ursache der Spannungsunterschiede nicht in der Bildung von Rissen wie es bei den Al-reichen Schichten beobachtet wurde.

Die Spannungsmessungen während des thermischen Zyklierens gaben weiteren Aufschluss über den Einfluss der Schichtdicke auf das thermomechanische Verhalten. Bei allen Schichten wurde beim Aufheizen von RT die Zugspannungen in der Schicht kontinuierlich abgebaut und bei Temperaturen über 400 °C entstanden Druckspannungen (Abbildung C-4). Beim Abkühlen werden dann wieder Zugspannung erzeugt, so dass bei RT nahezu die Ausgangspannung vor Beginn des Temperaturzyklus erreicht wurde. Während 3.0 µm dicke Schichten eine deutliche Hysterese in dem Spannungs-Temperatur-Verlauf zeigten, verhält sich die Spannung der 0.2 µm Schichten nahezu linear mit der Temperatur (siehe Abbildung C-4). Eine Abweichung vom linearen Bereich deutet auf plastische Verformung in der Schicht hin. Dickere NiAl-Schichten zeigten daher mehr plastische Verformung als dünnere Schichten.

Bei genauer Betrachtung der Spannungs-Temperatur-Kurven in Abbildung C-4 erkennt man, dass die Steigung des linearen Bereiches der Kurven mit zunehmender Schichtdicke abnimmt. Dies betrifft sowohl den Bereich des Aufheizens als auch den des Abkühlens. So wurde für eine 0.2 µm Schicht in einem Temperatur-Zyklus bis 700 °C eine Steigung von 2.8 MPa/K gemessen, während an einer 3.0 µm Schicht der gleichen chemischen Zusammensetzung die Auswertung des linearen Bereiches nur einen Steigung von 1.5 MPa/K ergab. Dies ist ein überraschendes Ergebnis, da die elastischen Eigenschaften eines Materials von der atomaren Bindung abhängen und sich bei gleich bleibender chemischer Zusammensetzung nicht ändern. Weitere Untersuchungen an 3.0 µm dicken Schichten zeigten, dass sich die Steigung des linearen Bereiches beim Abkühlen von 1.5 auf 3.0 MPa/K erhöhte, wenn die Probe statt bis 700 °C nur bis 400 °C zykliert wurde.

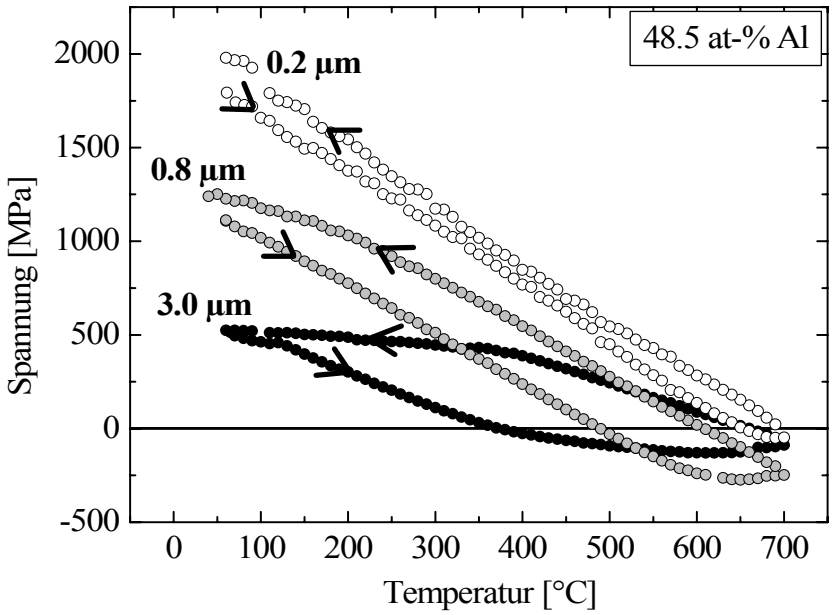

Abbildung C-4 Spannungsentwicklung in Ni-reichen NiAl-Schichten (48.5 at-% Al) während eines Temperaturzyklus bis 700 °C. In dünneren Schichten werden beim Abkühlen zur Raumtemperatur wesentlich höhere Spannungen erreicht.

Der Einfluss der chemischen Zusammensetzung auf das plastische Verhalten wurde besonders bei Temperaturen zwischen 650 und 700 °C deutlich: Durch eine Reduzierung des Al-Gehaltes von 50 auf 45 at-% wurden an 1 µm dicken Schichten die Druckspannungen von über 200 MPa auf unter 100 MPa reduziert. Durch die Verringerung des Al-Gehaltes wurde daher der Abbau von Spannungen durch plastische Verformung verstärkt.

Etwas komplizierter ist der Zusammenhang der Spannungen nahe 700 °C mit der Schichtdicke. Hier wurde eine Erhöhung der Druckspannungen von 50 MPa auf über 200 MPa mit zunehmender Schichtdicke von 0.2 auf 0.8 µm gemessen. Bei Schichten mit einer Dicke > 0.8 µm wurde der umgekehrte Trend gefunden. So betrug die Spannung einer 3 µm Schicht lediglich 100 MPa.

Diskussion

Rissverhalten der NiAl-Schichten

Al-reiche NiAl-Schichten zeigten eine größere Anfälligkeit für die Bildung von Rissen als stöchiometrische und Ni-reiche Schichten. Dieses Verhalten kann anhand von Bruchzähigkeitsmessungen an NiAl-Massivmaterial verstanden werden. Dabei spielen vor allem die Korngrenzen eine wesentliche Rolle, deren Festigkeit stark abnimmt sobald ein Überschuss an Al vorhanden ist [75]. Aufgrund der relativ kleinen Körnern in den NiAl-Schichten von oft weniger als 1 µm konnten sich die Risse leicht entlang der Korngrenzen ausbreiten.

Ein weiteres wesentliches Ergebnis dieser Arbeit ist die gemessene Zunahme der Bruchspannung mit abnehmender Schichtdicke. Dieser Zusammenhang konnte mit bestehenden Modellen zum Rissverhalten dünner Schichten korreliert werden [21, 22, 27]. Es wird angenommen, dass sich die Risse nach Erreichen der Bruchspannung mit einer konstanten Energiefreisetzungsrate durch den Schicht-Substrat-Verbund ausbreiten. Dabei skaliert die Bruchspannung σ_{fr} mit der Schichtdicke h_f nach der folgenden Beziehung:

$$\sigma_{fr} \propto h_f^{-0.5}$$

Dieser Zusammenhang wurde experimentell bestätigt und ist in Abbildung C-3 durch die Gerade mit einer Steigung von 0.5 gezeigt. Geringe Abweichungen von der eingezeichneten Gerade wurden mit Unterschieden in der Substratrisslänge erklärt.

Die Bruchzähigkeit der Al-reichen NiAl-Schichten (52 at-% Al) wurde mit Hilfe theoretischer Überlegungen von Beuth [21] und Ye et al. [27] und anhand der experimentellen Ergebnisse ermittelt. Dabei wurde neben der Bruchspannung und der Schichtdicke auch die Länge der Substratrisse und die Textur der Schichten berücksichtigt. Die Bruchzähigkeit K_C der Al-reichen Schichten wurde zu 2.2 bis 2.9 MPa $m^{1/2}$ bestimmt. Obwohl die Schichtdicke einen starken Einfluss auf die Bruchspannung hatte, ist die ermittelte Bruchzähigkeit nahezu unabhängig von der Schichtdicke. Die Schichtdicke entspricht einer kritischen Risslänge. Je größer die Schichtdicke desto weniger Spannung ist notwendig um die Rissausbreitung durch den Schicht-Substrat-Verbund zu erzwingen.

Im Vergleich zum NiAl-Massivmaterial wurden für die dünnen NiAl-Schichten geringere Bruchzähigkeiten gemessen. Es wird vermutet, dass dies vor allem auf den höheren Al-Gehalt zurückzuführen ist, da bisherige Untersuchungen zur Bruchzähigkeit von NiAl-Massivmaterial nur für stöchiometrische und Ni-reiche Zusammensetzungen durchgeführt wurden.

Plastisches Verhalten der NiAl-Schichten

Anhand der Spannungs-Temperatur-Kurven konnte die Fließspannung der NiAl-Schichten bestimmt werden. Dabei wurde das Abknicken vom linearen Bereich während des Abkühlens als der Beginn des Fließens definiert (siehe Abbildung C-4). In Analogie zu den gemessenen RT-Spannungen steigt die Fließspannung stark mit abnehmender Schichtdicke an (Abbildung C-5). Dieser Anstieg ist wesentlich ausgeprägter als es für Cu und Al bekannt ist [30, 31]. Es wird argumentiert, dass die Bildung von Versetzungen der limitierende Faktor für plastisches Fließen darstellt [36] und dies aufgrund des intermetallischen Charakters von NiAl noch ausgeprägter ist als bei Cu- und Al-Schichten. Diese Annahme wird durch TEM-Untersuchungen unterstützt: 3.0 µm dicke NiAl-Schichten zeigten eine Vielzahl von Versetzungen, in 0.2 µm dicken Schichten wurden stattdessen fast keine Versetzungen beobachtet.

Die Spannungs-Temperatur-Kurven der Ni-reichen NiAl-Schichten zeigten unterschiedliche Steigungen im linearen Bereich der Kurven obwohl sich die elastischen Eigenschaften nicht änderten. Zum besseren Verständnis dieses Effektes wurde anhand der Spannungs-Temperatur-Kurven die plastische Dehnung während des Aufheizens bestimmt und mit der Steigung im linearen Bereich beim Abkühlen korreliert. Dabei wurde gefunden, dass die Abweichung von der „rein elastischen“ Gerade beim Abkühlen direkt proportional zur eingebrachten plastische Verformung beim Aufheizen ist. Es wird vermutet, dass Versetzungen beim Aufheizen an Korngrenzen aufgestaut werden, die sich beim Abkühlen durch die Reduzierung der Spannung wieder lösen, obwohl die Fließspannung nicht erreicht ist. Die daraus resultierende Dehnung führt zu einem inelastischen Beitrag und zur Reduzierung der „elastischen“ Gerade.

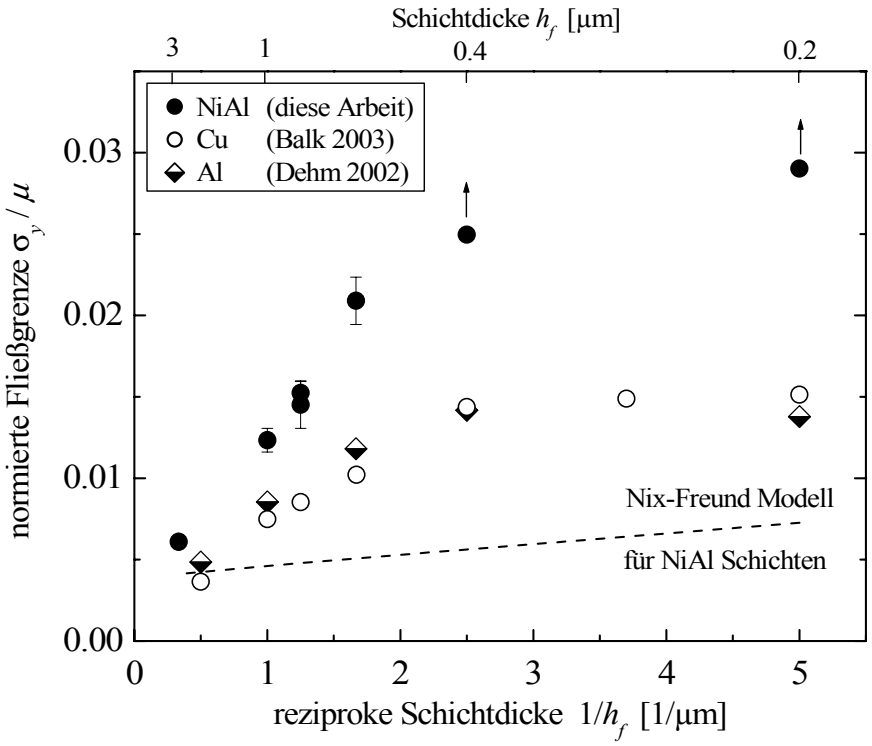

Abbildung C-5 Die auf den Schubmodul μ normierte Fließspannung σ_y von NiAl-Schichten (48.5 at-% Al) steigt mit abnehmender Schichtdicke stark an. Dieser Effekt ist in NiAl wesentlich ausgeprägter als in Cu [30] und in Al [31] und kann mit dem Modell von Nix [2] und Freund [33] nicht erklärt werden.

Die Änderungen in der Spannungsentwicklung durch die Variation von Schichtdicke und chemischer Zusammensetzung gaben Aufschluss über die zugrunde liegenden Verformungsprozesse beim thermischen Zyklieren. Die effektivere Spannungsreduzierung oberhalb 650 °C durch den Überschuss an Ni weist darauf hin, dass Diffusionsprozesse eine bedeutende Rolle spielen, da sich die Diffusivität mit Abweichung von der stöchiometrischen Zusammensetzung stark erhöht. So konnten Abweichungen vom linearen Verlauf der Spannung mit der Temperatur besonders bei Schichten dünner als 0.8 µm mit Diffusionskriechen erklärt werden. Dabei wurde das Modell von Gao et al. [41] angewandt, das die geometrischen Verhältnisse in dünnen Schichten berücksichtigt. Dem gegenüber zeigten NiAl-Schichten mit einer Dicke von mehr als 1.0 µm eine Spannungsentwicklung, die auch bei erhöhten Temperaturen auf Versetzungsplastizität hinweist.

Schlussfolgerung

In dieser Arbeit wurden dünne polykristalline NiAl-Schichten mittels eines Sputter-Prozesses auf Si-Substrate aufgebracht und ihr thermo-mechanisches Verhalten anhand Temperaturzyklen bis maximal 700 °C charakterisiert. Es ist gelungen, den Einfluss der chemischen Zusammensetzung und der Schichtdicke auf das mechanische Verhalten herauszustellen. So wurde gefunden, des Al-reiche Schichten eine geringere Bruchzähigkeit aufweisen als stöchiometrische und Ni-reiche Schichten. Variationen in der Schichtdicke an Al-reichen Schichten im Bereich von 0.4 bis 3.0 µm zeigten, dass dünnere Schichten wesentlich höheren Spannungen standhielten als dickere Schichten, bevor sich makroskopische Risse bildeten. Es konnte gezeigt werden, dass die Schichtdicke einer kritischen Risslänge entspricht, die für die Bildung von makroskopischen Rissen entscheidend ist. Die Bruchzähigkeit ist allerdings nahezu unabhängig von der Schichtdicke und wurde für die Al-reichen Schichten zu Werten zwischen 2.2 und 2.9 MPa $m^{1/2}$ bestimmt.

Die Fließspannung der Ni-reichen NiAl-Schichten bei Raumtemperatur stieg durch die Reduzierung der Schichtdicke von 3.0 auf 0.2 µm stark an. Dieser Effekt war wesentlich stärker ausgeprägt als es für Cu und Al bekannt ist. Durch das thermische Zyklieren und ergänzende mikrostrukturelle Untersuchungen konnten die zugrunde liegenden Verformungsmechanismen bei erhöhten Temperaturen bis 700 °C identifiziert werden. Dabei wurde ein Schichtdickeneffekt gefunden: NiAl-Schichten (48.5 at-% Al) mit Dicken unterhalb 1 µm zeigen ein für Diffusionskriechen typisches Verhalten, während das mechanische Verhalten von Schichten mit einer Dicke größer als 1 µm auf Versetzungsplastizität als dominierenden Verformungsmechanismus hinweist.

8 References

1. Rhys-Jones, T.N. and Bettridge, D.F.: *Adv. Mat. Proc. Techn. Struc. Appl.* (1988) 129-158.

2. Nix, W.D.: *Met. Trans. A* **20A** (1989) 2217-2245.

3. Singleton, M.F., Murray, J.L. and Nash, P.; Binary Alloy Phase Diagrams; Massalski, T.B. (eds.); ASM International (1990) 183.

4. Grabke, H.J., Brumm, M.W. and Wagemann, B.: *Materials and Corrosion* **47** (1996) 675-677.

5. Bradley, A.J. and Taylor, A.: *Proc. Royal Soc. London* **A159** (1937) 56-72.

6. Baker, I.: *Mat. Sci. Eng.* **A192/ 193** (1995) 1-13.

7. Hancock, G.F. and McDonnell, B.R.: *Phys. Stat. Sol. (a)* **4** (1971) 143-150.

8. Yang, W.J. and Dodd, R.A.: *Metal Sci. J.* **7** (1973) 41-47.

9. Ebrahimi, F. and Hoyle, T.G.: *Acta Mat.* **45** (1997) 4193-4204.

10. Chang, K.-M., Darolia, R. and Lipsitt, H.A.: *Acta Met. Mat.* **40** (1992) 2727-2737.

11. Darolia, R., Walston, W.S., Noebe, R., Garg, A. and Oliver, B.F.: *Interm.* **7** (1999) 1195-1202.

12. Gehling, M.G. and Vehoff, H.: *Mat. Sci. Eng.* **A329-331** (2002) 255-261.

13. Reuss, S. and Vehoff, H.: *Scripta Met. et Mat.* **24** (1990) 1021-1026.

14. Kumar, K.S., Mannan, S.K. and Viswanadham, R.K.: *Acta Met. Mat.* **40** (1992) 1201-1222.

15. Yoo, M.H., Takasugi, T., Hanada, S. and Izumi, O.: *Mat. Trans.* **31** (1990) 435-442.

16. Hsu, Y.-N., Laughlin, D.E. and Lambeth, D.N.: *Mat. Res. Soc. Symp. Proc.* **517** (1998) 199-204.

17. Zhong, D., Moore, J.J., Disam, J., Thiel, S. and Dahan, I.: *Surface and Coating Technology* **120-121** (1999) 22-27.

18. Almeida, P.d., Schäublin, R., Almazouzi, A., Victoria, M. and Levy, F.: *Thin Solid Films* **368** (2000) 26-34.

19. Hu, M.S. and Evans, A.G.: *Acta Met.* **37** (1989) 917-925.

20. Hutchinson, J.W. and Suo, Z.: *Adv. Appl. Mech.* **29** (1992) 63-191.

21. Beuth, J.L.: *Int. J. Sol. Struct.* **29** (1992) 1657-1675.

22. Xia, Z.C. and Hutchinson, J.W.: *J. Mech. Phys. Sol.* **48** (2000) 1107-1131.

23. Begley, M.R. and Ambrico, J.M.: *Int. J. Fracture* **119/120** (2003) 325-338.

24. Vlassak, J.J.: *Int. J. Fracture* **119/120** (2003) 299-323.

25. Evans, A.G., Drory, M.D. and Hu, M.S.: *J. Mat. Res.* **3** (1988) 1043-1049.

26. Hu, M.S., Thouless, M.D. and Evans, A.G.: *Acta Met.* **36** (1988) 1301-1307.

27. Ye, T., Suo, Z. and Evans, A.G.: *Int. J. Sol. Struct.* **29** (1992) 2639-2648.

28. Moody, N.R., Medlin, D., Boehme, D. and Norwood, D.P.: *Eng. Fracture Mech.* **61** (1998) 107-118.

29. Arzt, E.: *Acta Mat.* **46** (1998) 5611-5626.

30. Balk, T.J., Dehm, G. and Arzt, E.: *Acta Mat.* **51** (2003) 4471-4485.

31. Dehm, G., Inkson, B.J., Wagner, T., Balk, T.J. and Arzt, E.: *J. Mat. Sci. Techn.* **18** (2002) 113-117.

32. Kobrinsky, M.J. and Thompson, C.V.: *Appl. Phys. Let.* **73** (1998) 2429-2431.

33. Freund, L.B.: *J. Appl. Mech.* **54** (1987) 553-557.

34. Thompson, C.V.: *J. Mat. Res.* **8** (1993) 237-238.

35. Nix, W.D.: *Scripta Mat.* **39** (1998) 545-554.

36. Blanckenhagen, B.v., Gumbsch, P. and Arzt, E.: *Phil. Mag. Letters* **83** (2003) 1-8.

37. Flinn, P.A., Gardner, D.S. and Nix, W.D.: *IEEE Tran. Elect. Dev.* **34** (1987) 689-699.

38. Thouless, M.D., Rodbell, K.P. and Cabral, C.: *J. Vac. Sci. Techn.* **A 14** (1996) 2454-2461.

39. Kobrinsky, M.J. and Thompson, C.V.: *Acta Mat.* **48** (2000) 625-633.

40. Weiss, D., Gao, H. and Arzt, E.: *Acta Mat.* **49** (2001) 2395-2403.

41. Gao, H., Zhang, L., Nix, W.D., Thompson, C.V. and Arzt, E.: *Acta Mat.* **47** (1999) 2865-2878.

42. Baker, I., Nagpal, P., Liu, F. and Munroe, P.R.: *Acta Met. Mat.* **39** (1991) 1637-1644.

43. Schulson, E.M. and Barker, D.R.: *Scripta Met.* **17** (1983) 519-522.

44. Arzt, E. and Grahle, P.: *Acta Mat.* **46** (1998) 2717-2727.

45. Venkatraman, R. and Bravman, J.C.: *J. Mat. Res.* **7** (1992) 2040-2048.

46. Keller, R.-M., Baker, S.P. and Arzt, E.: *J. Mat. Res.* **13** (1998) 1307-1317.

47. Hommel, M. and Kraft, O.: *Acta Mat.* **49** (2001) 3935-3947.

48. Thouless, M.D.: *J. Am. Ceram. Soc.* **73** (1990) 2144-2146.

49. Totemeier, T.C., Gale, W.F. and King, J.E.: *Mat. Sci. Eng.* **A169** (1993) 19-26.

50. Affeldt, E.E.: *Adv. Eng. Mat.* **2** (2000) 811-813.

51. Chang, K.-M., Darolia, R. and Lipsitt, H.A.: *Mat. Res. Soc. Symp. Proc.* **213** (1991)

52. Hack, J.E., Brzeski, J.M. and Darolia, R.: *Mat. Sci. Eng. A* **192/193** (1995) 268-276.

53. Hoehn, J.W., Venkataraman, S.K., Huang, H. and Gerberich, W.W.: *Mat. Sci. Eng. A* **192/193** (1995) 301-308.

54. Flores, K.M. and Dauskardt, R.H.: *Scripta Mat.* **36** (1997) 1377-1382.

55. Ebrahimi, F. and Shrivastava, S.: *Mat. Sci. Eng. A* **239-240** (1997) 386-392.

56. Vehoff, H., Ochmann, P., Göken, M. and Gehling, M.G.: *Mat. Sci. Eng.* **A239-240** (1997) 378-385.

57. Nagpal, P. and Baker, I.: *Mat. Charact.* **27** (1991) 167-173.

58. Weaver, M.L., Levit, V., Kaufman, M.J. and Noebe, R.D.: *Mat. Res. Soc. Symp. Proc.* **364** (1995) 425-430.

59. Purvis, A.L. and Warnes, B.M.: *Surf. Coat. Tech.* **146-147** (2001) 1-6.

60. Antelo, M.A., Johnson, P.K., Ostolaza, K.M. and Bressers, J.: *Mat. Sci. Eng.* **A247** (1998) 40-50.

61. JCPDS No. 20-19; International Center for Diffraction Data, Swathmore, Pennsylvania (1991).

62. Stoney, G.G.: *Proc. R. Soc.* **A82** (1909) 172-175.

63. Flinn, P.A.: *Mat. Res. Soc. Symp. Proc.* **130** (1989) 41-51.

64. Handbook of Chemistry and Physics; Linde, D.R. (eds.); CRC Press (2001) 12-97.

65. Miracle, D.B.: *Acta Met. Mat.* **41** (1993) 649-684.

66. Wellner, P., Kraft, O. and Arzt, E.: *Mat. Res. Soc. Symp. Proc.* **695** (2002) L9.6.1-L9.6.6.

67. Cramer, T., Wanner, A. and Gumbsch, P.: *Phys. Rev. Letters* **85** (2000) 788-791.

68. Nakamura, T. and Kamath, S.: *Mech. Mat.* **13** (1992) 67-77.

69. Spence, J.C.H., Huang, Y.M. and Sankey, O.: *Acta Met. Mat.* **41** (1993) 2815-2824.

70. Lautenschlager, E.P., Kiewit, D.A. and Brittain, J.O.: *Trans. Met. Soc. AIME* **233** (1965) 1297-1302.

71. Vedula, K. and Khadkikar, P.S.; High Temperature Aluminides and Intermetallics; Whang, S.H., Liu, C.T., Pope, D.P. and Stieger, J.O. (eds.); The Minerals, Metals & Materials Society (1990) 197-217.

72. Schroll, R. and Gumbsch, P.: *Phys. Stat. Sol. (a)* **166** (1998) 457-488.

73. Cottrell, A.H.: *Mat. Sci. Techn.* **5** (1989) 1165-1167.

74. Mutasa, B. and Farkas, D.: *Surf. Sci.* **415** (1998) 312-319.

75. Mutasa, B. and Farkas, D.: *Metal. Mat. Trans. A* **29** (1998) 2655-2668.

76. Lane, M. and Dauskardt, R.H.: *J. Mat. Res.* **15** (2000) 2758-2769.

77. Wortman, J.J. and Evans, R.A.: *J. Appl. Phys.* **36** (1964) 153-156.

78. Rusovic, N. and Warlimont, H.: *Phys. Stat. Sol. (a)* **44** (1977) 609-619.

79. Kraft, O., Freund, L.B., Phillips, R. and Arzt, E.: *MRS Bulletin* **27** (2002) 30-37.

80. Ronay, M.: *Phil. Mag. A* **40** (1979) 145-160.

81. Shen, Y.-L., Suresh, S., He, M.Y., Bagchi, A., Kienzle, O., Rühle, M. and Evans, A.G.: *J. Mat. Res.* **13** (1998) 1928-1937.

82. Kobrinsky, M.J., Dehm, G., Thompson, C.V. and Arzt, E.: *Acta Mat.* **49** (2001) 3597-3607.

83. Nagpal, P., Baker, I., Liu, F. and Munroe, P.R.: *Mat. Res. Soc. Symp. Proc.* **213** (1991) 533-538.

84. Vedula, K., Hahn, K.H. and Boulogne, B.: *Mat. Res. Soc. Symp. Proc.* **133** (1989) 299-304.

85. Hansen, N. and Ralph, B.: *Acta Met.* **30** (1982) 411-17.

86. Kovacs-Csetenyi, E., Horvath, M., Chinh, N.Q. and Kovacs, I.: *Physica Status Solidi A* **166** (1998) 805-10.

87. Divinski, S. and Herzig, C.: *Interm.* **8** (2000) 1357-1368.

88. Hartmaier, A., Buehler, M.J. and Gao, H.: *submitted to: Defects and Diff. in Metals, Defects and Diff. Forum* (2003).

89. Brumm, M.W. and Grabke, H.J.: *Corr. Sci.* **33** (1992) 1677-1690.

90. Kraft, O., Wellner, P., Hommel, M., Schwaiger, R. and Arzt, E.: *Z. Metallk.* **93** (2002) 392-400.

91. Balk, T.J., Dehm, G. and Arzt, E.: *Mat. Res. Soc. Symp. Proc.* **779** (2003) W4.4.1 - 4.4.10.

92. Balk, T.J.: *unpublished results* (2003).